CHALMERS UNIVERSITY OF TECHNOLOGY
Gothenburg, Sweden
www.chalmers.se

LICENTIATE THESIS

AHAD HAMEDNIA • On Optimal Mission Planning for Conventional and Electric Heavy Duty Vehicles • 2020

On Optimal Mission Planning for Conventional and Electric Heavy Duty Vehicles

AHAD HAMEDNIA

DEPARTMENT OF ELECTRICAL ENGINEERING
CHALMERS UNIVERSITY OF TECHNOLOGY
Gothenburg, Sweden 2020
www.chalmers.se

THESIS FOR THE DEGREE OF LICENTIATE OF ENGINEERING

On Optimal Mission Planning for Conventional and Electric Heavy Duty Vehicles

Ahad Hamednia

CHALMERS
UNIVERSITY OF TECHNOLOGY

Department of Electrical Engineering
Chalmers University of Technology
Gothenburg, Sweden, 2020

On Optimal Mission Planning for Conventional and Electric Heavy Duty Vehicles

Ahad Hamednia

This thesis has been prepared using LaTeX.

Department of Electrical Engineering
Chalmers University of Technology
SE-412 96 Gothenburg, Sweden
Phone: +46 (0)31 772 1000
www.chalmers.se

Printed by Chalmers Reproservice
Gothenburg, Sweden, 2020

To my parents

Abstract

Ever-growing energy consumption and CO_2 emissions due to the increase in road transport are major challenges that attract international attention, especially policy makers, logistic service providers and customers considering environmental, ecological and economic issues. Other negative side-effects caused by the growth of the road transport are the extensive economic and social costs because of traffic congestion. Thus, there is a strong motivation to investigate possible ways of improving transport efficiency aiming at achieving a sustainable transport, e.g. by finding the best compromise between resource consumption and logistics performance. The transport efficiency can be improved by optimal planning of the transport mission, which can be interpreted as optimising mission start and/or finish time, and velocity profile of the driving vehicle. This thesis proposes a bi-layer mission planner for long look-ahead horizons stretched up to hundreds of kilometers. The mission planner consists of logistics planner as its top level and eco-driving supervisor as its bottom level. The logistics planner aims at optimising the mission start and/or finish time by optimising energy consumption and travel time, subject to road and traffic information, e.g. legal and dynamic speed limits. The eco-driving supervisor computes the velocity profile of the driving vehicle by optimising the energy consumption and penalising driver discomfort. To do so, an online-capable algorithm has been formulated in MPC framework, subject to road and traffic information, and the pre-optimised mission start and/or finish time. This algorithm is computationally efficient and enables the driving vehicle to adapt and optimally respond to predicted disturbances within a short amount of time. The mission planner has been applied to conventional and fully-electric powertrains. It is observed that total travel time is reduced up to 5.5 % by optimising the mission start time, when keeping an average cruising speed of about 75 km/h. Also, compared to standard cruise control, the energy savings of using this algorithm is up to 11.6 %.

Keywords: Transport efficiency, Mission planning, Logistics planning, Eco-driving, Optimal control, Model predictive control

List of Publications

This thesis is based on the following publications:

[A] **Ahad Hamednia**, Nikolce Murgovski, and Jonas Fredriksson, "Time optimal and eco-driving mission planning under traffic constraints". Accepted in 23rd *IEEE International Conference on Intelligent Transportation Systems (ITSC)*, Rhodos, Greece, Sep. 2020.

[B] **Ahad Hamednia**, Nalin K.Sharma, Nikolce Murgovski, Jonas Fredriksson, "Computationally efficient algorithm for eco-driving over long look-ahead horizons". Submitted to *IEEE Transactions on Intelligent Transportation Systems (ITS)* in Jan. 2020.

Other publications by the author, not included in this thesis, are:

[C] **A. Hamednia**, N. Murgovski, and J.Fredriksson, "Predictive velocity control in a hilly terrain over a long look-ahead horizon". 5th *IFAC Conference on Engine and Powertrain Control, Simulation and Modeling (E-CoSM)*, Changchun, China, Sep. 2018.

[D] S. E. T. Jacobsen, A. Gustafsson, N. Vu, S. Madhusudhana, **A. Hamednia**, N. K. Sharma, and N. Murgovski, "Predictive cruise control behind a stationary or slow moving object". 30^{th} *IEEE Intelligent Vehicles Symposium (IV)*, Paris, France, Jun. 2019.

[E] N. K. Sharma, **A. Hamednia**, N. Murgovski, E. R. Gelso, and J. Sjöberg, "Optimal eco-driving of a heavy-duty vehicle behinda leading heavy-duty vehicle". Accepted in *IEEE Transactions on Intelligent Transportation Systems (ITS)*, June, 2020.

Acknowledgments

First and foremost, I would like to express my sincere gratitude to my supervisor, Docent. Nikolce Murgovski, for his patient guidance, encouragement and advice throughout my PhD studies so far. Also, I would like to thank my co-supervisor, Prof. Jonas Fredriksson, for many fruitful discussions, which greatly helped me to gain a deeper understanding about my research field. I am very grateful for the time they both have spent to guide me and give me valuable comments on my work.

Many thanks to Dr. Nalin Kumar Sharma and Dr. Maryam Razi for their time and helpful discussions. Honestly, I learned a considerable amount from them.

Finally, my parents deserve the biggest recognition of all, for the endless support and having always faith in me. I love you both.

Acronyms

GDP:	Gross Domestic Product
NDC:	Nationally Determined Contributions
HDV:	Heavy Duty Vehicles
MP:	Mission Planner
MPC:	Model Predictive Control
ICE:	Internal Combustion Engine
EM:	Electric Machine
OCP:	Optimal Control Problem
CV:	Conventional Vehicle
EV:	Electric Vehicle
HEV:	Hybrid Electric Vehicle
SoC:	State of Charge
NLP:	Nonlinear Program
DP:	Dynamic Programming
MIQP:	Mixed-integer Quadratic Program
PMP:	Pontryagin's Maximum Principle
TPBVP:	Two-point Boundary Value Problem
MHMPC:	Moving Horizon Model Predictive Control
SHMPC:	Shrinking Horizon Model Predictive Control
RTI:	Real-time Iteration
SQP:	Sequential Quadratic Programming

QP:	Quadratic Program
MINLP:	Mixed-integer Nonlinear Program
PEV:	Plug-in Electrified Vehicle

Contents

Part I

Overview

CHAPTER 1

Introduction

1.1 Motivation

Transport demand is linked with several factors, such as economic environment, political will and technological development. The economic environment, characterized as gross domestic product (GDP), international trade and oil prices, plays a central role in the demand for transport. In particular, the growth of GDP has been historically identified as a major contributor to the growth of both freight and passenger transport, i.e. greater rise in goods production can lead to greater transport distances travelled [1]. International trade among different countries and people, known as a crucial matter for the development of civilizations, is enabled by the means of transport. The volume of international trade has grown twenty-seven fold in the post-war era between 1950 and 2007, three times faster than the growth of world GDP [1]. The recent precipitous drop in oil prices is an unexpected issue that strongly affects the transport demand. Transport sector has been a beneficiary of lower oil prices, where not only it attains direct savings taken from lower oil prices, but the expected rise in consumer spending, as the total money spent on final goods and services by individuals, can increase the amount of international

trade, and, accordingly, transportation [1].

Among all transport modes, surface transport, including road and rail, demands around 30 % of the freight transport demand and around 86 % of the passenger transport demand [1]. In a baseline scenario, defined as an extrapolation of current trends including current policies and policy developments, surface freight demand is projected to grow from 32 000 to 83 000 billion tonne-kilometres between 2015 to 2050, accounting road freight demand for about 60 % of the total, see Figure 1.1(a). Also, global surface passenger demand is expected to increase from 43 500 billion passenger-kilometres in 2015 to around 92 800 billion passenger-kilometres in 2050, see Figure 1.1(b), where road passenger-kilometres are estimated to account over 80 % of the total. Although surface transport is increasing, its growth rate is not the same in all countries. The future development path of the countries in service-oriented economies highly influences this transport sector [1].

Excessive energy consumption and CO_2 emissions caused by the growth of road transport are alarming concerns for policy makers, logistic service providers and customers due to economic, environmental and ecological issues. The nationally determined contributions (NDC) underlines the necessity of transport decarbonisation by addressing the important role of fuel-efficient technologies and development of electromobility [1]. In 2015, energy consumption due to the road transport in Europe amounted to around 11.5 million terajoules. Also, the calculated volume of the emissions is 60 % higher compared to the total amount in 1990 and is estimated to increase by more than 70 % until 2050 [2]. In relation to the oil prices, in the short to medium term, the risk of abandoning the commitments made against climate change is boosted by low oil prices, as they are encouraging more fossil fuel burning. Besides, the lower oil prices are known as a threat towards the companies introducing clean-energy technologies. However, in the longer term, the chance for clean investments may be raised, followed by the current low oil prices, since future possible cost-effective clean mobility solutions may win the competition with conventional fuel [1].

Extensive costs, e.g. economic and social, due to traffic congestion are other negative side effects caused by the increase in road transport. In 2010, the estimated cost due to the traffic congestion is $115 billion over 439 urban areas of the United States [3]. The traffic congestion engenders mainly because the traffic volume is too close to the maximum capacity of a road or network

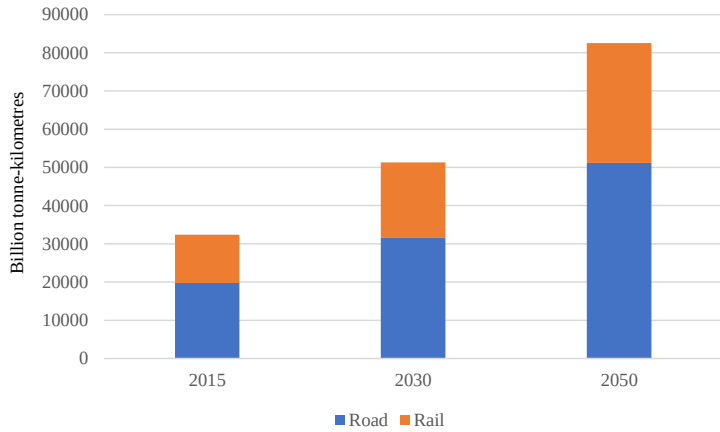

(a) Surface freight transport demand by mode.

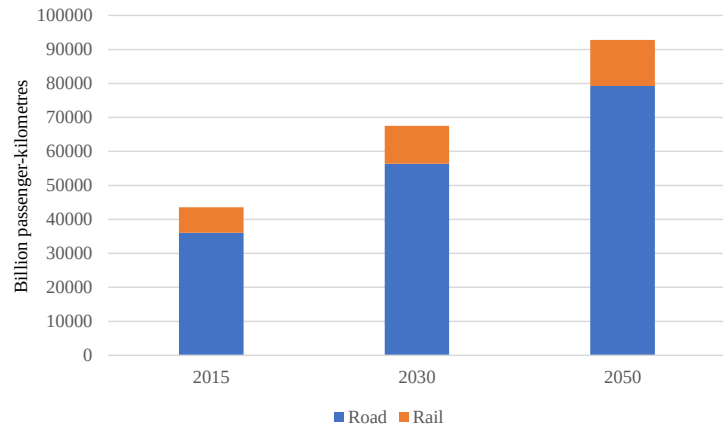

(b) Surface passenger transport demand by mode.

Figure 1.1: Surface transport demand including freight and passenger, baseline scenario. Data are extracted from [1].

for certain hours of a day. Current official forecasts point out that congestion will grow considerably within future decades [4]. In public opinion, the growing traffic congestion on motorways is indicated as a waste of money and time, which can be resolved by means of building more roads. However, road construction is not always cost-effective and can cause serious environmental issues. Thus, due to the enormous increase in the energy consumption, CO_2 emissions and traffic congestion costs, there is a strong incentive to achieve a sustainable transport by improving transport efficiency using current road infrastructure, which can be interpreted as providing service with less consumption of resources and not losing logistics performance, i.e. costs and delivery service [5].

Transport efficiency can be improved by optimal planning of the transport mission. To do so, it is essential to optimise the mission start time and increase the efficiency of *tank-to-meter*, which refers to the conversion of energy stored in fuel into potential and kinetic energy required for displacement, and accompanied losses [6]. The tank-to-meter efficiency can be improved in several ways by, e.g. alternative powertrains, better usage of vehicle components, reducing the vehicle mass, choosing the most energy-efficient route, or providing the vehicle's energy-efficient drive, so-called *eco-driving* [7]–[9]. In particular, it is revealed in [6] that there is a high potential of eco-driving in improving the tank-to-meter efficiency without having any requirement for structural changes in the vehicle. As for an example of a passenger car, sensitivity of vehicle mean square speed and mean acceleration are calculated as 0.6 and 0.35 respectively, where the sensitivity is defined as the percentage reduction of energy consumption per percentage reduction of the considered variable [6]. To achieve eco-driving it is necessary to optimally plan the velocity profile of the vehicle, subject to road and traffic flow information. One important factor in optimising the velocity profile is the speed limits, which are imposed by not only legal speed limits but also dynamic constraints [10], [11]. For instance, surrounding traffic sets such dynamic constraints due to the presence of e.g. traffic lights, intersections, ramps and junctions. Another example that dynamically affects the speed limits is the linking of two or more trucks in convoy in order to increase the energy efficiency [12]. As dynamic speed limits depend on day and time of day, the total travel time depends not only on the planned velocity profile, but also on the mission start time [13].

For non-urban road transport, heavy-duty vehicles (HDVs) have great po-

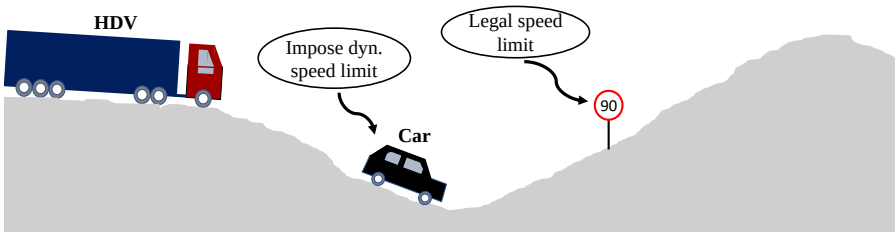

Figure 1.2: A truck is driving in a hilly terrain, where legal and dynamic speed limits are imposed. The truck is following the principles of eco-driving to improve its energy efficiency.

tential in improving the energy efficiency and reducing CO_2 [14], especially when driving in a hilly terrain. Thus, the vehicle accelerates when driving downhill and decelerates when climbing uphill, see Figure 1.2. This leads to less waste of non-recuperable energy compared to driving with constant speed [15]. To implement such behaviour over complex road topographies, advanced optimal control strategies [6] can be employed that maximise energy efficiency by optimal coordination of energy sources, utilizing information of the road topography.

1.2 Thesis focus and contributions

The focus of this thesis is the development of an optimal mission planner (MP) for an HDV driving in a hilly terrain, subject to road and traffic information. In particular, this thesis has the following three goals:

- Improve transport efficiency by controlling the speed profile and mission start and/or finish time under legal speed limits and dynamic speed limits imposed by surrounding traffic.
- Develop predictive controllers that employ communication and prediction abilities of modern transportation to anticipate future events and disturbances.
- Quantify the trade-off and perform sensitivity analyses among energy efficiency, travel time and driver comfort.

To address these goals, we propose an MP consisting of two layers, as shown in Figure 1.3. The MP's top layer calculates the mission start and/or finish

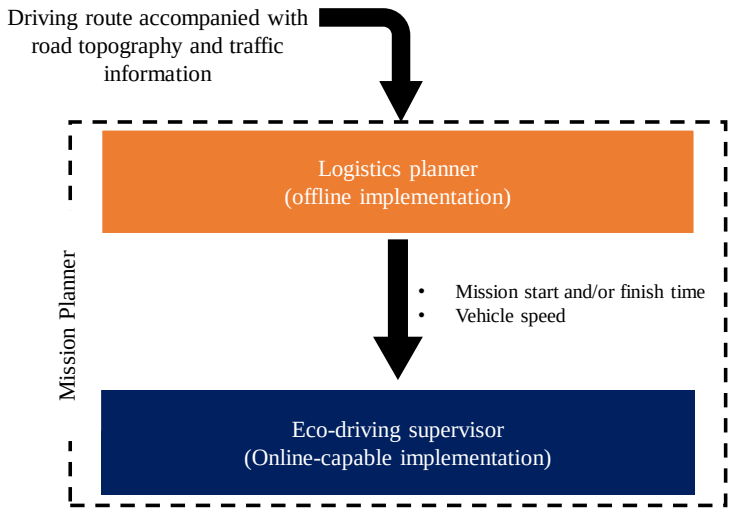

Figure 1.3: Two-layer mission planner.

time and generates a reference speed trajectory to its bottom level, by offline optimising energy consumption and travel time. Input to this layer is the road profile from a selected route and traffic information along the route compiled from look-ahead information and previous measurements. Then, the bottom layer optimises the vehicle speed by applying an online-capable computationally efficient algorithm, formulated in the model predictive control (MPC) framework. The MPC algorithm has the ability to incorporate look-ahead information and generate optimal predictive actions over look-ahead horizons of up to hundreds of kilometers.

1.3 Thesis outline

The thesis is divided into two parts. First part corresponds to illustration of the context given by the papers that are appended in the second part. Following paragraphs describe the thesis outline.

Chapter 2 describes modeling of the studied powertrain, dynamical equations governing to the driving vehicle, vehicle driving mission and the impact

of the vehicle's longitudinal drive on improving the energy efficiency. Chapter 3 begins with explaining the proposed bi-layer mission planner. Then, it is discussed that the tasks of each layer can be performed by solving an optimal control problem. Also, the proposed algorithm for solving each layer's optimisation program is explained. Finally, the selected simulation results are illustrated and discussed. Chapter 4 provides a short summary for each of the appended papers. Finally, the last chapter of introductory part concludes the thesis and presents the possible directions for future extension of current research.

CHAPTER 2

Modelling and energy analysis

In this chapter, modeling of the studied powertrain and dynamical equations governing to the driving vehicle are presented. Furthermore, driving mission of the vehicle is illustrated as a driving route accompanied with the road topography and speed limits in terms of travel distance and time of day. Finally, the impact of the vehicle's longitudinal drive on improving the energy efficiency is described.

2.1 Powertrain modelling

The focus of this work is on conventional and fully electric powertrains. Schematic diagram of the addressed powertrain in this thesis is depicted in Figure 2.1, which includes an energy storage unit, e.g. fuel tank or electric battery, an actuator, e.g. internal combustion engine (ICE) or electric machine (EM), and a transmission system. The torque and rotational speed at the shaft between the actuator and transmission are represented by M and ω, respectively. The actuators are modelled with static relations based on steady-state measurements. An example of efficiency maps of the ICE and EM for a given pair of rotational speed and torque are shown in Figure. 2.2. In Fig-

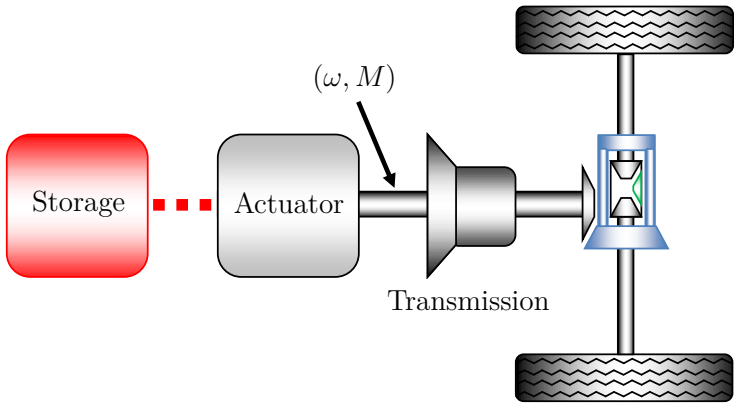

Figure 2.1: Powertrain schematic diagram, which consists of an energy storage unit, an actuator and a transmission system. The transmission translates shaft torque, M, with rotating speed ω, to traction force F with longitudinal velocity v.

ure 2.2(a), the negative torque limit corresponds to a lower bound on negative torque including a retarder, a compression release engine brake and/or an exhaust pressure governor. The additional braking is preferred over the service braking in order to reduce wear and avoid lockup of the braking pads. In Figure 2.2(b), the positive and negative torque regions indicate the motoring and the generating modes of operation, respectively.

The transmission system shown in Figure. 2.1, translates the shaft torque M and rotational speed ω to traction force F and longitudinal velocity v respectively, as

$$v(s) = \omega(s)R(\gamma), \quad F_{\mathrm{w}}(s) = \frac{M(s)}{R(\gamma)}, \quad R(\gamma) = \frac{\mathrm{r_w}}{\mathrm{r_{tg}}(\gamma)\mathrm{r_{fg}}}, \tag{2.1}$$

where s is traveled distance, γ is selected gear, $\mathrm{r_w}$ is wheel radius, $\mathrm{r_{tg}}$ and $\mathrm{r_{fg}}$ are transmission and final gear ratios, respectively. All over this thesis, all constants that are not dependent on s, for e.g. m, are shown in upright letters. Also, the explicit dependency on s of the variables that are trajectories in terms of s, e.g. $F_{\mathrm{w}}(s)$, is not shown in several places for simplicity.

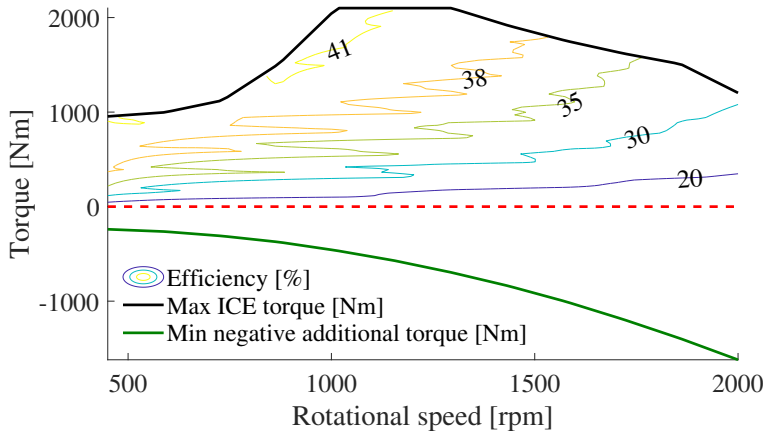

(a) Steady-state efficiency map together with ICE torque limits.

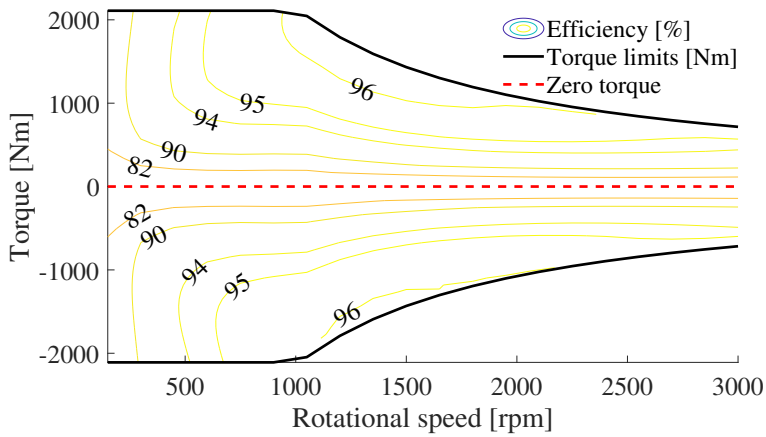

(b) Steady-state efficiency map together with EM torque limits.

Figure 2.2: Steady-state efficiency map together with actuator torque limits.

2.2 Travel time and longitudinal dynamics

Consider a vehicle driving a planned route in a hilly terrain, without stopping or changing direction of movement. The dynamics of travel time, t, is

$$t'(s) = \frac{1}{v(s)}. \tag{2.2}$$

According to the Newton's law of motion, longitudinal dynamics of the vehicle is

$$\mathrm{m}v(s)v'(s) = F_{\mathrm{w}}(s) + F_{\mathrm{brk}}(s) - F_{\mathrm{air}}(v) - F_{\alpha}(s), \tag{2.3}$$

where m is total lumped mass of the vehicle and the longitudinal acceleration is shown by $vv' = \mathrm{d}v/\mathrm{d}t$. Note that throughout this thesis, x' represents the space derivative of a variable x, as $x' = \mathrm{d}x/\mathrm{d}s$. Also, F_{brk} denotes a non-positive mechanical braking force that may include braking by the service brakes, a retarder, a compression release engine brake and/or an exhaust pressure governor. The nominal aerodynamic drag, F_{air}, and the roll resistance, $F_{\alpha}(s)$, are defined as

$$F_{\mathrm{air}}(v) = \frac{\rho_{\mathrm{a}} \mathrm{c_d} \mathrm{A_f} v^2}{2}, \tag{2.4}$$

$$F_{\alpha}(s) = \mathrm{mg}\left(\sin(\alpha(s)) + \mathrm{c_r}\cos(\alpha(s))\right), \tag{2.5}$$

where ρ_{a} is air density, $\mathrm{c_d}$ is aerodynamic drag coefficient, $\mathrm{A_f}$ is frontal area of the vehicle, g is gravitational acceleration, α is road gradient, and $\mathrm{c_r}$ is rolling resistance coefficient.

The vehicle longitudinal dynamics (2.3) is nonlinear, since the aerodynamical drag in (2.4) is a quadratic function of the longitudinal velocity. The nonlinearity may increase computational complexity. To alleviate this, it is possible to change the independent variable from v to kinetic energy E defined as

$$E(s) = \frac{\mathrm{m}v^2(s)}{2}. \tag{2.6}$$

To study variations on the driving vehicle's speed, the acceleration a, is

considered as

$$a(s) = \frac{1}{\mathrm{m}} \left(-\mathrm{c_a} E(s) + F_{\mathrm{w}}(s) + F_{\mathrm{brk}}(s) - F_{\alpha}(s) \right) \tag{2.7}$$

where $\mathrm{c_a} = \rho_{\mathrm{a}} \mathrm{c_d} \mathrm{A_f}/2$ gathers the drag related coefficients. Also, we introduce j as the change of acceleration in space coordinates, which hereafter is referred to as jerk. Thus, the governing equations of the vehicle are

$$t'(s) = \sqrt{\frac{\mathrm{m}}{2E(s)}} \tag{2.8}$$

$$E'(s) = \mathrm{m}a(s) \tag{2.9}$$

$$a'(s) = j(s) \tag{2.10}$$

where the $E' = \mathrm{m}vv'$ is the product of mass and vehicle acceleration.

2.3 Vehicle driving mission

We describe a driving mission by a map of maximum dynamic speed limits for a given pair of travel distance and time of day, as illustrated in Figure. 2.3. Figure. 2.3(a) includes a contour plot, where the lighter the contour color is, the greater the vehicle speed is. Figure. 2.3(b) is a double y-axis plot, where the left y-axis corresponds to the vehicle speed and the right axis is the road altitude, while the gray area represents the road topography. According to the max speed map, the vehicle's mission, characterised as the mission start time, total travel time and velocity profile, can be tailored in favour of the improved energy efficiency. One execution of the mission in terms of speed/time trajectory is also shown in Figure. 2.3, where the vehicle starts the mission at 10:00. It can be seen that the traffic speed drops to about 30 km/h in the congested area, at about 25 km.

2.4 Vehicle drive impact on energy efficiency

The impact of vehicle's longitudinal drive on improving the tank-to-meters efficiency can be investigated by studying the energy balance originating from

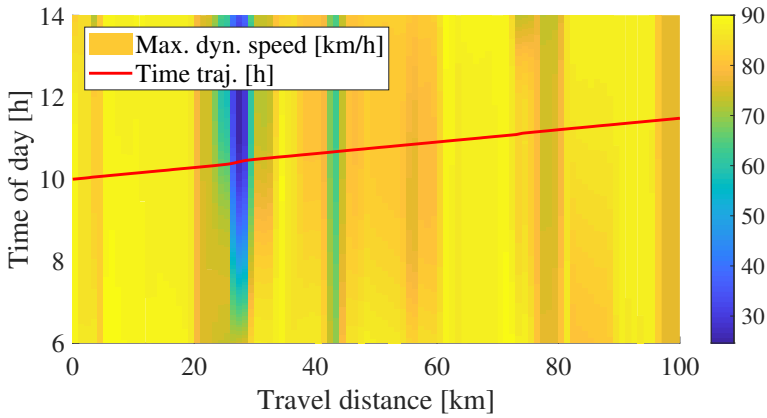

(a) Map of maximum dynamic speed limits together with one execution of the driving mission in terms of time trajectory.

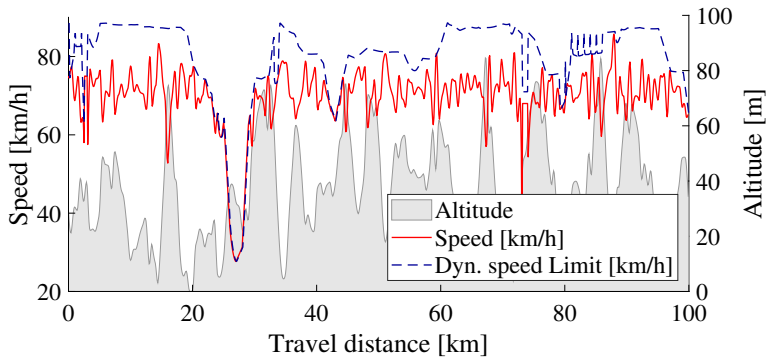

(b) Road topography with hilly terrain together with one execution of the driving mission in terms of longitudinal velocity and maximum dynamic speed limit.

Figure 2.3: Maximum dynamic speed limits map for a given pair of travel distance and time of day, together with associated road topography and one execution of the driving mission.

Newton's law of motion. Let

$$P_{\mathrm{t}}(s) = F_{\mathrm{w}}(s)v(s) + P_{\mathrm{loss}}(v, F_{\mathrm{w}}) + P_{\mathrm{aux}} \tag{2.11}$$

denote internal power drawn from the storage, where P_{loss} combines the storage and actuator power losses and P_{aux} is electrical load consumed by auxiliary devices. The energy consumed from the storage during a road segment can then be determined as

$$\begin{aligned} E_{\text{t}}(v, F_{\text{w}}) &= \int_{\text{s}_0}^{\text{s}_\text{f}} \frac{P_{\text{t}}(s)}{v(s)} \text{d}s = \\ &= \int_{\text{s}_0}^{\text{s}_\text{f}} F_{\text{w}}(s) \text{d}s + \int_{\text{s}_0}^{\text{s}_\text{f}} \frac{P_{\text{loss}}(v, F_{\text{w}}) + P_{\text{aux}}}{v(s)} \text{d}s, \end{aligned} \tag{2.12}$$

where s_0 and s_f represent initial and final position of the road segment. The division of the internal power with speed in (2.12) is obtained from the time to space transformation, i.e.

$$\int P_{\text{t}}(v, F_{\text{w}}) \text{d}t = \int P_{\text{t}}(v, F_{\text{w}})/v(s) \, \text{d}s = \int F_{\text{t}}(v, F_{\text{w}}) \, \text{d}s.$$

The first integral in (2.12) represents propelling energy at the wheels within the interval $[\text{s}_0, \text{s}_\text{f}]$, which is transformed into kinetic energy, potential energy, and the energy lost in service braking and for overcoming rolling resistance and aerodynamic drag, as

$$\begin{aligned} \int_{\text{s}_0}^{\text{s}_\text{f}} F_{\text{w}}(s) \text{d}s = \int_{\text{s}_0}^{\text{s}_\text{f}} \text{m} v(s) \text{d}v + \int_{\text{s}_0}^{\text{s}_\text{f}} \text{mg} \sin(\alpha(s)) \text{d}s + \\ + \int_{\text{s}_0}^{\text{s}_\text{f}} \left(\text{c}_\text{a} v^2 + \text{mgc}_\text{r} \cos(\alpha(s)) - F_{\text{brk}}(s) \right) \text{d}s. \end{aligned} \tag{2.13}$$

Looking at the first term in (2.13), which corresponds to the change in kinetic energy over the segment,

$$\int_{\text{s}_0}^{\text{s}_\text{f}} \text{m} v(s) \text{d}v = \frac{\text{m}}{2} \left(v^2(\text{s}_\text{f}) - v^2(\text{s}_0) \right) = E(\text{s}_\text{f}) - E(\text{s}_0),$$

one can notice that, if the initial and final longitudinal velocities are equal, the change in kinetic energy is zero. Also, the second term in (2.13) denotes the change in potential energy over the segment,

$$\int_{\text{s}_0}^{\text{s}_\text{f}} \text{mg} \sin(\alpha(s)) \text{d}s = \text{mg} \int_{\text{s}_0}^{\text{s}_\text{f}} h'(s) \text{d}s = \text{mg}(h(\text{s}_\text{f}) - h(\text{s}_0)),$$

considering $\sin\alpha(s) = h'(s)$ where h is the road altitude. In case of equal initial and final altitude, the change in potential energy is zero.

It is obvious from (2.12) and (2.13) that first priority in improving energy efficiency is to reduce non-recuperable energy waste due to service braking by controlling the vehicle speed. Furthermore, there is a trade-off between reduced aerodynamic drag by driving slower and increased travel time. Moreover, too slow driving will increase powertrain idling losses and the losses in auxiliaries. Thus, subject to road and traffic information as demonstrated in Figure. 2.3, and without changing structure of the powertrain, it is possible to minimise total losses and improve the energy efficiency by optimising velocity profile of the vehicle.

CHAPTER 3

Optimal mission planning

In this chapter, the proposed bi-layer mission planner is described. Primarily, it is shown that each layer has specific tasks, which can be performed by solving an optimal control problem. Then, the proposed algorithm for solving each layer's optimisation program is explained. Finally, selected simulation results of the layers are illustrated and discussed.

3.1 Mission planner

The mission planner consists of two layers, i.e. top layer is logistics planner and bottom layer is eco-driving supervisor, as visualised in Figure. 1.3. Several goals have stimulated us to design such a bi-layer structure, for e.g. reducing computational complexity, providing modularity and the ability to reject possible disturbances. Thus, specific tasks have been assigned to each layer that can be performed by solving an optimal control problem (OCP).

The ways of implementing optimal control actions obtained from solving the OCP can be categorised into offline and online. The logistics planner computes the optimal mission start and/or finish time by offline optimising energy consumption and travel time. It also generates a reference velocity

profile and, thus, an estimate of the time for reaching sparsely assigned positions along the route, at intervals of about 250 m. To do so, the logistics planner uses road information as well as traffic situation depicted as the map of maximum dynamic speed limits in terms of travel distance and time of day, see Figure. 2.3. The energy-efficient and time-optimal solution provided by the logistics planner offers the logistics centres a promising investigation in order to coordinate the shipping and receiving of goods, supplies, foods and people. The logistics planner will be discussed in more details later, in Section 3.2.

When solving the logistics planning OCP offline, reducing the computational time is often not the major bottleneck, since the problem solving is allowed to take a considerable amount of time. However, the offline implementation has drawbacks in situations where the disturbances and/or constraints, for e.g. traffic situation, change unpredictably and the vehicle is no longer able to exactly follow the planned solution. In such situations an alternative controller is needed to provide a solution, where in each instance the estimations and predictions of the vehicle and environment are utilised. Thus, an online-capable eco-driving supervisor has been developed in an MPC fashion for look-ahead horizons of up to hundreds of kilometers, subject to the pre-optimised mission start and/or finish time, and the reference velocity profile. The eco-driving supervisor will be discussed in more details later, in Section 3.3.

3.2 Logistics planner

In this section, the problem formulation and the proposed algorithm for designing the logistics planner are explained. Also, selected simulation results about the trade-off between energy efficiency and travel time, optimising the mission start time are presented.

Problem formulation

Here, the logistic planning OCP is formulated, which aims at planning optimal velocity trajectory for the entire mission, in a way that total energy consumption is minimised and the travel time is adjusted by a penalty factor.

The problem is summarised as

$$\min_{\mathbf{u}\in\mathcal{U}} \quad S(\mathbf{x}(\mathrm{s_f}),\mathrm{s_f}) + \int_{\mathrm{s_0}}^{\mathrm{s_f}} V(\mathbf{x}(s),\mathbf{u}(s),s)\mathrm{d}s \tag{3.1a}$$

subject to:

$$\frac{\mathrm{d}\mathbf{x}(s)}{\mathrm{d}s} = F(\mathbf{x}(s),\mathbf{u}(s),s) \tag{3.1b}$$

$$G(\mathbf{x}(s),\mathbf{u}(s),s) \leq 0 \tag{3.1c}$$

$$\mathbf{x}(\mathrm{s_0}) \in \mathcal{X}_0 \tag{3.1d}$$

$$\mathbf{x}(s) \in \mathcal{X} \tag{3.1e}$$

$$\mathbf{x}(\mathrm{s_f}) \in \mathcal{X}_\mathrm{f} \tag{3.1f}$$

$$\mathbf{u}(s) \in \mathcal{U} \tag{3.1g}$$

where $\mathrm{s_0}$ is initial position, $\mathrm{s_f}$ is final position, S and V are terminal and running cost, and include penalised total travel time and power consumption, respectively. The energy consumption in conventional vehicles (CVs) corresponds to consumed fossil fuel, while in electric vehicles (EVs) it corresponds to the electricity usage. The sets of the states $\mathbf{x}$, and control inputs $\mathbf{u}$ include a pair of travel time and longitudinal velocity (or kinetic energy), and a pair of traction and service braking forces, respectively. In conventional powertrains, gear is considered as an additional control input. Also, F and G are vectors of nonlinear functions in terms of the states, control inputs and traveled distance, where F corresponds to system dynamics (2.2) and (2.3), and G forms system general constraints including the maximum dynamic speed limit and actuator bounds. Moreover, $\mathcal{X}$, $\mathcal{X}_0$, $\mathcal{X}_\mathrm{f}$ and $\mathcal{U}$ denote the feasible sets of states, allowed initial states at $\mathrm{s_0}$, target states at $\mathrm{s_f}$ and control inputs, respectively. Note that our algorithm can accept different objective functions [16]–[20], with little, or almost no change, but we have not considered those objectives in the logistic planner. For more details about how such objectives can be used, interested readers may see Paper A and the references therein.

The problem (3.1) generally represents a mixed-integer nonlinear program (MINLP) if the set $\mathcal{U}$ is mixed-integer, e.g. when gear is chosen as one of the control inputs in CVs. When the set $\mathcal{U}$ does not include integer sub-sets, problem (3.1) is a dynamic nonlinear program (NLP). The MINLP (3.1) may generally be solved with dynamic programming (DP) [21] for only short look-ahead horizons, for e.g. up to 5 km [22], with the cost of high computation

effort. In addition to the two system states, travel time and longitudinal velocity (kinetic energy), having free initial and final time requires solving the DP in an additional loop, which is computationally equivalent to having a 3rd state in the problem. Furthermore, the problem may need to be solved multiple times, for different values of the time penalty factor. Moreover, since the logistics planner in this thesis addresses long look-ahead horizons, e.g. stretched up to hundreds of kilometers, there is a strong incentive to reduce the computation burden when solving the MINLP (3.1) by applying two steps described in the following two subsections.

Bi-level programming and gear optimisation

Here, the goal is to decouple gear optimisation defined as a static sub-problem from a dynamic NLP. Thus, the MINLP (3.1) can be reformulated as a bi-level program [23], where the optimisation of integer variables, i.e. gear, resides only in the bottom-level task, while all system dynamics reside in the top-level task. Static modelling of the actuator and transmission system allows separating the bottom level and solving it offline, where vehicle speed (or kinetic energy) and traction force are regarded as parameters, and optimal gear is computed as a function of these parameters.

To approach the offline-optimal gear selection that minimises energy consumption, it is first needed to translate the brake specific fuel consumption (BSFC) from the engine to the wheels, according to (2.1). The BSFC refers to the fuel efficiency of any prime mover that burns fuel and produces rotational, or shaft power. A given BSFC map of the engine translates to several equivalent maps at the wheels, one map for each gear. This is illustrated in Figure. 3.1, where BSFC is calculated over a grid of feasible vehicle speed and longitudinal traction force. It can be noticed that map regions with the same speed and force overlap for different gears. Then, the optimal BSFC map for the overlapping regions is derived by calculating the minimum BSFC value for each pair of speed and traction force, see Figure. 3.2. Thus, the optimal gear is computed as the corresponding gear that has minimised the BSFC for the given pair of speed and traction force, see Figure. 3.3.

Gear selection is relevant even in the negative force region, where a retarder, a compression release engine brake and/or an exhaust pressure governor can be used for braking. The maximum braking force that these units can deliver, also referred to as the minimum additional force limit, is calculated as the

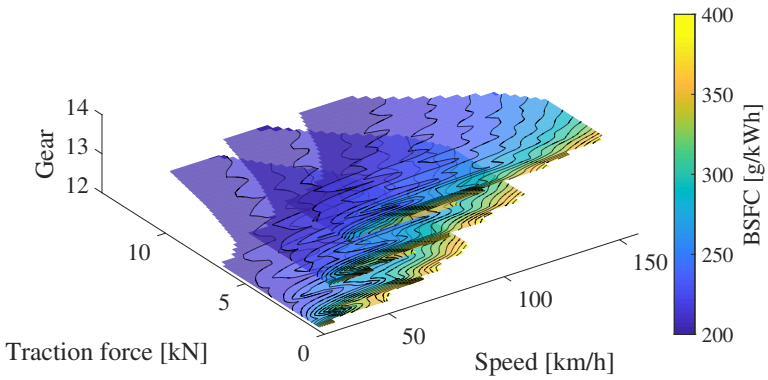

Figure 3.1: BSFC map for any feasible combination of speed and traction force for gears 12, 13 and 14.

minimum force at the wheels for a combination of speed and gear, as shown in Figure. 3.3. The goal is to use these units, and thus avoid wear of the service brakes. If the total negative demanded force is higher than the minimum negative additional force, the highest possible gear is selected, which avoids unnecessary down-shifting. On the other hand, if total demanded force is lower than the minimum negative additional force, the lowest possible gear is selected, since it provides the most possible negative additional force and thus reduces the need for using the service brakes.

A similar procedure can be adopted by minimising energy consumption of an electric vehicle, although in this thesis we consider only a single-gear-transmission EV. For more details about the offline gear optimisation, see Paper B.

Dynamic nonlinear programming

After gear map is optimised offline, the remaining problem is a smooth NLP that looks exactly as in problem (3.1), but with a reduced input vector, as optimal gear can be derived later, after the optimal vehicle speed and traction force are computed. The problem includes a modified set $\mathcal{U}$, where integer subsets have been removed by embedding constraints from the offline optimised gear map. The objective function of the NLP is the energy consumption, computed as an aggregation of the internal power on the wheels side of the vehicle, appended by the total travel time that is adjusted by a penalty factor.

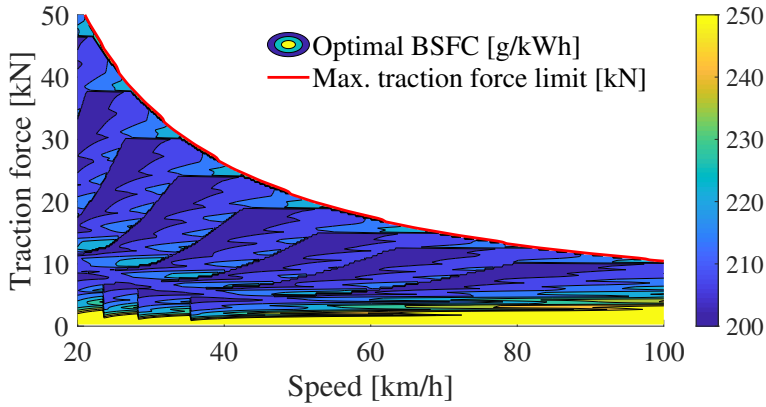

Figure 3.2: Offline-optimised BSFC map with maximum traction force limit. The map is shown for the speed range of 20-100 km.

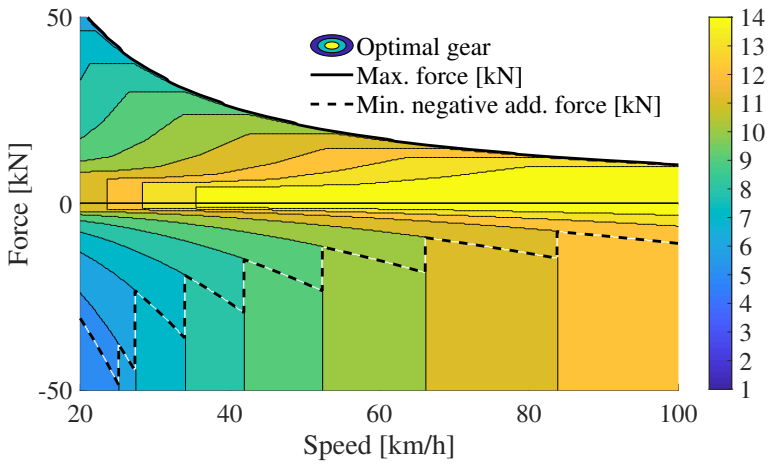

Figure 3.3: Offline-optimised gear map together with maximum traction force and minimum negative additional force limits. The map is shown for the speed range of 20-100 km.

In the following, modelling procedures of the speed limits, traction force limits and internal power are described, which help the top-level task to be solved efficiently.

Maximum total speed limit for a given pair of travel distance and time of day, is computed as minimum value of the maximum legal speed limit, $v_{\max}^{\mathrm{lg}}$, and maximum dynamic speed limit, $v_{\max}^{\mathrm{dyn}}$, as

$$v_{\max}(s,t) = \min\left(v_{\max}^{\mathrm{lg}}(s), v_{\max}^{\mathrm{dyn}}(s,t)\right). \tag{3.2}$$

The maximum legal speed limit can generally change abruptly for different segments of the driving road, see Figure. 3.4(a). However, the dynamic speed limits generally vary smoothly in terms of s and t, see Figure. 3.4(b), since there is no instantaneous change in traffic flow neither in terms of s and nor in terms of t. Thus, the maximum dynamic speed limit is modelled by a smooth function in terms of t. As for an example, a sum of sigmoidal functions in terms of time of day is chosen as the smooth function in Paper A, which gives the flexibility to model flat regions, as well as steep and shallow transitions as shown in Figure. 3.4(b).

The original maximum traction force limit for the CVs is computed as the maximum force at the wheels for any feasible combination of speed and gear. As depicted in Figure. 3.5, the original maximum force for the CVs and force limits for the EVs are generally piece-wise smooth curves. Thus, they have been modelled as piece-wise functions, where each of the pieces is a smooth function, see Figure. 3.5. Moreover, the internal power has been modelled as a function of state variables and control inputs, as for e.g. it is presented in Paper A. Several other polynomials are also used for modelling the internal power in the technical literature, see [18] and the references therein.

Selected results

Here, selected simulation results about the logistics planner's impact on optimal coordination of the vehicle mission are presented. To this end, an EV is driving in a 100 km long hilly terrain, as illustrated in Figure. 2.3(b), subject to a legal speed limit of 90 km/h. For pedagogical purposes, a simple scenario is considered with a single traffic jam, occurring at about 35 km, see Figure. 3.7. The traffic jam imposes dynamic speed limits, which depending on the time of the day, may constrain EV speed down to 30 km/h. Also, the

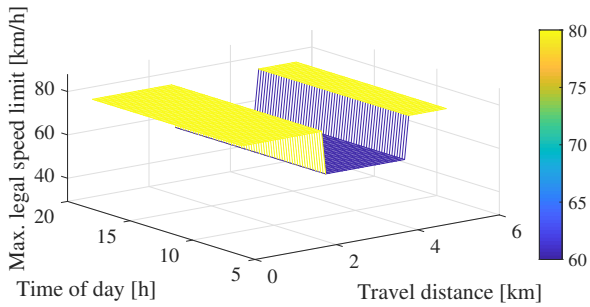

(a) Maximum dynamic speed limit.

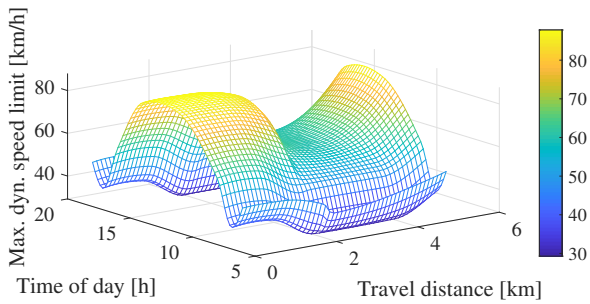

(b) Maximum legal speed limit.

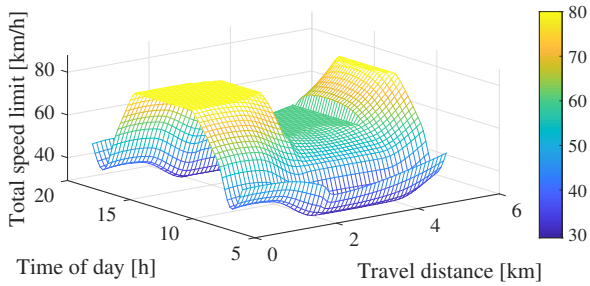

(c) Total speed limit as a minimum of legal and dynamic speed limit.

Figure 3.4: Maximum speed limits in terms of travel distance and time of day. The legal speed limits can change abruptly in terms of travel distance, however dynamic speed limits vary smoothly in terms of travel distance and time of day.

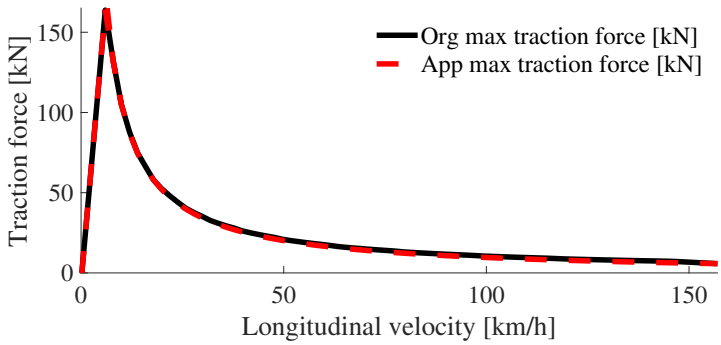

(a) Original and approximated maximum traction force limit of CV.

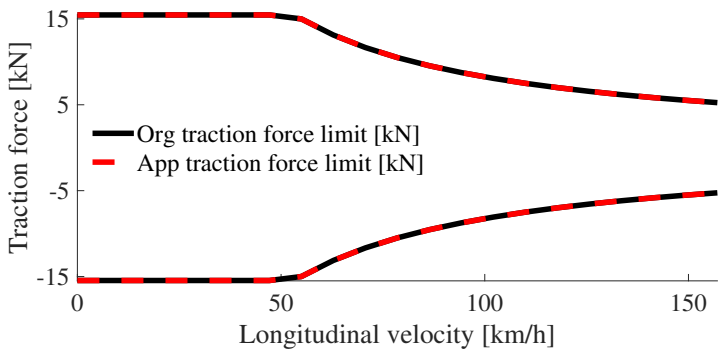

(b) Original and approximated traction force limits of EV.

Figure 3.5: Original and approximated actuator traction force limits. The traction force limits are approximated by piece-wise smooth functions.

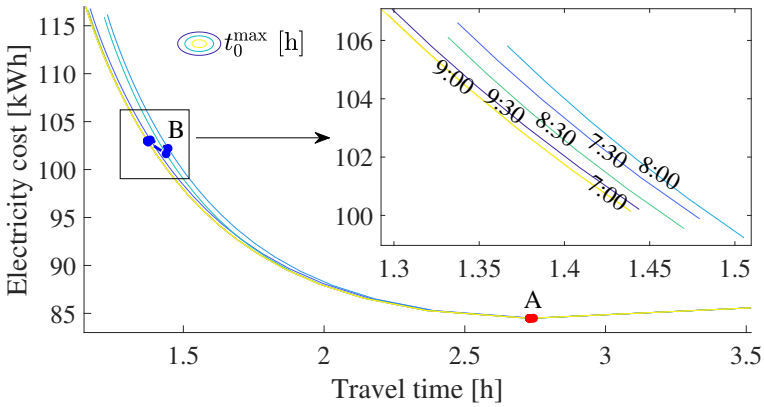

Figure 3.6: Contour plot of upper bound on each half-hour start time interval for a given pair of travel time and electricity use.

travel time at initial position of the route is not fixed, but is allowed to vary within a half-hour interval. Final travel time is kept free. The NLP is solved in Matlab with the solver IPOPT using the open source optimisation tool CasADi [24]. For more details about problem discretization, and vehicle and simulation parameters, see Paper A.

Energy efficiency versus travel time

Penalising total travel time in (3.1a) strongly influences the energy consumption. To investigate this, the NLP (3.1) is solved for a wide range of the time penalty factor, where the mission start time is allowed to vary within half-hour time intervals starting from 6:30. Figure. 3.6 shows a contour plot of upper bound on each half-hour mission start time, $t_0^{\max}$, for a given combination of the consumed electrical energy and total travel time. It is observed that there is a trade-off between the electrical energy consumption and travel time, i.e. by increasing the penalty factor, the travel time decreases, but it leads to higher electricity use. Unsurprisingly, the curves of electricity use versus travel time overlap for the start time intervals of 6:30-7:00 and 9:00-9:30, since the vehicle never encounters the traffic jam in either cases. The demonstrated profile in Figure. 3.6, provides promising information for e.g. logistics service managers, who have wide range of choices to customise the vehicle's mission. In this profile, the region A corresponds to a case with zero time penalty

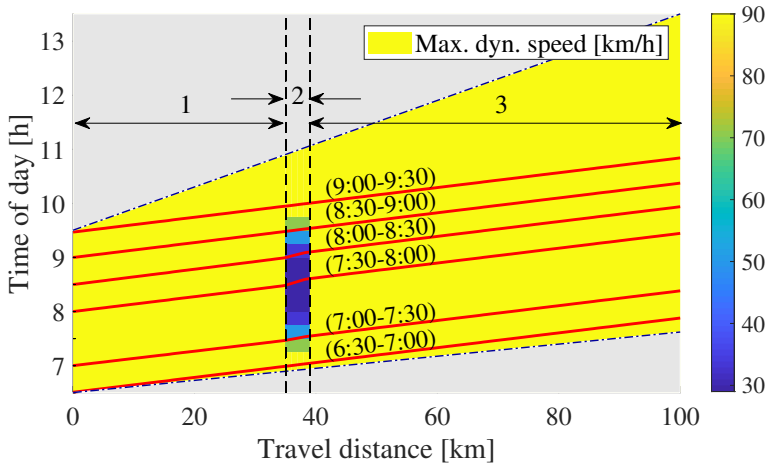

Figure 3.7: A map of maximum dynamic speed limit in terms of travel distance and time of day, together with optimal time trajectories for each mission start time interval; corresponding to region B.

factor, i.e. the most energy efficient driving. By letting the penalty factor be negative, it is possible to further increase travel time, which will actually cause increase in energy consumption. This implies that there is a low speed threshold, here about 35 km/h, below which the benefit of reduced air drag is negated by the increased time of accumulating powertrain losses.

Optimal mission start time

Region B in Figure. 3.6 corresponds to a positive penalty factor that results in keeping an average cruising speed of about $v_{cru} = 75$ km/h when traffic jam is avoided. Optimal time trajectory for the region B, for each half-hour interval of the mission start time, is depicted in Figure. 3.7, where the gray areas correspond to infeasible regions. It is observed that by applying the proposed algorithm, the vehicle tries to avoid the low speed regions. The travel distance in Figure. 3.7 is divided into three segments; (1): before traffic congestion, (2): during traffic congestion and (3): after traffic congestion. By comparing the results of the intervals 6:30-7:00 and 7:30-8:00, travel time is reduced by 5.5 %, when the mission starts at 6:30 instead of 8:00. For detailed results see Paper A.

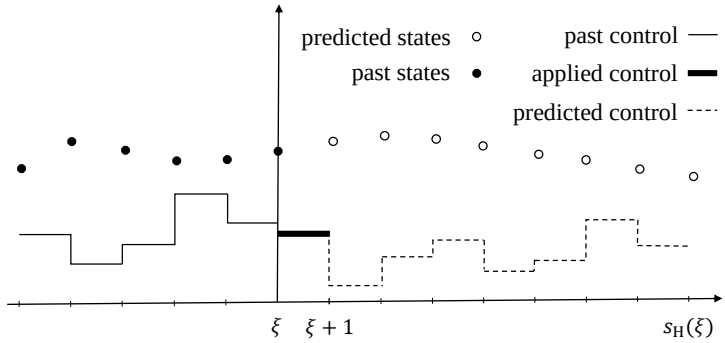

Figure 3.8: Concept of a model predictive controller in discrete domain, where ζ is current instance and s_H is prediction horizon length.

3.3 Eco-driving supervisor

The eco-driving supervisor utilises the calculated optimal mission start and/or finish time by the logistics planner, in order to provide the vehicle's energy-efficient drive with the ability of anticipating disturbances and future events. In this section, the problem formulation and the proposed computationally efficient algorithm for designing the eco-driving supervisor are explained. Also, selected simulation results about the trade-off between energy efficiency and driver comfort, disturbance rejection and computation time are presented.

Problem formulation

Here, the eco-driving supervision problem is formulated as an OCP in MPC fashion that allows horizons to cover the entire route. MPC is an online-capable framework that iteratively solves (3.1). The main advantage of MPC is that it engages future instances in optimising the current instance. In other words, a finite horizon of instances is optimised, but only the optimal solution of current instance is implemented. This process repeatedly continues up to the end of the horizon. Thus, MPC is able to anticipate future events, e.g. disturbances, and can take appropriate control action accordingly. The concept of MPC in discrete domain is demonstrated in Figure. 3.8.

As computational resources are always limited, we impose an upper bound

on horizon length, s_{Hmax}, hopefully in the range of hundreds of kilometers. Thus, the eco-driving supervision OCP can be solved in a moving horizon MPC (MHMPC) framework if $s_{\mathrm{Hmax}} < \mathrm{s_f}$, or in a shrinking horizon MPC (SHMPC) framework if $s_{\mathrm{Hmax}} \geq \mathrm{s_f}$. The optimisation variables are predicted at samples $s \in [\zeta, \zeta + s_{\mathrm{H}}]$, given information of the actual vehicle's states at ζ. Thus, the actual horizon length can be computed as

$$s_{\mathrm{H}}(\zeta) = \min\{s_{\mathrm{Hmax}}, \mathrm{s_f} - \zeta\}. \tag{3.3}$$

The problem can now be summarised as follows

$$\min_{\mathbf{u}\in\mathcal{U}} \quad S(\mathbf{x}(s_{\mathrm{H}}|\zeta), s_{\mathrm{H}}) + \int_{\zeta+\mathrm{s_0}}^{\zeta+s_{\mathrm{H}}(\zeta)} V(\mathbf{x}(s|\zeta), \mathbf{u}(s|\zeta), s)\mathrm{d}s \tag{3.4a}$$

subject to:

$$\frac{\mathrm{d}\mathbf{x}(s|\zeta)}{\mathrm{d}s} = F(\mathbf{x}(s|\zeta), \mathbf{u}(s|\zeta), s) \tag{3.4b}$$

$$G(\mathbf{x}(s|\zeta), \mathbf{u}(s|\zeta), s) \leq 0 \tag{3.4c}$$

$$\mathbf{x}(\mathrm{s_0}|\zeta) \in \mathcal{X}_0(\zeta) \tag{3.4d}$$

$$\mathbf{x}(s|\zeta) \in \mathcal{X}(\zeta) \tag{3.4e}$$

$$\mathbf{x}(\mathrm{s_f}|\zeta) \in \mathcal{X}_{\mathrm{f}}(\zeta) \tag{3.4f}$$

$$\mathbf{u}(s|\zeta) \in \mathcal{U}(\zeta). \tag{3.4g}$$

The full statements of problem (3.4) for CVs and EVs are given in Paper B, in which travel time, kinetic energy and acceleration are real-valued state variables, jerk and service braking force are real-valued control inputs, and traction force is an output variable. In CVs, gear is an integer control input. The problem (3.4) is generally a non-convex MINLP if the set $\mathcal{U}$, for e.g. in CVs; otherwise, it is simply an NLP.

Methods for solving the eco-driving problem

Problems, such as the MINLP (3.4), have been addressed in literature by different methods. DP [21] is the most commonly used algorithm to optimise the eco-driving problem due to its potential to guarantee global optimum for non-convex, nonlinear and mixed-integer optimisation problems [16], [22], [25]–[28]. Fuel-optimal look-ahead control strategies have been proposed in

[16] and [25] using DP, where in addition to optimising velocity, optimal gear shifting of conventional trucks is also investigated. Furthermore, a DP-based method is applied in [26] to minimise the energy consumption in fully electric vehicles (EVs) by optimising vehicle speed on short-range trips, e.g. driving between two consecutive traffic lights. A combined energy management and eco-driving approach using discrete DP is devised in [27] for hybrid electric vehicles (HEVs) driving over limited horizons, where the velocity profile is allowed to be optimised to further enhance fuel efficiency. Despite the promising contributions in solving optimal control problems, DP-based methods suffer from the *curse of dimensionality*, which denotes to a fact that computational time increases exponentially with the number of state variables and control signals, [21]. Several ways have been taken to decrease computational effort, for example by limiting the look-ahead horizon of cruise controllers for HEVs. At the current state, real-time capable DP-based control can only be applied for short prediction horizon scenarios of HEVs [22].

Other approaches focus on simplifying the powertrain model, by e.g. using a simplified internal combustion engine (ICE) model or discarding system states, such as travel time, ICE on/off and gear [28].

For high-dimensional optimisation problems, e.g. optimal control of HEVs with more energy states, several alternative approaches have been proposed. In [29] a mixed-integer quadratic program (MIQP) [30] has been applied for power allocation of HEVs. A way to diminish computational complexity of the high-dimensional problems is by adjoining system dynamics to the cost function and neglecting constraints on state variables, as shown in [31]–[33]. In [33] Pontryagin's maximum principle (PMP) [34] has been applied to optimise longitudinal velocity, gear selection and energy use of HEVs, where integer state variables have been neglected. Furthermore, in [10], [35] minimisation of energy consumption using PMP and considering varying speed requirements has been studied. Although PMP-based methods are computationally efficient for optimal velocity problems over long look-ahead horizons, they do not provide the same computational advantage for problems where state variables often activate their bounds. This is especially relevant for single shooting methods used for solving two-point boundary value problems (TPBVPs), as in e.g. [36]. A TPBVP refers to a system of ordinary differential equations, where the solution and derivatives are given at just two points.

Another portion of the conducted research benefits from the combination

of DP and other methods. Such approaches have been proposed by [18], [37]–[39], where real-valued decisions, e.g., planing optimal velocity, are made by sequential convex optimisation, while integer decisions are taken by DP. These strategies have also been shown to be effective when considering surrounding traffic [38], or cooperative energy management of multiple vehicles [18], [39]. In [40] a PMP-DP method has been proposed to solve the optimal control of longitudinal velocity, battery energy, gear selection and ICE on/off state. However, the computational effort of the control algorithms is still highly susceptible to long horizon lengths and high update frequencies.

The synergy among different optimisation methods is generally performed by splitting the problem into sub-problems arranged into multi-level or bi-level control architectures, where different tasks are delegated to distinct layers based on horizon length, time constants, sampling interval and update frequency. To this end, multi-level and bi-level MPC algorithms have been proposed for CVs, [41], and HEVs, [42]–[45], respectively. The multi-level architectures allow solving computationally intensive sub-problems, e.g. mixed-integer programs. Such programs are typically solved by an MPC, tracking a certain reference or a target state, typically over look-ahead horizons of several of kilometers. Even though such horizons may appear long, in this thesis problems are addressed that are naturally defined for even longer horizons.

The proposed computationally efficient algorithm

Here, we propose an algorithm to solve the eco-driving problem (3.4), with a significant boost in computational efficiency. This algorithm consists of: 1) gear optimisation using problem decomposition into two sub-problems formulated as a bi-level program as described in Section. 3.2; 2) a combination of an indirect PMP solution and a direct nonlinear programming for reducing the number of states in top-level dynamic sub problem of the bi-level program; 3) a real-time iteration (RTI) sequential quadratic programming (SQP), which allows a single quadratic program (QP) to be solved in a single MPC update.

Having the gear optimisation been performed offline as a bottom-level task of a bi-level program, the top-level task represents a dynamic NLP. Let the Hamiltonian function of this NLP be defined as

$$\mathcal{H}(s, \mathbf{x}, \mathbf{u}_{\mathrm{r}}, \lambda) = V(\mathbf{x}(s), \mathbf{u}_{\mathrm{r}}(s), s) + \lambda^T F(\mathbf{x}(s), \mathbf{u}_{\mathrm{r}}(s), s), \tag{3.5}$$

where $\mathbf{u}_\mathrm{r} = \begin{bmatrix} j & F_\mathrm{brk} \end{bmatrix}^\top$ is the top-level real-valued decision vector. Also, λ denotes the vector of Lagrange multipliers known as costate vector to the state vector $\mathbf{x}$. The Hamiltonian (3.5) for (3.4) is not an explicit function of travel time as it is discussed in Paper B, thus optimal time costate, λ_t^*, i.e. the value for λ_t that satisfies maximum travel time constraint, is a constant value, i.e.

$$\lambda'^*_\mathrm{t}(s) = -\left(\frac{\partial \mathcal{H}(\cdot)}{\partial t}\right)^* = 0. \tag{3.6}$$

Furthermore, the travel time is a strictly monotonically increasing function that may activate the maximum travel time constraint only at the final instance. Consequently, if λ_t^* is known, it will be possible to adjoin the nonlinear dynamics on travel time to the objective function. The optimal λ_t^* can be calculated by solving a TPBVP. To do so, it is considered that the optimal energy consumption corresponds in general to driving slow, so it can be assumed that the vehicle will use the entire travel time, i.e. $t^*(\lambda_\mathrm{t}, s_\mathrm{H}) \approx t_\mathrm{H}$, where t^* is optimised travel time and t_H is desired travel time at final position of the horizon, obtained by the logistic planner. Thus, it is possible to try different values for λ_t and then use search methods, e.g. Newton or bisection, that minimises the cost

$$\min_{\lambda_\mathrm{t}} ||t^*(\lambda_\mathrm{t}, s_\mathrm{H}|\zeta) - t_\mathrm{H}(\zeta)|| \tag{3.7}$$

where $||\cdot||$ may indicate any norm. For more details on finding λ_t^* see Paper B.

Having λ^* been adjoined to the objective function, the resultant top-level task NLP can be solved using SQP [46]. SQP is an iterative method for solving NLPs, in which the objective function and the constraints are twice continuously differentiable. This method solves a sequence of quadratic optimization sub-problems, i.e. with quadratic model of the objective function and linearized constraints. This thesis proposes an algorithm for solving the top-level task NLP with the term adjoined to its objective, which consists of three nested loops as illustrated in Figure. 3.9(a). The outermost loop updates the MPC horizon, the middle loop finds the optimal value for the time costate and the innermost loop sequentially solves a QP in order to find the solution of the dynamic problem for a given value of λ_t. The procedure is still computationally inefficient, as it requires solving multiple QPs for given

multiple λ_t values in each MPC update. The goal in order to improve computational efficiency, is to eliminate the inner most loops in Figure. 3.9(a), and for a given λ_t, solve only a single QP in each MPC update, as illustrated in Figure. 3.9(b).

For an SHMPC implementation of the top-level NLP and for a given λ_t, if predicted disturbances do not change and there is no miss-match between the control and plant model, then

$$t^*(\lambda_t, s_H|\zeta) = t^*(\lambda_t, s_H|\zeta + \delta\zeta), \quad \forall \delta\zeta \in [0, s_f - \zeta], \tag{3.8}$$

holds, i.e. the optimal travel time at the end of the horizon does not change for different SHMPC updates. The proof follows directly from Bellman's principle of optimality, i.e. *any tail of an optimal trajectory is an optimal solution as well* [21]. Thus, validly the middle loop for an SHMPC is removed, i.e. the time costate update is spread over the MPC loop.

For an MHMPC, the expression (3.8) does not hold even if disturbances are predicted exactly and there is no model miss-match. This is because new information is added as the prediction horizon moves forward at each MPC update. However, if the prediction horizon is much longer than the interval between two consecutive updates, then for different ζ, it can be assumed

$$t^*(\lambda_t, s_H|\zeta) - t_H(\zeta) \approx t^*(\lambda_t, s_H|\zeta^+) - t_H(\zeta^+) \tag{3.9}$$

where ζ^+ is the instance of the MHMPC update following that at ζ. Figure 3.10 demonstrates the overlapped curves of the final time difference versus the time costate for a CV and an EV, where $\zeta = 0\,\mathrm{m}$ and $\zeta^+ = 300\,\mathrm{m}$. Thus, it is also possible for an MHMPC to update the time costate over the MPC loop. For more details on how the time costate can be updated in MPC framework, see Paper B.

RTI [47] facilitates the SQP loop's removal, where the idea is to solve only a single QP per an MPC update, without waiting for a full convergence. The obtained solution is possibly sub-optimal, but due to the contractivity of the RTI scheme as shown in [48], the real-time iterates quickly approach the optimal solution during the runtime of the process. As the SQP is stopped prematurely, it is important to show that the obtained solution by solving a single QP is feasible in the original NLP. Feasibility can be guaranteed if the domain of the QP, obtained by linearizing nonlinear constraints is inner

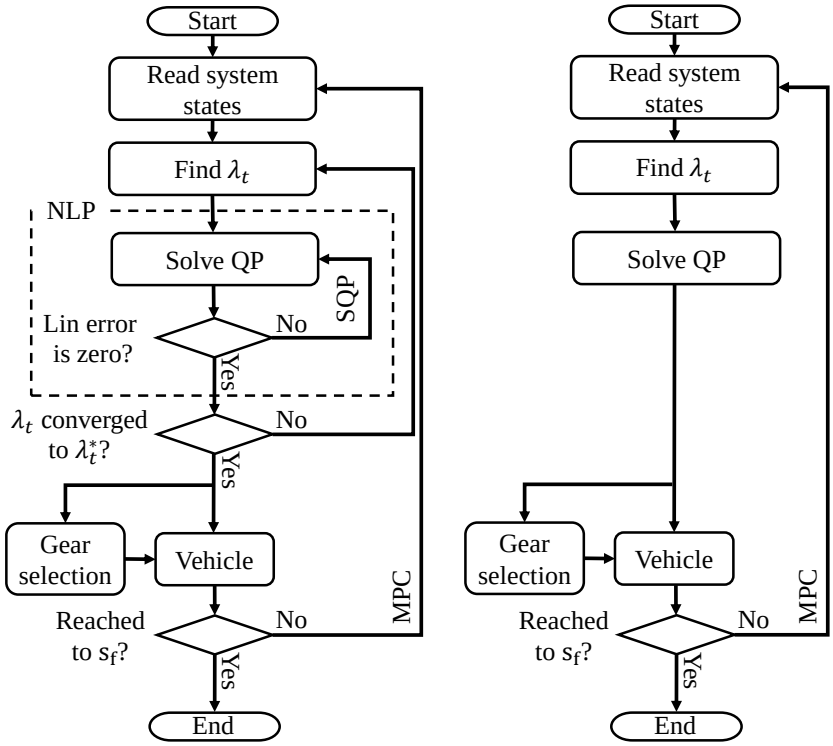

(a) With three nested loops.

(b) Without two innermost loops to solve NLP using SQP, and to find λ.

Figure 3.9: Flowchart of the proposed algorithm to solve mixed-integer NLP in MPC framework, (a) with three nested loops, innermost loop to solve NLP using SQP and middle loop to find λ^*; (b) using real-time iterations SQP, which solves a single QP in each MPC update.

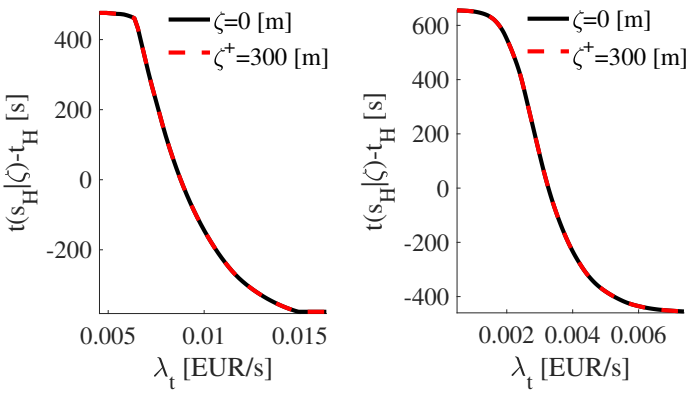

(a) For CV case study.

(b) For EV case study.

Figure 3.10: Difference between calculated time at the end of horizon and the desired maximum time for varying time costate using MHMPC scheme, where $\zeta = 0\,\text{m}$ and $\zeta^+ = 300\,\text{m}$. Overlap of the curves for different ζ values shows that λ_t can be evaluated only once per each MPC update, rather than waiting for a full convergence.

approximation of the feasible set of the NLP. To gain more insight on feasibility of the presented method for CV and EV case studies see Paper B.

Selected results

Here, selected simulation results about the eco-driving supervisor's impact on optimal coordination of the vehicle mission are presented. To this end, the proposed computationally efficient algorithm has been applied to CV and EV case studies driving in 118 km long road from Södertälje to Norrköping in Sweden. For most of the simulation the sampling interval is kept at about 250 m, unless stated otherwise. Thus, the top-level NLP is solved in an SHMPC framework, where travel time at the final position (end of the route) is upper bounded. For more details about problem discretization, and vehicle and simulation parameters see Paper B.

Energy efficiency versus driver comfort

To study the cost components, i.e. energy cost and the cost due to penalising driver discomfort, we investigate two case studies: in Case 1, i.e. performance drive, the driver discomfort is not penalised; and in Case 2, i.e. comfortable drive, penalising the vehicle jerk leads to obtain a smooth velocity profile. As an index to measure the drive comfort, the root mean square (RMS) value of jerk

$$j_{\mathrm{RMS}} = \sqrt{\frac{1}{\mathrm{s_f}} \int_0^{\mathrm{s_f}} j^2(s) \mathrm{d}s} \tag{3.10}$$

is used. Note that we have observed the smooth speed profile could be achieved by only penalising jerk, thus there is no penalty coefficient on the acceleration for either of the cases.

There is a trade-off between the energy cost and comfort, i.e. lower values of RMS jerk yield higher energy cost, see Figure. 3.11(a) and Figure. 3.11(b) for such trade-off for the CV and the EV respectively. Thus, vehicle manufacturers have wide range of choice to tailor the vehicle's performance for a desired energy use and comfort. The driver discomfort in Case 2 is penalised in a way that the RMS jerk is equal to $0.0027\,\mathrm{m/s^3}$ for the CV and the EV.

Disturbance rejection

The convergence curve of the time costate versus shrinking prediction horizon length is shown in Figure. 3.12. According to the algorithm given in Paper A, the time costate is updated once per each MPC stage rather than waiting for the full costate convergence. It can be observed that after few initial MPC stages, the time costate converges to its optimum value. The disturbance rejection properties of the algorithm are verified in Figure. 3.12. At the prediction horizon of 85 km, maximum travel time changes due to e.g. traffic congestion. It can be seen in Figure. 3.12 that the travel time costate converges to its new value, which leads the vehicle to arrive to the final position within the updated maximum travel time.

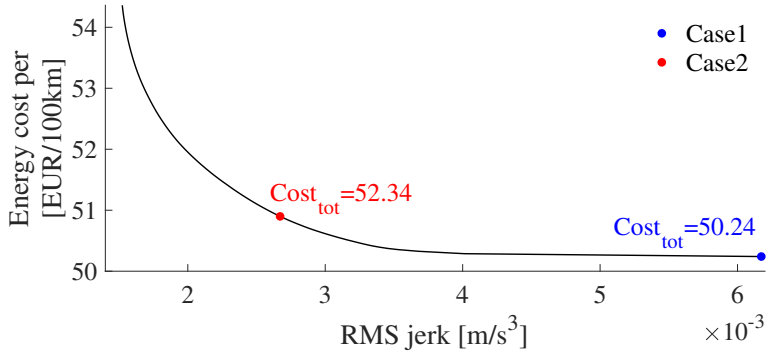

(a) Fuel cost vs. RMS jerk.

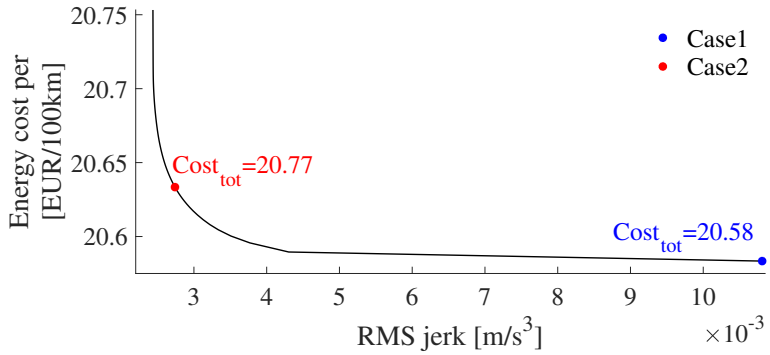

(b) Electricity cost vs. RMS jerk.

Figure 3.11: Comparison between non-approximate original problem with approximate problem. Energy cost investigation for different jerk penalty factors. For the large penalty factors, RMS jerk is saturated.

Computation time

The computation time profile for various sampling intervals is depicted in Figure. 3.13 using HPIPM [49], where the entire route, 118 km, is considered as the prediction horizon. The optimisation was run on a laptop PC with 6600K CPU at 2.81GHz and 16GB RAM. The trend is that as the number of samples increases, the computation time also increases. For real-time applications, it is preferable to have small sampling interval, however the information on the topography should not be lost. The corresponding computation time for

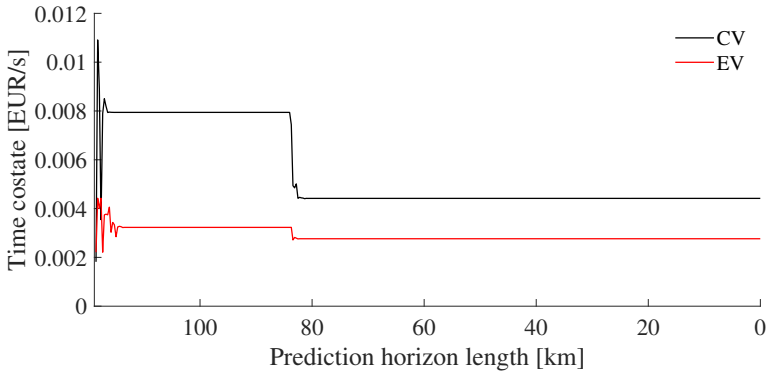

Figure 3.12: Travel time costate vs. prediction horizon length. The costate converges after few MPC updates, even after disturbance is introduced (at horizon length of 85 km) by suddenly increasing maximum travel time, e.g. due to traffic congestion.

solving the top-level task NLP with the sampling interval of about 250 m is less than 20 ms, which is considerably low value for a horizon of 118 km.

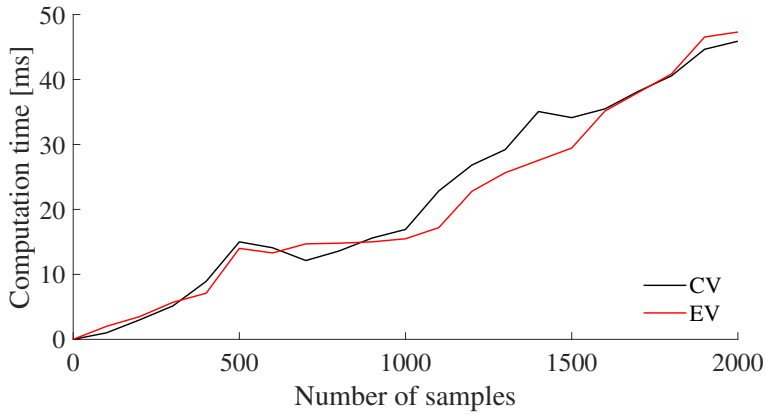

Figure 3.13: Computation time vs. prediction horizon length using HPIPM for various resolutions of the prediction horizon. The computation time increases linearly with the number of samples.

CHAPTER 4

Summary of included papers

This chapter provides a summary of the included papers.

4.1 Paper A

Ahad Hamednia, Nikolce Murgovski, and Jonas Fredriksson
Time optimal and eco-driving mission planning under traffic constraints
Accepted in 23rd *IEEE International Conference on Intelligent Transportation Systems (ITSC)* .

This paper addresses logistics planning problem which aims at controlling the mission start time and velocity profile of an electric vehicle driving in a hilly terrain, subject to legal and dynamic speed limits imposed by traffic congestion. To this end, an NLP is formulated, where total energy consumption is minimised and the travel time is adjusted by a penalty factor, subject to road and traffic information. Total speed limits have been calculated as the minimum value of the legal and dynamic speed limits. The legal speed limits can change abruptly for different segments of the travelled distance. However, considering the smooth variations of the dynamic speed limits in terms of travel distance and time of day, they have been modelled by smooth

sigmoidal functions, which gives the flexibility to model flat regions, as well as steep and shallow transitions for combinations of travel distance and time of day. The traction force limits at the wheels are modelled as piece-wise functions, which sufficiently describe the original piece-wise smooth traction force limits. Moreover, the electric battery power has been modelled as a function of state variables and control inputs. With these modeling procedures, the NLP is solved in a computationally efficient manner. The trade-off between energy consumption and travel time has also been investigated, while allowing a flexibility in starting time and a certain variation of vehicle speed around an average. It is observed that total travel time is reduced up to 5.5% by adjusting the mission start time, when keeping an average cruising speed of about 75 km/h.

4.2 Paper B

Ahad Hamednia, Nalin K.Sharma, Nikolce Murgovski, Jonas Fredriksson
Computationally efficient algorithm for eco-driving over long look-ahead horizons
Submitted to IEEE Transactions on Intelligent Transportation Systems in Jan. 2020 .

This paper addresses designing an eco-driving supervisor, which aims at obtaining a velocity profile by optimising energy consumption. To do so, an online-capable algorithm has been developed in an MPC framework for long prediction horizons of up to hundreds of kilometers. The controller is capable of using communication and prediction abilities of modern transportation to anticipate future events and disturbances. This implies that the controller is able to re-optimise the velocity profile online, considering possible changes in the condition of the vehicle and/or the driving road. As a central concern for such online-implementable supervisor, the computational efficiency has been considered by developing a bi-level algorithm where integer variable, i.e. gear, is decoupled from the real-valued variables. In the bottom level, the optimal gear map is derived in a way that the total energy consumption is minimised. In the top level, the remaining nonlinear problem has been solved by gaining insights from PMP conditions for optimality and real-time iterations SQP. To provide more comfortable way of driving, acceleration and

jerk of the vehicle have been appended to the top level's objective function. The proposed algorithm has been applied to a CV and an EV. This algorithm is able to solve the optimisation in a very short amount of time, i.e. for a horizon length of 118 km with the sampling interval kept at about 250 m, the computation time is less than 20 ms. Compared to standard cruise control, the energy savings of using this algorithm is up to 11.6 %. Also, Pareto frontier illustrating the trade-off between energy efficiency and driver comfort has been presented, which provides valuable information for vehicle manufacturers to customise the vehicle's performance for a desired energy use and comfort.

CHAPTER 5

Conclusion and future work

In this chapter, the thesis is concluded by addressing the research goals and possible directions for future research.

5.1 Discussion and conclusion

Automotive industry leaders and transport service providers constantly consider reducing ever-growing energy consumption and CO_2 emissions by improving transport efficiency and not losing logistics performance. This thesis has investigated how these goals are achievable by optimal planning of the transport mission, which is characterized as optimising the start and/or finish time of vehicle driving mission and increasing the tank-to-meter efficiency. It has been shown that optimising the vehicle's longitudinal drive has a significant impact on enhancing the tank-to-meter efficiency. Thus, the core idea has been introduced as formulating a driving mission as an optimal control problem. To do so, several factors have been considered that strongly influence solving the optimal control problem, such as speed limits, travel time, driver comfort, and future events and disturbances.

In order to increase feasibility in realistic driving situations, the control

problem incorporates speed limits that include not only legal, but also dynamic limits using the information about the road and traffic available. Surrounding traffic can impose such dynamic constraints on the vehicle speed due to presence of e.g. traffic lights, intersections, ramps and junctions. Furthermore, the trade-offs between the energy efficiency and travel time, and between the energy efficiency and driver comfort, are considered in the control problem, i.e. lower energy cost generally yields non-smooth saw-tooth shape velocity profiles and longer travel times. Moreover, predictive controllers are developed that employ communication and prediction abilities of modern transportation to anticipate future events and disturbances.

To improve the transport efficiency and not lose the logistics performance, with all above-mentioned factors considered, a mission planner with a bi-layer structure has been proposed. The mission planner consists of a *logistics planner* as its top level and an *eco-driving supervisor* as its bottom level. The logistics planner provides the optimal mission start and/or finish time by offline optimising energy consumption and travel time. It also provides a reference speed profile and, thus, an estimate of the time for reaching sparsely assigned positions along the route, at intervals of about 250 m. To do so, the logistics planner uses road information as well as traffic situation characterized as a map of total maximum speed limits given in terms of travel distance and time of day. Here, the trade-off between energy efficiency and total travel time has been investigated, which offers the logistics service provider a valuable information to tailor the vehicle's trip in terms of energy costs and delivery service. It is observed that total travel time is reduced up to 5.5 % by adjusting the mission start time, when keeping an average cruising speed of about 75 km/h.

In cases that the traffic situation and/or the driving road change unpredictably for any reason, an algorithm is needed to generate a valid solution by solving the optimal control problem, and consequently should be real-time implementable. To achieve this, an online-capable algorithm for the eco-driving supervisor has been developed in an MPC fashion, subject to the pre-optimised mission start and/or finish time, and the reference velocity profile. It obtains a velocity profile by optimising the energy consumption and penalising driver discomfort. The algorithm is able to solve the optimisation in a very short amount of time, i.e. for a horizon length of 118 km with the sampling interval kept at about 250 m, the computation time is less than 20 ms. For on-line applications, such small computation time can strongly enhance the optimality,

since the suggested optimal state of vehicle can be updated more frequently. Also, this algorithm is applicable to offline analysis of multi-path problems, where the optimal path of the driving vehicle in terms of energy consumption can be obtained by iterativelly solving the eco-driving problem within a small amount of time. The proposed algorithm has been applied to CV and EV, where compared to standard cruise control, the energy savings are up to 11.6 %. Also, Pareto frontier describing the trade-off between energy efficiency and comfortable driving has been presented. This offers a wide range of choice for vehicle manufacturers to customise the vehicle's performance for a desired energy use and comfort.

Apart from the attached two papers, the mission planning problem has also been investigated for a vehicle driving behind a slow moving leading vehicle that does not communicate its future speed plan, see Paper D and Paper E. To do so, a leading vehicle observer has been designed to estimate maximum force to mass ratio of the leading vehicle and subsequently predict its future speed. Then the predicted speed is utilised by the ego vehicle to optimally plan its energy-efficient way of driving. Thus, unnecessary braking and usage of traction force can be avoided, and the aerodynamic drag can be reduced by keeping a short time headway. The proposed algorithm provides fuel savings of up to 8 % compared to a standard cruise control. This algorithm has also been applied to the traffic light scenario, where position of the traffic light and the timing of its signals are considered to be known, see Paper D.

5.2 Future work

In this section, several possible directions for future research on the topic mission planning are presented.

Optimal mission planning of HEVs

The current developed mission planner can also be extended to be applicable to HEVs. To this end, an optimisation problem can be formulated, which aims at planning optimal velocity trajectory for the entire route, in a way that total energy consumption is minimised, travel time is upper bounded, and battery SoC at final position is specified. Having the fixed travel time and the battery SoC at the end of the route, indicate that the mission planning of HEVs is

also a long-horizon type of problem. Thus, the problem can be treated by using an SHMPC considering the information to the end of the driving route per each MPC update. This results in gradual battery depletion and reaching the desired battery SoC at end of the route. Note that an important step in designing the mission planner for HEVs is the offline gear optimisation, where both fuel and electricity consumption are required to be incorporated in finding the optimal gear map.

Optimal electricity charging coordination of electrified vehicles

The current developed mission planner can also be extended with a new functionality that optimally coordinates electricity charging of plug-in electrified vehicles (PEVs) for long look-ahead horizons, subject to road and traffic information and systems dynamics. A key factor is to incorporate uncertain information on electricity pricing that may vary from charger to charger and time of day, costs for overstay at charging locations and charging capabilities. When the uncertainties are bounded, robust MPC can be designed to guarantee that constraints on system states and control inputs are always respected. If the uncertainties are unbounded, stochastic MPC can be employed to ensure that constraints are satisfied on average or with a given probability. The main challenge in stochastic optimization over long horizons is in the development of efficient numerical methods to comply to the real-time requirements and limitations of computational units. Another crucial issue is to find a good balance between optimality, robustness and real-time computational feasibility. Thus, current investigations on mathematical transformations, such as bi-level formulation, variable changes and time-to-space coordinate transformation can be extended by studying implications on conservativeness, convexity, accuracy and optimality.

References

[1] I. T. Forum, *ITF Transport Outlook 2017*. 2017, p. 224.

[2] I. E. Agency, *World Energy Outlook 2015*. 2015, p. 600.

[3] D. Schrank, B. Eisele, and T. Lomax, "Tti's 2012 urban mobility report", *Texas A&M Transportation Institute. The Texas A&M University System*, vol. 4, 2012.

[4] C. Lee, Y. Kim, S. M. Jin, D. Kim, R. Maciejewski, D. Ebert, and S. Ko, "A visual analytics system for exploring, monitoring, and forecasting road traffic congestion", *IEEE transactions on visualization and computer graphics*, 2019.

[5] H. Aronsson and M. H. Brodin, "The environmental impact of changing logistics structures", *The international journal of logistics management*, 2006.

[6] A. Sciarretta, G. D. Nunzio, and L. L. Ojeda, "Optimal ecodriving control: Energy-efficient driving of road vehicles as an optimal control problem", *IEEE Control Systems Magazine*, vol. 35, no. 5, pp. 71–90, 2015.

[7] M. A. S. Kamal, M. Mukai, J. Murata, and T. Kawabe, "Model predictive control of vehicles on urban roads for improved fuel economy", *IEEE Transactions on control systems technology*, vol. 21, no. 3, pp. 831–841, 2012.

[8] M. Vajedi and N. L. Azad, "Ecological adaptive cruise controller for plug-in hybrid electric vehicles using nonlinear model predictive control", *IEEE Transactions on Intelligent Transportation Systems*, vol. 17, no. 1, pp. 113–122, 2015.

[9] Y. Luo, T. Chen, S. Zhang, and K. Li, "Intelligent hybrid electric vehicle acc with coordinated control of tracking ability, fuel economy, and ride comfort", *IEEE Transactions on Intelligent Transportation Systems*, vol. 16, no. 4, pp. 2303–2308, 2015.

[10] M. Held, O. Flärdh, and J. Mårtensson, "Optimal speed control of a heavy-duty vehicle in urban driving", *IEEE Transactions on Intelligent Transportation Systems*, vol. 20, no. 4, pp. 1562–1573, 2018.

[11] R. Basso, P. Lindroth, B. Kulcsár, and B. Egardt, "Traffic aware electric vehicle routing", in *2016 IEEE 19th International Conference on Intelligent Transportation Systems (ITSC)*, IEEE, 2016, pp. 416–421.

[12] A. Alam, B. Besselink, J. Mårtensson, and K. H. Johansson, "Heavy-duty vehicle platooning for sustainable freight transportation: A cooperative method to enhance safety and efficiency", *IEEE Control Systems Magazine*, vol. 35, no. 6, pp. 34–56, 2015.

[13] M. Gendreau, G. Ghiani, and E. Guerriero, "Time-dependent routing problems: A review", *Computers & operations research*, vol. 64, pp. 189–197, 2015.

[14] OECD, *Moving Freight with Better Trucks*. 2011, p. 360.

[15] J. N. Barkenbus, "Eco-driving: An overlooked climate change initiative", *Energy Policy*, vol. 38, no. 2, pp. 762–769, 2010.

[16] E. Hellström, M. Ivarsson, J. Åslund, and L. Nielsen, "Look-ahead control for heavy trucks to minimize trip time and fuel consumption", *Control Engineering Practice*, vol. 17, no. 2, pp. 245–254, 2009.

[17] B. Passenberg, P. Kock, and O. Stursberg, "Combined time and fuel optimal driving of trucks based on a hybrid model", in *European Control Conference*, Budapest, Hungary, 2009, pp. 4955–4960.

[18] N. Murgovski, B. Egardt, and M. Nilsson, "Cooperative energy management of automated vehicles", *Control Engineering Practice*, vol. 57, pp. 84–98, 2016.

[19] H. Rakha and R. K. Kamalanathsharma, "Eco-driving at signalized intersections using v2i communication", in *2011 14th international IEEE conference on intelligent transportation systems (ITSC)*, IEEE, 2011, pp. 341–346.

[20] G. Heppeler, M. Sonntag, and O. Sawodny, "Fuel efficiency analysis for simultaneous optimization of the velocity trajectory and the energy management in hybrid electric vehicles", *IFAC Proceedings Volumes*, vol. 47, no. 3, pp. 6612–6617, 2014.

[21] R. Bellman, *Dynamic Programming*. New Jersey: Princeton Univ Pr, 1957.

[22] H.-G. Wahl, K.-L. Bauer, F. Gauterin, and M. Holzäpfel, "A real-time capable enhanced dynamic programming approach for predictive optimal cruise control in hybrid electric vehicles", in *16th International IEEE Conference on Intelligent Transportation Systems (ITSC 2013)*, IEEE, 2013, pp. 1662–1667.

[23] J. F. Bard, *Practical bilevel optimization: algorithms and applications*. Springer Science & Business Media, 2013, vol. 30.

[24] J. A. Andersson, J. Gillis, G. Horn, J. B. Rawlings, and M. Diehl, "Casadi: A software framework for nonlinear optimization and optimal control", *Mathematical Programming Computation*, vol. 11, no. 1, pp. 1–36, 2019.

[25] E. Hellström, J. Åslund, and L. Nielsen, "Design of an efficient algorithm for fuel-optimal look-ahead control", *Control Engineering Practice*, vol. 18, no. 11, pp. 1318–1327, 2010.

[26] W. Dib, L. Serrao, and A. Sciarretta, "Optimal control to minimize trip time and energy consumption in electric vehicles", in *2011 IEEE Vehicle Power and Propulsion Conference*, IEEE, 2011, pp. 1–8.

[27] G. Heppeler, M. Sonntag, U. Wohlhaupter, and O. Sawodny, "Predictive planning of optimal velocity and state of charge trajectories for hybrid electric vehicles", *Control Engineering Practice*, vol. 61, pp. 229–243, 2016.

[28] L. Bühler, "Fuel-efficient platooning of heavy duty vehicles through road topography preview information", Master's thesis, KTH, Stockholm, Sweden, 2013.

[29] P. Themann, A. Zlocki, and L. Eckstein, "Energieeffiziente fahrzeuglängsführung durch v2x-kommunikation", in *Fahrerassistenzsysteme und Effiziente Antriebe*, W. Siebenpfeiffer, Ed. Wiesbaden: Springer Fachmedien Wiesbaden, 2015, pp. 27–33, ISBN: 978-3-658-08161-4.

[30] S. Boyd and L. Vandenberghe, *Convex Optimization*. Cambridge University Press, 2004.

[31] E. Hellström, J. Åslund, and L. Nielsen, "Management of kinetic and electric energy in heavy trucks", *SAE International Journal of Engines*, vol. 3, no. 1, pp. 1152–1163, 2010.

[32] T. van Keulen, B. de Jager, D. Foster, and M. Steinbuch, "Velocity trajectory optimization in hybrid electric trucks", in *American Control Conference*, Marriott Waterfront, Baltimore, MD, USA, 2010, pp. 5074–5079.

[33] T. van Keulen, B. de Jager, and M. Steinbuch, "Optimal trajectories for vehicles with energy recovery options", in *IFAC World Congress*, Milan, Italy, 2011, pp. 3831–3836.

[34] L. S. Pontryagin, V. G. Boltyanskii, R. V. Gamkrelidze, and E. F. Mishchenko, *The Mathematical Theory of Optimal Processes*. Interscience Publishers, 1962.

[35] M. Held, "Fuel-efficient look-ahead control for heavy-duty vehicles with varying velocity demands", PhD thesis, KTH Royal Institute of Technology, 2020.

[36] T. van Keulen, J. Gillot, B. de Jager, and M. Steinbuch, "Solution for state constrained optimal control problems applied to power split control for hybrid vehicles", *Automatica*, vol. 50, no. 1, pp. 187–192, 2014.

[37] L. Johannesson, N. Murgovski, E. Jonasson, J. Hellgren, and B. Egardt, "Predictive energy management of hybrid long-haul trucks", *Control Engineering Practice*, vol. 41, pp. 83–97, 2015.

[38] L. Johannesson, M. Nilsson, and N. Murgovski, "Look-ahead vehicle energy management with traffic predictions", in *IFAC Workshop on Engine and Powertrain Control, Simulation and Modeling (E-COSM)*, vol. 48, Columbus, Ohio, USA, 2015, pp. 244–251.

[39] M. Hovgard, O. Jonsson, N. Murgovski, M. Sanfridson, and J. Fredriksson, "Cooperative energy management of electrified vehicles on hilly roads", *Control Engineering Practice*, vol. 73, pp. 66–78, 2018.

[40] S. Uebel, N. Murgovski, C. Tempelhahn, and B. Bäker, "Optimal energy management and velocity control of hybrid electric vehicles", *IEEE Transactions on Vehicular Technology*, vol. 67, no. 1, pp. 327–337, 2017.

[41] L. Guo, H. Chen, Q. Liu, and B. Gao, "A computationally efficient and hierarchical control strategy for velocity optimization of on-road vehicles", *IEEE Transactions on Systems, Man, and Cybernetics: Systems*, vol. 49, no. 1, pp. 31–41, 2018.

[42] V. Turri, B. Besselink, and K. H. Johansson, "Cooperative look-ahead control for fuel-efficient and safe heavy-duty vehicle platooning", *IEEE Transactions on Control Systems Technology*, vol. 25, no. 1, pp. 12–28, 2016.

[43] L. Guo, B. Gao, Y. Gao, and H. Chen, "Optimal energy management for hevs in eco-driving applications using bi-level mpc", *IEEE Transactions on Intelligent Transportation Systems*, vol. 18, no. 8, pp. 2153–2162, 2016.

[44] N. Stroe, S. Olaru, G. Colin, K. Ben-Cherif, and Y. Chamaillard, "A two-layer predictive control for hybrid electric vehicles energy management", *IFAC-PapersOnLine*, vol. 50, no. 1, pp. 10 058–10 064, 2017.

[45] S. Uebel, N. Murgovski, B. Baker, and J. Sjoberg, "A 2-level mpc for energy management including velocity control of hybrid electric vehicle", *IEEE Transactions on Vehicular Technology*, 2019.

[46] A. Parkinson and M. Wilson, "Development of a hybrid sqp-grg algorithm for constrained nonlinear programming", 1988.

[47] M. Diehl, "Real-time optimization for large scale nonlinear processes", PhD thesis, University of Heidelberg, 2001.

[48] M. Diehl, H. G. Bock, and J. P. Schlöder, "A real-time iteration scheme for nonlinear optimization in optimal feedback control", *SIAM Journal on control and optimization*, vol. 43, no. 5, pp. 1714–1736, 2005.

[49] G. Frison and M. Diehl, "Hpipm: A high-performance quadratic programming framework for model predictive control", *arXiv preprint*, 2020.

Part II

Papers

PAPER A

Time optimal and eco-driving mission planning under traffic constraints

Ahad Hamednia, Nikolce Murgovski, and Jonas Fredriksson

Accepted in 23rd *IEEE International Conference on Intelligent Transportation Systems (ITSC)*

The layout has been revised.

Abstract

This paper addresses optimising a transport mission by controlling the mission start time and velocity profile of an electric vehicle (EV) driving in a hilly terrain, subject to legal and dynamic speed limits imposed by traffic congestion. To this end, a nonlinear program (NLP) is formulated, where the mission start time is allowed to vary within an interval and final time is kept free. The goal is to find the optimal trade-off between energy consumption and travel time, while allowing a flexibility in starting time and a certain variation of vehicle speed around an average. It is observed that total travel time is reduced up to 5.5% by adjusting the mission start time, when keeping an average cruising speed of about 75 km/h.

1 Introduction

Transportation plays an important role in the current global trade system, where the demand for transportation is highly connected to economic development. Particularly, road transportation's influence in the economy is crucial, since it includes nearly 60 % of all surface freight transportation [1]. Although the road transportation positively contributes to the economy, it is facing serious challenges, e.g. increasing energy consumption and CO_2 emissions.

In order to alleviate the destructive consequences from ever-growing CO_2 emissions, one promising alternative for future transportation systems is to electrify the vehicles ranging from hybrid to fully electric [2]. Furthermore, time loss due to traffic congestion is an additional negative side effect of the road transportation that greatly costs the society. The traffic congestion cost is estimated to $115 billion over 439 urban areas of the United States in 2010 [3]. Thus, there is a strong motivation to achieve a sustainable transportation system by improving transport efficiency, which can be interpreted as providing a service with less consumption of resources and not losing logistics performance, i.e. costs and delivery service [4].

Logistics service providers are considered among major actors that are involved in increasing the transport efficiency. *The service providers can optimally plan the transport mission by controlling the mission start time and*

following the principles of energy-efficient driving, referred to as eco-driving [5]–[7]. To achieve eco-driving it is necessary to optimally plan the velocity profile of a vehicle, subject to road and traffic flow information. One important factor in optimising the velocity profile is the knowledge about speed limits, which are imposed by not only legal speed limits, but also dynamic constraints [8], [9]. For instance, surrounding traffic sets such dynamic constraints due to presence of e.g. traffic lights, intersections, ramps and junctions. Another example that dynamically affects the speed limits is the linking of two or more trucks in convoy in order to increase the energy efficiency [10]. The dynamic speed limits make the travel time to be time-dependent, since the optimised speed can vary depending on time of the day [11].

In case of driving in a hilly terrain, preferably the optimal velocity varies within a bound, which originates from the legal and dynamic speed limits and the utilization of the road topography, i.e. the vehicle accelerates when driving downhill and decelerates when climbing uphill. This leads to less waste of non-recuperable energy compared to driving with constant speed [12]. To implement such behaviour over complex road topographies, advanced control strategies [13] could be employed that maximise energy efficiency by optimal coordination of energy sources, using information of the road topography and traffic flow.

Among the optimal control strategies, dynamic programming (DP) [14], which can handle mixed-integer, non-convex and nonlinear optimisation problems, is the most commonly used algorithm to optimise the velocity profile of a vehicle. For instance, information about the road topography ahead is used to optimise the velocity profile using DP in [15] to minimize fuel consumption and travel time.

Although DP is a powerful tool in solving optimal control problems, its main drawback is so-called *curse of dimensionality*, which refers to exponential increase in computational time with the increase in problem dimension [14]. The high computation burden due to using DP can be reduced by employing a heuristic method, which priorities exploring to the most promising solutions, utilizing the knowledge about considered problem [16]. As an alternative approach to DP, Pontryagin's Maximum Principle (PMP) [17] has been widely applied to the velocity optimisation of vehicles, especially in order to tackle the computational complexity due to high-dimensional optimisation problems. An algorithm for optimising the velocity profile is proposed in [18]

incorporating gear shifting, road grade constraints and speed limits. Necessary optimality conditions as stated by the PMP have been exploited in the well known equivalent consumption minimisation strategy (ECMS) to optimally manage energy flows in hybrid electric vehicles [19]. ECMS provides computational advantages by converting the optimisation problem to a two-point boundary-value program. However, for problems where states' bounds are frequently activated, multiple-shooting techniques are preferred, where the problem is directly transcribed to a nonlinear program (NLP) [20].

A combination of DP and other approaches for optimal control of vehicles have also been investigated. In [21]–[23], a mixture of DP and (sequential) convex optimisation is developed, where integer decisions, e.g. gear selection, are optimised by DP and real-valued decisions are taken by sequential convex optimisation. A PMP-DP method has been proposed in [24] to optimally plan the vehicle speed, gear selection, battery energy and ICE on/off state.

The combination of eco-driving and start time of the vehicle's mission by considering the dynamic speed limits is not addressed in the technical literature. This paper formulates a nonlinear program (NLP), which aims at optimal planning of the transport mission on long horizons that possibly stretches up to 100 km. The goal is to find a possible solution for energy-efficient driving considering both legal and dynamic speed limits, where the mission start time is allowed to vary within certain bounds. The method is demonstrated and applied on electric vehicle (EV) example.

2 Vehicle modelling

This section addresses modelling of the dynamics of an EV as a lumped mass, characteristics of EM and transmission system, and driving mission.

2.1 Travel time and longitudinal dynamics

Consider a vehicle driving on a planned route with a hilly terrain, where the vehicle does not stop or change direction of movement. This allows choosing travel distance, s, as an independent variable instead of travel time, t, i.e. decisions are taken with respect to s. The reason for such transformation is to alleviate high computational complexity due to nonlinearity in resistive force originating from roll resistance, which is shown in the following. Similar

transformations in the governing equations of the vehicle are done in [25]–[27] and references therein. Thus, the dynamics on travel time is

$$t'(s) = \frac{1}{v(s)}, \tag{A.1}$$

where v is longitudinal velocity.

Longitudinal dynamics of the vehicle, according to the Newton's law of motion, is

$$\mathrm{m}v(s)v'(s) = F(s) + F_{\mathrm{brk}}(s) - F_{\mathrm{air}}(v) - F_{\alpha}(s), \tag{A.2}$$

where $v' = \mathrm{d}v/\mathrm{d}s$ is the space derivative and $vv' = \mathrm{d}v/\mathrm{d}t$ denotes the longitudinal acceleration. Also, m is total lumped mass of the vehicle, F is EM force at the wheel side of the vehicle generated by the EM, and F_{brk} is non-positive mechanical braking force. The nominal aerodynamic drag, F_{air}, and the roll resistance, $F_{\alpha}(s)$, are defined as

$$F_{\mathrm{air}}(v) = \frac{\rho_{\mathrm{a}} \mathrm{c_d} \mathrm{A_f} v^2}{2}, \tag{A.3}$$

$$F_{\alpha}(s) = \mathrm{mg}\left(\sin(\alpha(s)) + \mathrm{c_r}\cos(\alpha(s))\right), \tag{A.4}$$

where α is road inclination, ρ_{a} is air density, $\mathrm{c_d}$ is aerodynamic drag coefficient, $\mathrm{A_f}$ is frontal area of the vehicle, g is the gravitational acceleration, and $\mathrm{c_r}$ is rolling resistance coefficient. Throughout this paper, all constants that are not dependent on s are displayed in upright letters, e.g. m, does not depend on s. Also, the dependency on s of the variables that are trajectories in terms of s, e.g. $F(s)$, is not shown in several places for simplicity.

2.2 Electric machine and transmission system

A schematic diagram of the studied fully electric powertrain is demonstrated in Fig. 1. The powertrain includes an electric battery as an energy storage unit, an EM, and a transmission system. The torque and rotational speed at the shaft between the electric machine and transmission are represented by M and ω, respectively.

The EM is represented using a steady-state model. The steady-state efficiency map of the EM for a given pair of rotational speed and torque is

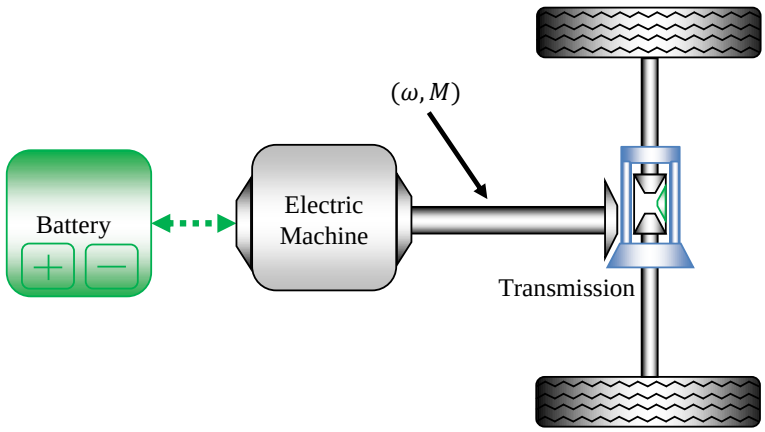

Figure 1: Schematic diagram of a fully electric powertrain. The powertrain consists of electric battery as energy storage unit, electric machine and transmission system, which transfers shaft torque, M, with rotating speed ω.

shown in Fig. 2, where positive and negative torque regions correspond to the motoring and the generating modes of operation, respectively.

The transmission system for the studied powertrain is solely a final gear ratio, which translates the shaft torque and rotational speed to the EM force and longitudinal velocity respectively, as

$$F(s) = \frac{M(s)}{R}, \quad v(s) = \omega(s)R, \quad R = \frac{\mathrm{r_w}}{\mathrm{r_{fg}}} \tag{A.5}$$

where γ denotes selected gear, $\mathrm{r_w}$ is wheel radius and $\mathrm{r_{fg}}$ is final gear ratio respectively.

2.3 Driving mission

We describe a driving mission by a map of maximum dynamic speed limits for a given pair of travel distance and time of day, as given in Figure. 6.3(a) and the associated road topography, see Figure. 6.3(b). Figure. 6.3(a) includes a contour plot, where the lighter the contour color is, the greater the vehicle speed is. Figure. 6.3(b) is a double y-axis plot, where the left y-axis corresponds to the vehicle speed and the right axis is the road altitude, while the gray area represents the road topography. According to the max speed map,

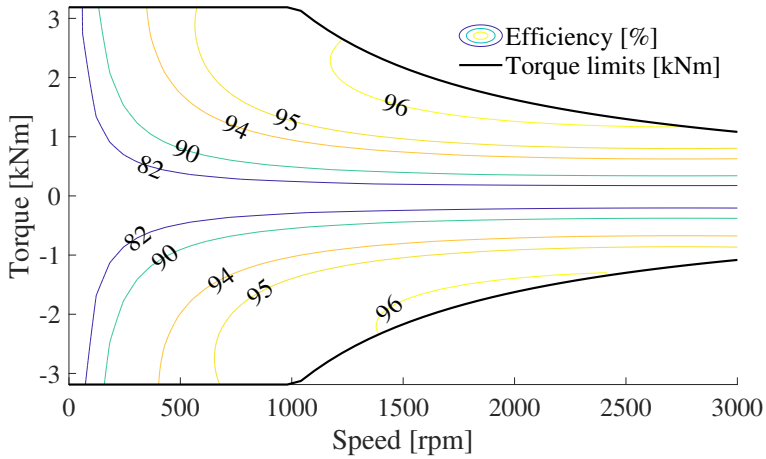

Figure 2: Steady-state efficiency map and torque limits of the electric machine.

the vehicle's mission, characterised as the mission start time, total travel time and velocity profile, can be tailored in favour of the improved energy efficiency. One execution of the mission in terms of speed/time trajectory is also shown in Figure. 3, where the vehicle starts the mission at 10:00. It can be seen that the traffic speed drops to about 30 km/h in the congested area, at travel distance of about 25 km.

3 Problem statement

In this section an optimisation problem is formulated, which aims at planning optimal velocity trajectory for the entire mission, in a way that total energy consumption is minimised and the travel time is adjusted by a penalty factor. Note that the travel time at initial position of the route is not fixed, but is allowed to vary within a bound. Final travel time is kept free.

Based on the models derived in the previous section, the energy optimization problem can be formulated as:

$$\min_{F,F_{\mathrm{brk}}} \lambda_{\mathrm{t}} \left(t(\mathrm{s_f}) - t(\mathrm{s_0})\right) + \int_{\mathrm{s_0}}^{\mathrm{s_f}} \frac{P_{\mathrm{b}}(v,F)}{v(s)} \mathrm{d}s \tag{A.6a}$$

subject to:

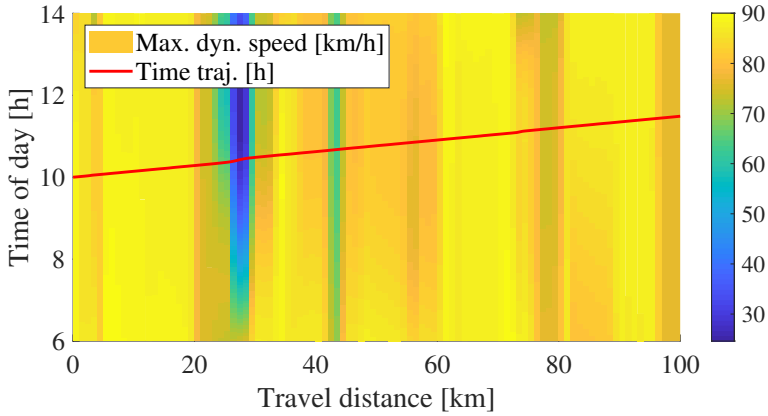

(a) Map of maximum dynamic speed limits together with one execution of the driving mission in terms of time trajectory.

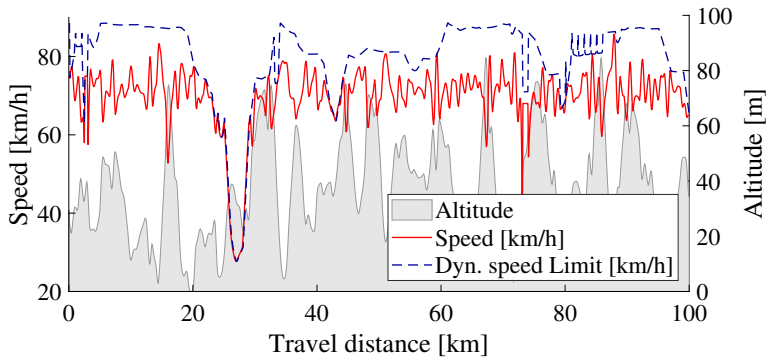

(b) Road topography with hilly terrain together with one execution of the driving mission in terms of longitudinal velocity and maximum dynamic speed limit.

Figure 3: Maximum dynamic speed limits map for a given pair of travel distance and time of day, together with associated road topography and one execution of the driving mission.

$$t'(s) = \frac{1}{v(s)} \tag{A.6b}$$

$$\mathrm{m}v(s)v'(s) = F(s) + F_{\mathrm{brk}}(s) - F_{\mathrm{air}}(v) - F_{\alpha}(s) \tag{A.6c}$$

$$v(s) \in [v_{\min}(s,t), v_{\max}(s,t)] \tag{A.6d}$$

$$F(s) \in [F_{\min}(v), F_{\max}(v)] \tag{A.6e}$$
$$F_{\text{brk}}(s) \leq 0 \tag{A.6f}$$
$$t(\mathrm{s}_0) \in [\mathrm{t}_0^{\min}, \mathrm{t}_0^{\max}], \quad v(\mathrm{s}_0) = \mathrm{v}_0 \tag{A.6g}$$

where $\mathrm{t}_0^{\min}$ is the minimum and $\mathrm{t}_0^{\max}$ is the maximum allowed initial time, and v_0 is initial longitudinal velocity. The longitudinal velocity limits including legal speed limits and dynamics constraints are shown by $v_{\min}(s,t)$ and $v_{\max}(s,t)$. Also, $F_{\min}(v)$ and $F_{\max}(v)$ represent the EM force limits for a given longitudinal velocity. In (A.6a), s_0 and s_f are initial and final positions of the driving vehicle respectively, and λ_t is a coefficient for penalising the travel time. The division of the battery power with speed in (A.6a) is obtained from the time to space transformation, i.e.

$$\int P_\mathrm{b}(v,F)\mathrm{d}t = \int P_\mathrm{b}(v,F)/v(s)\,\mathrm{d}s.$$

The constraints (A.6b)-(A.6f) are enforced for all $s \in [\mathrm{s}_0, \mathrm{s}_\mathrm{f}]$. Problem (A.6) has two states, t and v, and two control inputs, F and F_{brk}.

4 Smooth nonlinear programming

In this paper we define an NLP to be smooth if it is not mixed-integer. On the other hand, if the program is non-smooth, i.e. it is mixed-integer NLP, then there is at least one non-smooth or discontinuous function in the program with unbounded derivative. Accordingly, the direction in which the function is decreasing (or increasing) cannot generally be determined by using its derivative or gradient information. Thus, having one feasible solution provides very little information about how to search for a better solution, which makes the NLP extremely difficult to solve. Therefore, there is a strong motivation to model the non-smooth functions within an optimisation program by smooth or piece-wise smooth functions to alleviate the computational complexity.

The limits on longitudinal velocity (A.6d) and EM force (A.6e) may not be smooth functions. Such problems may generally be solved with DP, with the cost of high computation effort, which is exponential in the number of system states. In addition to the two system states, travel time and longitudinal velocity, having free initial and final time requires solving DP in an additional loop, which is computationally equivalent to having a 3rd state in the problem.

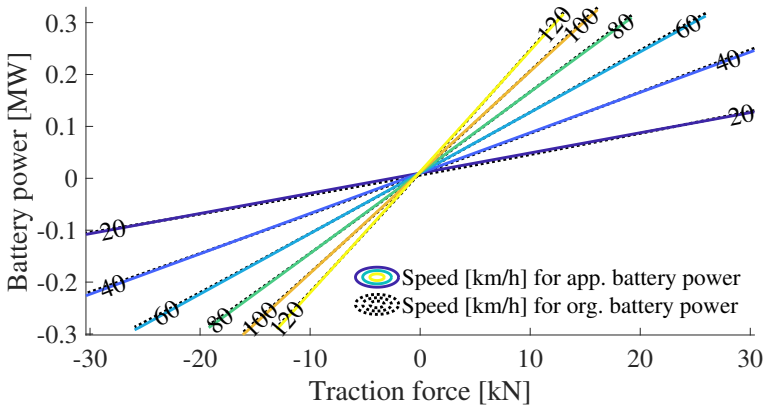

Figure 4: Measured and modelled electric battery power for a given longitudinal velocity and EM force.

Moreover, the problem may need to be solved multiple times, for different values of the time penalty factor, or may involve additional states to model driving comfort. Thus, there is a strong incentive to solve problem (A.6) in a computationally efficient way. To this end, the EM force limits are modeled as piecewise functions, where each of the pieces is a smooth function, and speed limits are approximated by smooth functions. This allows the problem to be translated to a smooth NLP that can be solved efficiently with Newton-based methods.

Electric battery power is modeled as

$$\begin{aligned} P(v,F) \approx \mathrm{p}_0 + \mathrm{p}_1 v(s) + \mathrm{p}_2 v^3(s) + \mathrm{p}_3 v^5(s) + \\ + \mathrm{p}_4 v(s) F(s) + \mathrm{p}_5 v(s) F^2(s), \end{aligned} \tag{A.7}$$

with $\mathrm{p}_0, \mathrm{p}_1, \mathrm{p}_2, \mathrm{p}_3, \mathrm{p}_4, \mathrm{p}_5 \geq 0$. Fig. 4 shows that the model fits well original steady-state measurements.

The EM force limits are modelled as piecewise functions

$$F_{\min}(v) \approx \max\left\{\underline{F}, \mathrm{x}_0 + \frac{\mathrm{x}_1}{v(s)}\right\} \tag{A.8}$$

$$F_{\max}(v) \approx \min\left\{\overline{F}, \mathrm{y}_0 + \frac{\mathrm{y}_1}{v(s)}\right\} \tag{A.9}$$

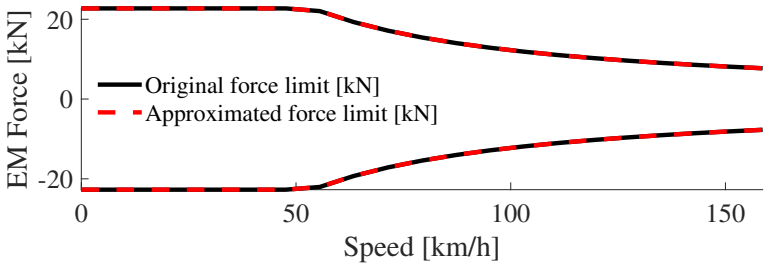

Figure 5: Measured and modelled EM force limits of the EM.

where $\underline{F}$ is constant minimum and $\overline{F}$ is constant maximum EM force, while the coefficients x_1 and y_1 denote maximum and minimum power limits. An illustration of the modelled and measured force limits is given in Fig. 5.

The maximum speed limit is computed as the minimum between the maximum legal speed limit, $v_{\max}^{\mathrm{lg}}$, and maximum dynamic speed limit that is modelled as a sum of sigmoidal functions

$$v_{\max}(s,t) = \min\left(v_{\max}^{\mathrm{lg}}(s), \sum_i \frac{a_i(s)}{1+e^{b_i(s)t+c_i(s)}}\right), \tag{A.10}$$

using traffic information. The proposed model for maximum dynamic speed limit gives the flexibility to model flat regions, as well as steep and shallow transitions. Here, $a_i(s)$, $b_i(s)$ and $c_i(s)$ are distance dependant coefficients. Our analyses showed that (A.10) is able to model many realistic scenarios, but the proposed method can identically be applied for other functions, as long as the smoothness of the NLP (A.6) is preserved.

5 Case study and results

In this section, optimal planning of a driving mission is investigated for a particular case study. An EV is driving in a 100 km long hilly terrain, as illustrated in Fig. 6.3(b), subject to a legal speed limit of 90 km/h. For pedagogical purposes, a simple scenario is considered with a single traffic jam, occurring at about 35 km, see Fig. 6. The traffic jam imposes dynamic speed limits, which depend on the time of the day, may constrain EV speed down to 30 km/h. Vehicle and simulation parameters are given in Table 1.

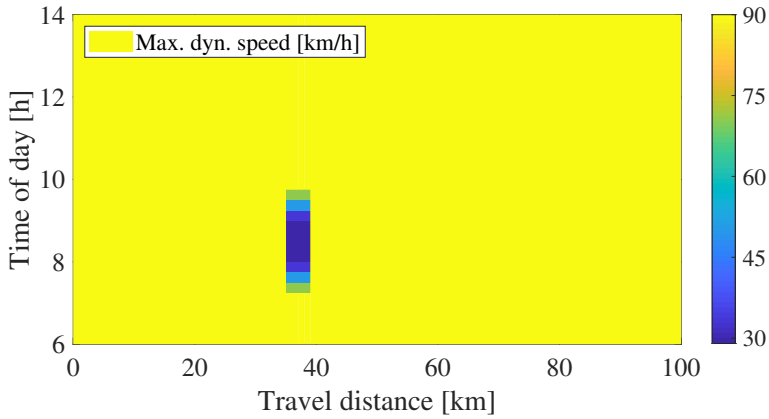

Figure 6: Map of maximum dynamic speed limits, a simple scenario.

The resulting NLP (A.6) is discretized using the forward Euler method with a sampling interval of 400 m. It is then solved in Matlab with the solver IPOPT using the open source optimisation tool CasADi [28]. To alleviate computational complexity due to nonlinearity in terms of the longitudinal velocity in (A.3), kinetic energy, $E(s)$, is used instead of longitudinal velocity, as proposed in [27], using the one-to-one relation

$$E(s) = \frac{\mathrm{m}v^2(s)}{2}. \tag{A.11}$$

The NLP is warm-started by providing an initial guess, further detailed in Appendix 1.

5.1 Choosing penalty factor for travel time

Penalising total travel time in (A.6a) strongly influences the electrical energy consumption. To investigate this, problem (A.6) is solved for a wide range of the time penalty factor, where the mission start time is allowed to vary within half-hour time intervals starting from 6:30. Fig. 7 shows a contour plot of upper bound on each half-hour mission start time for a given combination of the consumed electrical energy and total travel time. It is observed that there is a trade-off between the electrical energy consumption and travel time, i.e. by increasing the penalty factor, the travel time decreases, but it leads to higher

Table 1: Simulation parameters

Gravitational acceleration	$g = 9.81\,m/s^2$
Air density	$\rho = 1.29\,kg/m^3$
Vehicle frontal area	$A_f = 10\,m^2$
Rolling resistance coefficient	$c_r = 0.006$
Vehicle mass	$m = 40\,000\,kg$
Aerodynamic drag coefficient	$c_d = 0.5$
Wheel radius	$r_w = 0.50\,m$
Final gear ratio	$r_{fg} = 3$
Cruising set speed	$v_{cru} = 75\,km/h$
Route length	$100\,km$
Number of samples	$N = 250$

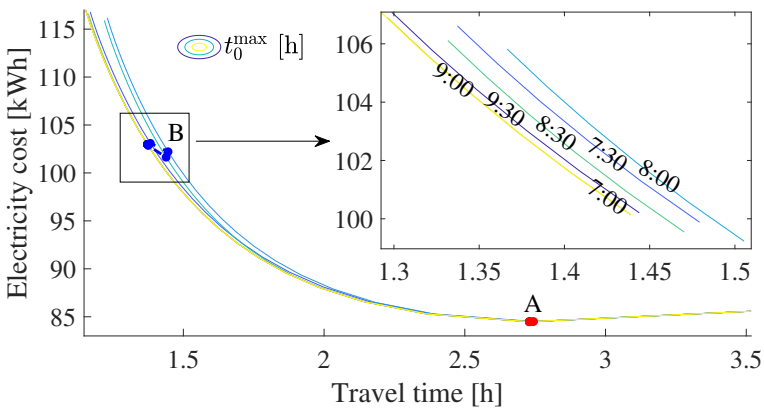

Figure 7: Contour plot of upper bound on each half-hour start time interval for a given pair of travel time and electricity use.

electricity use. Unsurprisingly, the curves of electricity use versus travel time overlap for the start time intervals of 6:30-7:00 and 9:00-9:30, since the vehicle never encounters the traffic jam in either cases. The demonstrated profile in Fig. 7, provides promising information for e.g. logistics service managers, who have wide range of choices to customise the vehicle's mission. In this profile, the region A corresponds to $\lambda_t = 0$, i.e. the most energy efficient driving. By letting the penalty factor be negative, it is possible to further increase travel time, which will actually cause increase in energy consumption. This implies

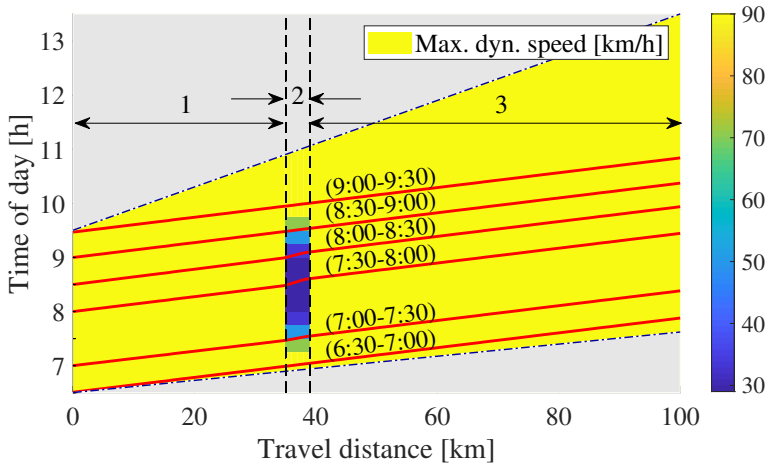

Figure 8: Optimal time trajectories for each mission start time interval; corresponding to region B.

that there is a low speed threshold, here about 35 km/h, below which the benefit of reduced air drag is negated by the increased time of accumulating powertrain losses.

Region B in Fig. 7 corresponds to a positive penalty factor that results in keeping an average cruising speed of about $v_{cru} = 75$ km/h when traffic jam is avoided. For the remaining results in this paper, we use the time penalty factor that enables operation in region B. Optimal time trajectory for the region B, for each interval of the mission start time, is depicted in Fig. 8. It is observed that by applying the proposed algorithm, the vehicle tries to avoid the low speed area. The gray areas correspond to the infeasible time regions. The travel distance in Fig. 8 is divided into three segments; (1): before traffic congestion, (2): during traffic congestion and (3): after traffic congestion. The mean optimal speed values per each distance segment and mission start time interval together with electrical energy use and travel time are given in Table 2. For instance, by comparing the results of the intervals 6:30-7:00 and 7:30-8:00, travel time is reduced by 5.5%, when the mission starts at 6:30 instead of 8:00.

As an example, optimal longitudinal velocity profiles for the start time intervals of 6:30-7:00 and 7:00-7:30 are shown in Fig. 9, together with their corresponding guess velocity profiles. It is observed that for the interval of

Table 2: Mean optimal speed for given road segment and time interval together with electricity use and travel time, region B.

Start time interval	$\overline{v}_1$ [km/h]	$\overline{v}_2$ [km/h]	$\overline{v}_3$ [km/h]	Elec. [kWh]	Travel time [h]
6:30-7:00	73.07	74.00	73.08	102.99	1.37
7:00-7:30	75.34	55.75	73.08	103.09	1.38
7:30-8:00	72.92	40.33	73.08	102.22	1.45
8:00-8:30	70.93	45.27	73.08	101.64	1.44
8:30-9:00	72.93	71.64	73.08	102.86	1.38
9:00-9:30	73.07	74.00	73.08	102.99	1.37

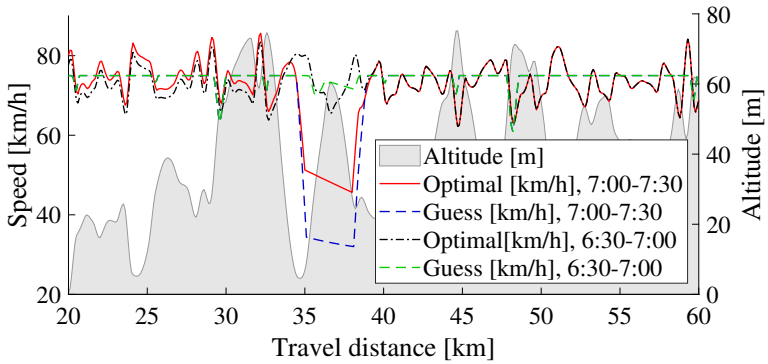

Figure 9: Optimal longitudinal velocity profiles for the start time intervals of 6:30-7:00 and 7:00-7:30 together with their corresponding guess velocity profiles.

7:00-7:30 the vehicle speeds up in the first distance segment compared to the interval of 6:30-7:00 to avoid the traffic congestion. Optimal EM force and braking force trajectories are depicted in Fig. 6.10(a). Also, optimal force-speed operating points are given in Fig. 6.10(b). Note that Fig. 9 and Fig. 6.10(a) are shown for zoomed distance segment of 20 km-60 km.

6 Conclusion

In this paper, an NLP is formulated in order to improve the transport efficiency for an EV driving in a hilly terrain, by optimising the velocity profile and mission start time. To alleviate the computational complexity, non-smooth

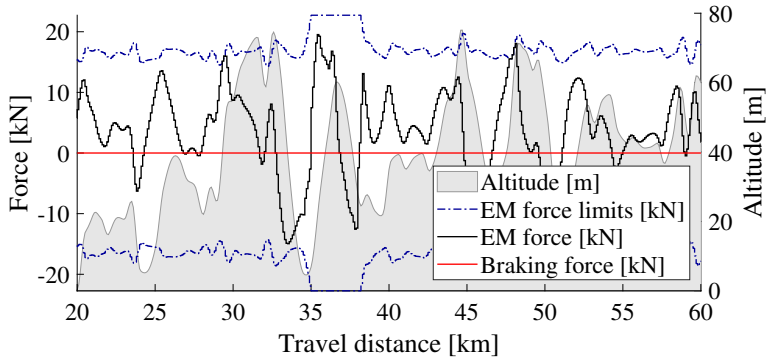

(a) Optimal EM force and braking force trajectories.

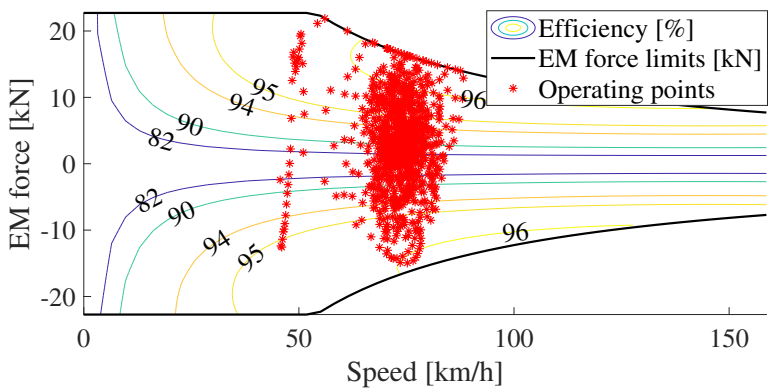

(b) Optimal force-speed points.

Figure 10: Optimal EM force and braking force trajectories together with optimal force-speed points, when the mission start time is allowed to vary over 7:00 to 7:30.

EM force and dynamic speed limits are modeled by smooth functions. The mission start time is allowed to vary over half-hour intervals starting from 6:30. For pedagogical purposes a scenario with a single traffic jam is studied. According to the simulation results, the proposed algorithm can find a possible solution such that the vehicle avoids the traffic jam.

1 Initial guess for warm-starting

An initial guess of speed limits

$$v^{\mathrm{g}}_{\min}(s,t) = \max\left\{v^{\mathrm{lg}}_{\min}(s), v^{\mathrm{dyn}}_{\min}(s,t)\right\}, \tag{A.12}$$

$$v^{\mathrm{g}}_{\max}(s,t) = \min\left\{v^{\mathrm{lg}}_{\max}(s), v^{\mathrm{dyn}}_{\max}(s,t)\right\}, \tag{A.13}$$

are obtained by considering legal speed limits of the road, $v^{\mathrm{lg}}_{\min}(s)$ and $v^{\mathrm{lg}}_{\max}(s)$, and dynamic speed limits, $v^{\mathrm{dyn}}_{\min}(s,t)$ and $v^{\mathrm{dyn}}_{\max}(s,t)$, for a given pair of travel distance and travel time. To initialize the problem (A.6), a velocity profile, $v_{\mathrm{g}}(s,t) \in [v^{\mathrm{g}}_{\min}(s,t), v^{\mathrm{g}}_{\max}(s,t)]$, can be derived as a guess by filtering cruising speed, $\mathrm{v_{cru}} \in [v^{\mathrm{lg}}_{\min}(s), v^{\mathrm{lg}}_{\max}(s)]$, where the cruising speed can be set manually by driver or automatically by a telemetry system. To compute $v_{\mathrm{g}}(s)$, the rated power of EM and legal/dynamic limits on speed are taken into consideration in filtering the cruise speed [22], i.e. the vehicle will try to maintain $\mathrm{v_{cru}}$ unless EM and/or speed limit is reached.

Let

$$F_{\mathrm{Wmax}}(v) = F_{\max}(v) - F_{\mathrm{air}}(v) - F_{\alpha}(s) \tag{A.14}$$

represent the maximum EM force to be delivered at the wheels, for the vehicle driving at the speed v. The guess longitudinal velocity, $v_{\mathrm{g}}(s)$, and travel time, $t_{\mathrm{g}}(s)$, are computed in discrete space domain using the forward Euler method as in Algorithm 1. In this algorithm, $\mathrm{t_{0g}}$ is a guess for the travel time at the first position, N is number of samples, $\mathrm{a_{max}}$ is the maximum allowed acceleration within a comfort zone, and Δs is the sampling interval.

References

[1] OECD/ITF, “ITF transport outlook 2013”, 2013.

[2] S. PELLETIER, O. JABALI, and G. LAPORTE, “Goods distribution with electric vehicles: Review and research perspectives. montrál”, Canada, 2014: Technical Report CIRRELT-2014-44, CIRRELT, Tech. Rep., 2014.

Algorithm 1 Initial guess for warm-starting.

$t_{\mathrm{g}}^{0} \in [\mathrm{t}_{0}^{\min}, \mathrm{t}_{0}^{\max}]$
$v_{\mathrm{g}}^{0} = \mathrm{v}_{\mathrm{cru}}$
for $\mathrm{k} = 1, \ldots, \mathrm{N}$ **do**
    $v_{\mathrm{g}}^{\mathrm{k}} \leftarrow v_{\mathrm{g}}^{\mathrm{k}-1} + \frac{\Delta s}{v_{\mathrm{g}}^{\mathrm{k}-1}} \min \left\{ \mathrm{a}_{\max},\ \frac{F_{\mathrm{Wmax}}(v_{\mathrm{g}}^{\mathrm{k}-1})}{\mathrm{m}} \right\}$
    $v_{\mathrm{g}}^{\mathrm{k}} \leftarrow \min \left\{ \mathrm{v}_{\mathrm{cru}},\ v_{\mathrm{g}}^{\mathrm{k}} \right\}$
    $t_{\mathrm{g}}^{\mathrm{k}} \leftarrow t_{\mathrm{g}}^{\mathrm{k\text{-}1}} + \frac{\Delta s}{v_{\mathrm{g}}^{\mathrm{k}}}$
    $v_{\mathrm{g}}^{\mathrm{k}} \leftarrow \min \left\{ v_{\mathrm{g}}^{\mathrm{k}},\ v_{\max}^{\mathrm{dyn}}(s, t_{\mathrm{g}}^{\mathrm{k}}) \right\}$
    $t_{\mathrm{g}}^{\mathrm{k}} \leftarrow t_{\mathrm{g}}^{\mathrm{k\text{-}1}} + \frac{\Delta s}{v_{\mathrm{g}}^{\mathrm{k}}}$
end

[3] D. Schrank, B. Eisele, and T. Lomax, "Tti's 2012 urban mobility report", *Texas A&M Transportation Institute. The Texas A&M University System*, vol. 4, 2012.

[4] H. Aronsson and M. H. Brodin, "The environmental impact of changing logistics structures", *The international journal of logistics management*, 2006.

[5] M. A. S. Kamal, M. Mukai, J. Murata, and T. Kawabe, "Model predictive control of vehicles on urban roads for improved fuel economy", *IEEE Transactions on control systems technology*, vol. 21, no. 3, pp. 831–841, 2012.

[6] M. Vajedi and N. L. Azad, "Ecological adaptive cruise controller for plug-in hybrid electric vehicles using nonlinear model predictive control", *IEEE Transactions on Intelligent Transportation Systems*, vol. 17, no. 1, pp. 113–122, 2015.

[7] Y. Luo, T. Chen, S. Zhang, and K. Li, "Intelligent hybrid electric vehicle acc with coordinated control of tracking ability, fuel economy, and ride comfort", *IEEE Transactions on Intelligent Transportation Systems*, vol. 16, no. 4, pp. 2303–2308, 2015.

[8] M. Held, O. Flärdh, and J. Mårtensson, "Optimal speed control of a heavy-duty vehicle in urban driving", *IEEE Transactions on Intelligent Transportation Systems*, vol. 20, no. 4, pp. 1562–1573, 2018.

[9] R. Basso, P. Lindroth, B. Kulcsár, and B. Egardt, "Traffic aware electric vehicle routing", in *2016 IEEE 19th International Conference on Intelligent Transportation Systems (ITSC)*, IEEE, 2016, pp. 416–421.

[10] A. Alam, B. Besselink, J. Mårtensson, and K. H. Johansson, "Heavy-duty vehicle platooning for sustainable freight transportation: A cooperative method to enhance safety and efficiency", *IEEE Control Systems Magazine*, vol. 35, no. 6, pp. 34–56, 2015.

[11] M. Gendreau, G. Ghiani, and E. Guerriero, "Time-dependent routing problems: A review", *Computers & operations research*, vol. 64, pp. 189–197, 2015.

[12] J. N. Barkenbus, "Eco-driving: An overlooked climate change initiative", *Energy Policy*, vol. 38, no. 2, pp. 762–769, 2010.

[13] A. Sciarretta, G. D. Nunzio, and L. L. Ojeda, "Optimal ecodriving control: Energy-efficient driving of road vehicles as an optimal control problem", *IEEE Control Systems Magazine*, vol. 35, no. 5, pp. 71–90, 2015.

[14] R. Bellman, *Dynamic Programming*. New Jersey: Princeton Univ Pr, 1957.

[15] E. Hellström, M. Ivarsson, J. Åslund, and L. Nielsen, "Look-ahead control for heavy trucks to minimize trip time and fuel consumption", *Control Engineering Practice*, vol. 17, no. 2, pp. 245–254, 2009.

[16] Z. Ajanović, M. Stolz, and M. Horn, "A novel model-based heuristic for energy-optimal motion planning for automated driving", *IFAC-PapersOnLine*, vol. 51, no. 9, pp. 255–260, 2018.

[17] L. S. Pontryagin, V. G. Boltyanskii, R. V. Gamkrelidze, and E. F. Mishchenko, *The Mathematical Theory of Optimal Processes*. Interscience Publishers, 1962.

[18] E. Ozatay, U. Ozguner, and D. Filev, "Velocity profile optimization of on road vehicles: Pontryagin's maximum principle based approach", *Control Engineering Practice*, vol. 61, pp. 244–254, 2017.

[19] A. Rezaei, J. B. Burl, and B. Zhou, "Estimation of the ecms equivalent factor bounds for hybrid electric vehicles", *IEEE Transactions on Control Systems Technology*, vol. 26, no. 6, pp. 2198–2205, 2017.

[20] H. W. Kuhn and A. W. Tucker, "Nonlinear programming", in *Traces and emergence of nonlinear programming*, Springer, 2014, pp. 247–258.

[21] L. Johannesson, M. Nilsson, and N. Murgovski, "Look-ahead vehicle energy management with traffic predictions", in *IFAC Workshop on Engine and Powertrain Control, Simulation and Modeling (E-COSM)*, vol. 48, Columbus, Ohio, USA, 2015, pp. 244–251.

[22] N. Murgovski, B. Egardt, and M. Nilsson, "Cooperative energy management of automated vehicles", *Control Engineering Practice*, vol. 57, pp. 84–98, 2016.

[23] M. Hovgard, O. Jonsson, N. Murgovski, M. Sanfridson, and J. Fredriksson, "Cooperative energy management of electrified vehicles on hilly roads", *Control Engineering Practice*, vol. 73, pp. 66–78, 2018.

[24] S. Uebel, N. Murgovski, C. Tempelhahn, and B. Bäker, "Optimal energy management and velocity control of hybrid electric vehicles", *IEEE Transactions on Vehicular Technology*, vol. 67, no. 1, pp. 327–337, 2017.

[25] B. Saerens, "Optimal control based eco-driving", *Theoretical Approach and Practical Applications. Heverlee: Katholieke Universiteit Leuven*, 2012.

[26] A. Hamednia, N. Murgovski, and J. Fredriksson, "Predictive velocity control in a hilly terrain over a long look-ahead horizon", *IFAC PapersOnLine*, vol. 51, no. 31, pp. 485–492, 2018.

[27] A. Hamednia, N. K. Sharma, N. Murgovski, and J. Fredriksson, *Computationally efficient algorithm for eco-driving over long look-ahead horizons*, 2020.

[28] J. A. Andersson, J. Gillis, G. Horn, J. B. Rawlings, and M. Diehl, "Casadi: A software framework for nonlinear optimization and optimal control", *Mathematical Programming Computation*, vol. 11, no. 1, pp. 1–36, 2019.

PAPER B

Computationally efficient algorithm for eco-driving over long look-ahead horizons

Ahad Hamednia, Nalin K.Sharma, Nikolce Murgovski, Jonas Fredriksson

Submitted to IEEE Transactions on Intelligent Transportation Systems in Jan. 2020

The layout has been revised.

Abstract

This paper presents a computationally efficient algorithm for eco-driving along horizons of over 100 km. The eco-driving problem is formulated as a bi-level program, where the bottom level is solved offline, pre-optimising gear as a function of longitudinal velocity (kinetic energy) and acceleration. The top level is solved online, optimising a nonlinear dynamic program with travel time, kinetic energy and acceleration as state variables. To further reduce computational effort, the travel time is adjoined to the objective by applying necessary Pontryagin's Maximum Principle conditions, and the nonlinear program is solved using real-time iteration sequential quadratic programming scheme in a model predictive control framework. Compared to average driver's driving cycle, the energy savings of using the proposed algorithm is up to 11.60 %.

1 Introduction

Excessive energy consumption of vehicles is recently being regarded as a crucial concern for automotive industry leaders and transport service providers due to economic, ecological and environmental issues. For instance, the Organisation for Economic Co-operation and Development (OECD) forecasts a rapid growth in transport demand over the coming years, which may lead to 60 % increase in worldwide transport CO_2 emissions by 2050, due to increase in fossil fuel consumption [1]. One effective way to mitigate destructive consequences from ever growing energy consumption by vehicles is to improve *transport efficiency*. The transport efficiency can also be characterised as *tank-to-meter efficiency*, referred to as the conversion of energy stored in fuel into potential and kinetic energy required for displacement, and accompanied losses.

Eco-driving has been concerned widely as an approach for increasing the tank-to-meter efficiency by optimising velocity profile when considering road information and traffic flow [2]–[6]. When driving in a hilly terrain, it is preferable to vary the vehicle speed over a narrow interval while keeping the maximum allowed travel time, i.e., speeding up when driving downhill and

decreasing speed when climbing uphill, to have less energy waste at braking pads compared to a constant speed driving [7]. Implementing this behaviour over complex road topographies is generally achieved by model-based optimal control methods that maximise energy efficiency by optimally coordinating the energy use.

Dynamic programming (DP) [8] is the most commonly used algorithm to optimise the velocity profile of vehicles due to its potential to tackle non-convex, nonlinear and mixed-integer optimisation problems [9]–[14]. Fuel-optimal look-ahead control strategies have been proposed in [9] and [10] using DP, where in addition to optimising velocity, optimal gear shifting of conventional trucks is also investigated. Furthermore, a DP-based method is applied in [11] to minimise the energy consumption in fully electric vehicles (EVs) by optimising vehicle speed on short-range trips, e.g. driving between two consecutive traffic lights. A combined energy management and eco-driving approach using discrete DP is devised in [12] for hybrid electric vehicles (HEVs) driving over limited horizons, where the velocity profile is allowed to be optimised to further enhance fuel efficiency. Despite the promising contributions in solving optimal control problems (OCPs), DP-based methods suffer from the *curse of dimensionality*, which denotes to a fact that computational time increases exponentially with the number of state variables and control signals [8]. Several ways have been taken to decrease computational effort, for example by limiting the look-ahead horizon of cruise controllers for HEVs. At the current state, real-time capable DP-based control can only be applied for short prediction horizon scenarios of HEVs [13]. Other approaches focus on simplifying the powertrain model, by e.g. using a simplified internal combustion engine (ICE) model or discarding system states, such as travel time, ICE on/off and gear [14].

For high-dimensional optimisation problems, e.g. optimal control of HEVs with more energy states, several alternative approaches have been proposed. In [15] a mixed-integer quadratic program (MIQP) [16] has been applied for power allocation of HEVs. A way to diminish computational complexity of the high-dimensional problems is adjoining system dynamics to the cost function and neglecting constraints on state variables, as shown in [17]–[19]. In [19] Pontryagin's Maximum Principle (PMP) [20], [21] has been applied to optimise vehicle speed, gear selection and energy use of HEVs, where integer state variables have been neglected. Also, optimal speed and gear selection

of vehicles driving on highways have been addressed in [22] under varying parameters. Furthermore, in [23], [24] minimisation of energy consumption using PMP and considering varying speed requirements has been studied. Although PMP-based methods are computationally efficient for optimal velocity problems over long look-ahead horizons, they do not provide the same computational advantage for problems where state variables often activate their bounds. This is especially relevant for single shooting methods used for solving two-point boundary value problems (2PBVPs), as in e.g. [25].

Another portion of the conducted research benefits from the combination of DP and other methods. Such approaches have been proposed by [26]–[29], where real-valued decisions, e.g., planing optimal velocity, are made by sequential convex optimisation, while integer decisions are taken by DP. These strategies have also been shown to be effective when considering surrounding traffic [28], or cooperative energy management of multiple vehicles [26], [29]. In [30] a PMP-DP method has been proposed to solve the optimal control of vehicle speed, battery energy, gear selection and ICE on/off state. However, the computational effort of the control algorithms is still highly susceptible to long horizon lengths and high update frequencies.

High computational complexity may not be crucial when the eco-driving problem is implemented offline, since the problem solving is generally allowed to take a considerable amount of time. However, the offline implementation has drawbacks in situations where disturbances and/or constraints, for e.g. traffic situation, change unpredictably and the vehicle is no longer able to exactly follow the planned solution. Thus, the synergy among different optimisation methods is generally performed by splitting the problem into sub-problems arranged into multi-level or bi-level control architectures, where different tasks, for e.g. disturbance rejection, are delegated to distinct layers based on horizon length, time constants, sampling interval and updating frequency. To this end, multi-level and bi-level model predictive control (MPC) algorithms have been proposed for conventional vehicles (CVs), [31], and HEVs, [32]–[35], respectively. The multi-level architectures allow solving computationally intensive sub-problems, e.g. mixed-integer programs. When solving such programs in an MPC fashion, a certain reference or a target state are tracked, typically over look-ahead horizons of up to several of kilometers. Even though such horizons may appear long, there are problems that are naturally defined for even longer horizons.

Problems with very long look-ahead horizons, in the order of hundreds of kilometres, are typically addressed in electrified vehicles or logistics [36]. In the case of electrified vehicles, a target battery state of charge may be provided at charging locations along the route. For the logistics case, a target state over the long horizon is the travel time, which is often given at the end of the route by a logistics planner. Within the multi-level control architecture mentioned earlier, these problems are delegated to the highest supervisory level, generating reference travel time and battery state of charge trajectories over hundreds of kilometres. Early results on developing online implementable controllers that operate over long horizons, hereafter referred to as the eco-driving supervisors, have been published in our previous work for the case of CV, see [37].

In this paper, the eco-driving supervisor designed in [37] is generalised to both CVs and EVs. The purpose of the eco-driving supervisor is to generate optimal reference trajectories for the entire route, or for look-ahead horizons that may stretch over hundreds of kilometres, using road and traffic information compiled from look-ahead data and previous measurements. To do so, an online-capable algorithm is developed in an MPC framework that has the ability to anticipate future events and react to disturbances. For solving the eco-driving supervision problem online, reducing the computational complexity is the main concern, to allow the online solution to be obtained within the update frequency of real-time execution. Furthermore, having small computation time can strongly enhance the optimality, since the suggested optimal state of vehicle can be updated more frequently. Accordingly, the algorithm's computational effort is decreased in three steps: 1) a problem decomposition into two sub-problems, where velocity and travel-time trajectory are optimised online and gear shifting strategy is optimised offline; 2) a combination of an indirect PMP solution and a direct nonlinear programming for reducing the number of states in the online optimisation sub problem; 3) a real-time iteration (RTI) sequential quadratic programming (SQP) [38], which allows a single quadratic program (QP) to be solved in an MPC manner [39].

The outline of the paper is as follows. In Section 2, dynamic model of vehicle is presented. In Section 3, the energy minimisation problem is formulated. Section 4 describes the computationally efficient algorithm. In Section 5 the proposed algorithm is applied to a CV and an EV. In Section 6, the simulation results are demonstrated. Finally, Section 7 concludes the paper.

2 Physical Modelling

This section addresses vehicle dynamics, i.e. travel time and longitudinal vehicle dynamics. Furthermore, static relations are given that translate torque and rotational speed of actuator to traction force and longitudinal velocity. Finally, lower bounds and upper bounds on longitudinal velocity, traction force and acceleration are presented.

2.1 Travel time and longitudinal dynamics

According to Newton's law of motion, preliminary governing equations of a point mass vehicle model are

$$\dot{s}(t) = v(t) \tag{B.1}$$

$$\mathrm{m}\,\dot{v}(t) = F(t) + F_{\mathrm{brk}}(t) - F_{\mathrm{air}}(v) - F_{\alpha}(s) \tag{B.2}$$

where m is total lumped mass of the vehicle, t is travel time, s is travelled distance, v is longitudinal velocity, F is traction force at the wheel side of the vehicle generated by the actuator, and F_{brk} is a non-positive force that includes braking by the service brakes, a retarder, a compression release engine brake and/or an exhaust pressure governor. For the case of a conventional vehicle, more details on the braking force will be discussed later, in Section 5.1. Note that the travelled distance and longitudinal velocity are functions of travel time in (B.2). However, the explicit dependence is not shown for brevity, when these signals are input arguments to functions, such as $F_{\alpha}(s(t))$ and $F_{\mathrm{air}}(v(t))$. The nominal aerodynamic drag, F_{air}, and resistive forces that depend on road gradient α, $F_{\alpha}(s)$, are defined as

$$F_{\mathrm{air}}(v) = \frac{\rho_{\mathrm{a}} \mathrm{c_d} \mathrm{A_f} v^2}{2}, \tag{B.3}$$

$$F_{\alpha}(s) = \mathrm{mg}\left(\sin(\alpha(s)) + \mathrm{c_r}\cos(\alpha(s))\right), \tag{B.4}$$

where ρ_{a} is air density, $\mathrm{c_d}$ is aerodynamic drag coefficient, $\mathrm{A_f}$ is vehicle frontal area, g is the gravitational acceleration, and $\mathrm{c_r}$ is rolling resistance coefficient. The road gradient can be directly obtained from a standard global positioning system (GPS).

The vehicle longitudinal dynamics (B.1) and (B.2), are nonlinear due to

the quadratic dependency of longitudinal velocity in the aerodynamical drag function in (B.3) and the road gradient that can be an arbitrary nonlinear function of distance in (B.4). Such nonlinearities may increase computational complexity. To overcome this issue, it is possible to modify (B.1) and (B.2) by changing independent variables. Thus, distance s is used as independent variable instead of time t in (B.1), i.e. decisions are planned with respect to s, as presented in [40]–[43]. Subsequently, for a given road topography, the function F_α now becomes a fixed trajectory for the entire route. In addition, the nonlinearity in (B.3) can be removed by a change of state variable v to kinetic energy,

$$E(s) = \frac{\mathrm{m}v^2(s)}{2} \tag{B.5}$$

where E represents the kinetic energy of the vehicle. These transformations are non-approximate as long as the studied vehicle does not stop or change direction of its movement. Also, to study variations on speed and acceleration of the driving vehicle, we introduce acceleration, a, as an additional state variable. The change of acceleration in space coordinates, which resembles jerk, j, now becomes the input signal to the vehicle system. The resulting vehicle dynamics model becomes

$$t'(s) = \sqrt{\frac{\mathrm{m}}{2E(s)}} \tag{B.6}$$

$$E'(s) = \mathrm{m}a(s) \tag{B.7}$$

$$a'(s) = j(s) \tag{B.8}$$

where t' and a' are used as short hand notations for $\mathrm{d}t/\mathrm{d}s$ and $\mathrm{d}a/\mathrm{d}s$, respectively. The relation $E' = \mathrm{m}vv'$ is the product of mass and vehicle acceleration, and

$$a(s) = \frac{1}{\mathrm{m}}\left(-\mathrm{c_a}E(s) + F(s) + F_{\mathrm{brk}}(s) - F_\alpha(s)\right) \tag{B.9}$$

where $\mathrm{c_a} = \rho_\mathrm{a}\mathrm{c_d}\mathrm{A_f}/\mathrm{m}$, gathers the drag related coefficients.

It can be noticed that (B.6) is still nonlinear with respect to E. More information on how to tackle the nonlinearity in (B.6) is presented in Section 4.

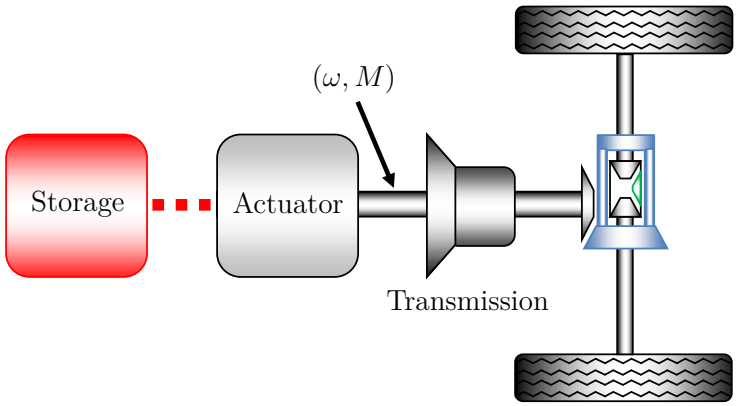

Figure 1: Schematic diagram of the studied powertrain. The powertrain consists of energy storage unit, actuator and transmission system, which transfers shaft torque, M, with rotating speed ω.

Throughout this paper, all constants, which are not dependent on s are shown in upright letters, e.g. $\mathrm{m}, \mathrm{A_f}, \mathrm{c_d}, \rho_\mathrm{a}$ do not depend on s. Also, all the states and control inputs are trajectories in terms of s, e.g. $t(s)$ and $E(s)$ are the trajectories dependent on s, where in several places the dependency is not displayed for simplicity.

2.2 Vehicle powertrain

A schematic diagram of the considered powertrain is illustrated in Fig. 1. The powertrain consists of an energy storage unit, an actuator, e.g. an ICE or an electric machine (EM), and a transmission system. The torque and speed at the shaft between the actuator and transmission are denoted by M and ω, respectively.

The transmission system is modelled considering the transmission and final gear ratios as

$$v(s) = \omega(s)R(\gamma), \quad F(s) = \frac{M(s)}{R(\gamma)}, \tag{B.10}$$

where γ denotes selected gear, and

$$R(\gamma) = \frac{\mathrm{r_w}}{\mathrm{r_{tg}}(\gamma)\mathrm{r_{fg}}} \tag{B.11}$$

where $\mathrm{r_w}$ is the wheel radius, $\mathrm{r_{tg}}$ and $\mathrm{r_{fg}}$ are transmission and final gear ratios, respectively.

The traction force is bounded

$$F(s) \in [F_{\gamma\min}(E), F_{\gamma\max}(E)], \tag{B.12}$$

where

$$F_{\gamma\min}(E) = \min_{\gamma} F_{\min}(E, \gamma), \tag{B.13}$$

$$F_{\gamma\max}(E) = \max_{\gamma} F_{\max}(E, \gamma). \tag{B.14}$$

The functions $F_{\min}(E, \gamma)$ and $F_{\max}(E, \gamma)$ are the traction force limits for a given pair of kinetic energy (longitudinal velocity) and gear.

In turn, the acceleration limits,

$$a(s) \in [a_{\min}(E), a_{\max}(E)],$$

can be derived using (B.9) as a function of kinetic energy (longitudinal velocity) and considering the limits on traction force, as

$$a_{\min}(E) = \max\left\{\underline{\mathrm{a}}, \frac{F_{\gamma\min}(E) - \mathrm{c_a}E + \underline{\mathrm{F_{brk}}} - F_\alpha}{\mathrm{m}}\right\} \tag{B.15}$$

$$a_{\max}(E) = \min\left\{\overline{\mathrm{a}}, \frac{F_{\gamma\max}(E) - \mathrm{c_a}E - F_\alpha}{\mathrm{m}}\right\} \tag{B.16}$$

where $\underline{\mathrm{a}}$ is the minimum and $\overline{\mathrm{a}}$ is the maximum allowed acceleration within a comfort zone and $\underline{\mathrm{F_{brk}}}$ denotes constant minimum total braking force. Here, $a_{\min}$ and $a_{\max}$ are not necessarily smooth functions, as $F_{\gamma\min}$ and $F_{\gamma\max}$ may not be smooth functions. This will be discussed in more details in Section 5.

In order to deliver a certain traction force, the actuator draws power from the energy storage unit. Let $P_{\mathrm{w}}(v, F, \gamma)$ denote the drawn power, which in the case of a combustion engine is a chemical, fossil fuel power, and in the case of an electric machine, it is an electric power. Explicit representations of

the internal power in terms of the kinetic energy (longitudinal velocity) and traction force will be provided later, in Section 5.

3 Problem Statement

This section formulates the eco-driving OCP, which aims at planning an optimal velocity trajectory for the entire route such that the total energy consumption is minimised and the travel time is upper bounded by the target time given by a logistics planner.

3.1 Performance function

The performance function of the OCP is formulated as

$$\int_0^{\mathrm{s_f}} \left(\frac{\mathrm{c_{eg}} P_{\mathrm{w}}(v, F, \gamma)}{v(s)} + \mathrm{w}_1 a^2(s) + \mathrm{w}_2 j^2(s) \right) \mathrm{d}s \tag{B.17}$$

that incorporates total energy consumption by integrating the internal power drawn from the storage unit, and the driver's discomfort via the acceleration and jerk. Here, $\mathrm{c_{eg}}$ denotes the price of energy storage, and w_1 and w_2 are penalty factors associated with the acceleration and jerk. The division of the internal power with speed in (B.17) derives from the time to space transformation,

$$\int P_{\mathrm{w}}(v, F, \gamma) \mathrm{d}t = \int P_{\mathrm{w}}(v, F, \gamma)/v(s)\, \mathrm{d}s.$$

3.2 Speed limits and travel time

In order to increase feasibility in realistic driving situations, we consider speed limits that include not only legal, but also dynamic speed limits using available information about the road and traffic. Surrounding traffic can impose such dynamic constraints on the vehicle speed due to presence of e.g. traffic lights, intersections, ramps and junctions. Total speed limits are computed as

$$v_{\min}(s) = \min \left\{ v_{\min}^{\mathrm{legal}}(s), v_{\mathrm{fl}}(s) \right\}, \tag{B.18}$$

$$v_{\max}(s) = \min \left\{ v_{\max}^{\mathrm{legal}}(s), v_{\max}^{\mathrm{dyn}}(s) \right\}, \tag{B.19}$$

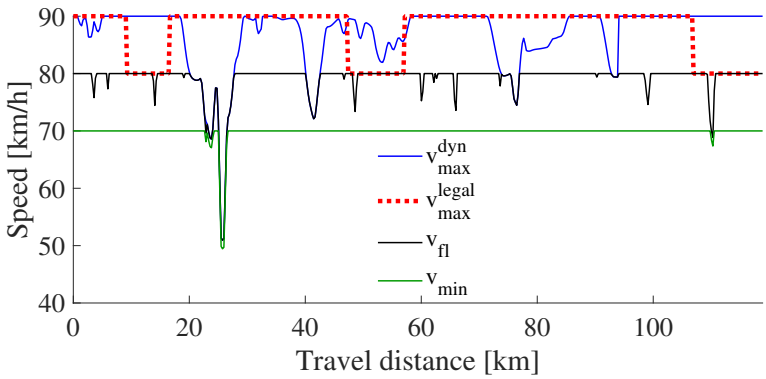

Figure 2: Examples of maximum legal and dynamic speed limits together with minimum allowed speed limit and filtered speed trajectory, v_{fl}. For calculating v_{fl} maximum power (acceleration) capability of the actuator has been considered.

where $v_{\min}^{\text{legal}}$ and $v_{\max}^{\text{legal}}$ are legal speed limits, $v_{\max}^{\text{dyn}}$ is maximum dynamic speed limit, and v_{fl} is a filtered speed that will be discussed later in this section. The legal and dynamic speed limits can be provided by new modern systems, e.g. e-horizon technologies [44]. An illustration of the speed limits are shown in Fig. 2, where the legal speed limits can generally change abruptly for different segments of the driving road, whereas the maximum dynamic speed limit vary smoothly in terms of travel distance. To avoid singularity in (B.6), the vehicle speed is not allowed to drop to zero. However, with the use of variable scaling, very small speed values are acceptable, and the speed may be rounded to zero after the optimisation is finished. This could be useful when short duration traffic stops are to be considered. For longer stops, it could be more convenient to split the trip into two distinct trips, and optimise each individually [45].

To compute the upper bound on travel time, $\mathrm{t_f}$, it is possible to obtain the velocity profile, $v_{\text{fl}}(s) \in [v_{\min}(s), v_{\max}(s)]$, as the average driver's driving cycle, by filtering cruising speed, $\mathrm{v_{cru}} \in [v_{\min}(s), v_{\max}(s)]$. The logistics planner may send $\mathrm{v_{cru}}$ via a telemetry system, or it can be set manually by the driver. The rated power of the actuator and road/traffic limits on speed are taken into consideration in the cruise speed filtering [26], [27], [37]. When deriving v_{fl}, it is assumed that the vehicle will try to maintain $\mathrm{v_{cru}}$ unless instantaneous

dynamic speed limit and/or actuator limit are reached.

$$v_{\text{fl}}(s) = \min \left\{ v_{\max}^{\text{dyn}}, \mathrm{v_{cru}}, \int_0^s \frac{a_{\max}(v_{\text{fl}})}{v_{\text{fl}}(\sigma)} \mathrm{d}\sigma \right\} \tag{B.20}$$

By computing maximum arrival time as

$$\mathrm{t_f} = \int_0^{\mathrm{s_f}} \frac{\mathrm{d}s}{v_{\text{fl}}(s)}, \tag{B.21}$$

where $\mathrm{s_f}$ is the final position at the end of the route, a constraint can be imposed

$$t(\mathrm{s_f}) \leq \mathrm{t_f} \tag{B.22}$$

that requires finishing the route in the same time or sooner than what would be required when driving with v_{fl}.

3.3 MPC for minimising energy consumption

The problem (B.17) is optimised in an MPC framework with a prediction horizon of length s_{H}, aiming at anticipating future events and reacting to disturbances. The main goal of this paper is to develop a computationally efficient algorithm that allows horizons that cover the entire route. However, as computational resources are always limited, we impose an upper bound, $\mathrm{s_{Hmax}}$, hopefully in the range of hundreds of kilometres. The optimisation problem can then be solved in a moving horizon MPC (MHMPC) framework if $\mathrm{s_{Hmax}} < \mathrm{s_f}$, or in a shrinking horizon MPC (SHMPC) framework if $\mathrm{s_{Hmax}} \geq \mathrm{s_f}$. The optimisation variables are predicted at distance samples $s \in [\zeta, \zeta + s_{\mathrm{H}}]$, given information of the actual vehicle's states at ζ. Thus, the actual horizon length can be computed as

$$s_{\mathrm{H}}(\zeta) = \min\{\mathrm{s_{Hmax}}, \mathrm{s_f} - \zeta\}. \tag{B.23}$$

The problem can now be summarised as follows

$$\min_{j,F_{\mathrm{brk}},\gamma} \int_{\zeta}^{\zeta+s_{\mathrm{H}}(\zeta)} \left(\frac{\mathrm{c_{eg}} P_{\mathrm{w}}(E,F,\gamma)}{\sqrt{\frac{2E(s|\zeta)}{\mathrm{m}}}} + \mathrm{w}_1 a^2(s|\zeta) + \mathrm{w}_2 j^2(s|\zeta) \right) \mathrm{d}s, \tag{B.24a}$$

subject to:

$$t'(s|\zeta) = \sqrt{\frac{\mathrm{m}}{2E(s|\zeta)}} \tag{B.24b}$$

$$E'(s|\zeta) = \mathrm{m}a(s|\zeta) \tag{B.24c}$$

$$a'(s|\zeta) = j(s|\zeta) \tag{B.24d}$$

$$F(s|\zeta) = \mathrm{m}a(s|\zeta) + \mathrm{c_a}E(s|\zeta) - F_{\mathrm{brk}}(s|\zeta) + F_{\alpha}(s) \tag{B.24e}$$

$$E(s|\zeta) \in \frac{\mathrm{m}}{2}[v^2_{\min}(s|\zeta), v^2_{\max}(s|\zeta)] \tag{B.24f}$$

$$a(s|\zeta) \in [a_{\min}(E), a_{\max}(E)] \tag{B.24g}$$

$$j(s|\zeta) \in [\underline{\mathrm{j}}, \bar{\mathrm{j}}] \tag{B.24h}$$

$$F_{\mathrm{brk}}(s|\zeta) \in [\underline{\mathrm{F_{brk}}}, 0] \tag{B.24i}$$

$$t(\zeta|\zeta) = t_0(\zeta), \quad E(\zeta|\zeta) = E_0(\zeta), \quad a(\zeta|\zeta) = a_0(\zeta) \tag{B.24j}$$

$$t(\zeta + s_{\mathrm{H}}|\zeta) \leq t_{\mathrm{H}}(\zeta) \tag{B.24k}$$

$$\gamma(s|\zeta) \in \{1, 2, \ldots, \gamma_{\max}\} \tag{B.24l}$$

where $\underline{\mathrm{j}}$ is the minimum and $\bar{\mathrm{j}}$ is the maximum allowed jerk within a comfort zone, t_0, E_0 and a_0 are the values of the system states at instance ζ, and $\gamma_{\max}$ is the highest gear. The constraints (B.24b)-(B.24l) are enforced for all $s \in [\zeta, \zeta + s_{\mathrm{H}}(\zeta)]$ and the problem is re-evaluated for all $\zeta \in [0, \mathrm{s_f}]$. The maximum allowed travel time over the prediction horizon, t_{H}, is computed as in (B.21) for the distance s_{H}. The problem (B.24) is a non-convex, mixed-integer and dynamic nonlinear program, where t, E and a are real-valued state variables, j and F_{brk} are real-valued control inputs, γ is an integer control input and F is an output variable. Although from a control point of view j is the control signal, in practice, a is applied to the vehicle. When solving such computationally complex problem online, reducing the computational time is the major bottleneck, since the online solution must be at least within the up-

date frequency of real-time execution. Thus, we propose several reformulation steps in the following that break down the problem (B.24) into optimisation sub problems, which is solved with significantly reduced computational complexity compared to the original problem.

For the sake of simplicity, the dependence on ζ will not be shown in most following parts of the paper and the method is explained via a single MPC update, e.g. the one with $\zeta = 0$.

4 Computationally Efficient Algorithm

This section proposes three reformulation steps for reducing computational complexity of the problem (B.24). These steps are: 1) formulating a bi-level optimisation program that allows decoupling the integer variable, i.e. gear, from a nonlinear optimisation program (NLP); 2) adjoining nonlinear dynamics of travel time to the objective using necessary PMP conditions for optimality; 3) Removing a loop on finding optimal time costate and applying RTI SQP scheme.

4.1 Bi-level programming and gear optimisation

The mixed-integer problem (B.24) can be reformulated as a bi-level program:

$$\min_{j,F_{\mathrm{brk}}} \int_0^{s_{\mathrm{H}}} \left(\frac{\mathrm{c_{eg}} P_{\mathrm{w}}(E,F,\gamma^*)}{\sqrt{\frac{2E(s)}{\mathrm{m}}}} + \mathrm{w}_1 a^2(s) + \mathrm{w}_2 j^2(s) \right) \mathrm{d}s \tag{B.25a}$$

subject to:(B.24b)-(B.24k)

$$\gamma^*(s) = \arg\min_{\gamma} P_{\mathrm{w}}(E,F,\gamma) \tag{B.25b}$$

$$\text{subject to: } \gamma(s) \in \{1,2,...,\gamma_{\max}\} \tag{B.25c}$$

$$F(s) \in [F_{\gamma\min}(E), F_{\gamma\max}(E)] \tag{B.25d}$$

where the gear optimisation resides only in the bottom level program, while all the system dynamics reside in the top level program. Static modelling of the actuator and transmission system allows separating the bottom level and solving it offline, where v (or E) and F are regarded as parameters, and optimal gear is computed as a function of these parameters. To this end, the

bottom level can be solved as

$$f_\gamma^*(E,F) = \arg\min_\gamma P_\mathrm{w}(E,F,\gamma) \tag{B.26a}$$

$$\text{subject to: } \gamma \in \{1,2,...,\gamma_\mathrm{max}\} \tag{B.26b}$$

$$F \in \mathcal{F}(E) = [F_{\gamma\mathrm{min}}(E), F_{\gamma\mathrm{max}}(E)] \tag{B.26c}$$

$$E \in \mathcal{E}(\gamma) = \frac{\mathrm{m}[\omega_\mathrm{idle}^2, \omega_\mathrm{max}^2]\mathrm{R}^2(\gamma)}{2} \tag{B.26d}$$

where $f_\gamma^*(E,F)$ is a two-dimensional function describing the optimal gear choices for all traction force versus speed (kinetic energy) combinations, $\mathcal{E}$ and $\mathcal{F}$ are the feasible sets for kinetic energy and traction force respectively, and ω_idle and ω_max are rotational speed limits. By replacing the optimal gear with the parametric function, the internal power can be written as

$$P_\gamma(E,F) = P_\mathrm{w}(E,F,f_\gamma^*(E,F)), \tag{B.27}$$

indicating power consumption when gear is optimally chosen. Note that for CV case study the offline-optimised gear selection algorithm is extended, which covers the negative force area originating from negative additional force. More details will be given later in Section 5.

4.2 Necessary PMP conditions for optimality

In the second step of the algorithm, the problem (B.25) is reformulated, which is facilitated by the necessary PMP conditions for optimality. The Hamiltonian is defined as

$$\begin{aligned}\mathcal{H}(\cdot) = \mathrm{c_{eg}} P_\gamma(E,F)\sqrt{\frac{\mathrm{m}}{2E(s)}} + \mathrm{w}_1 a^2(s) + \mathrm{w}_2 j^2(s) + \\ + \lambda_\mathrm{t}(s)\sqrt{\frac{\mathrm{m}}{2E(s)}} + \lambda_E(s)\mathrm{m}a(s) + \lambda_a(s)j(s).\end{aligned} \tag{B.28}$$

where the symbol $\cdot$ is a compact notation for a function of multiple variables. Here, λ_t, λ_E and λ_a denote the costates of travel time, kinetic energy and acceleration, respectively. It can be observed that the Hamiltonian is not an explicit function of travel time, thus the optimal time costate, λ_t^*, i.e. the value for λ_t that satisfies the maximum travel time constraint (B.24k), is a

constant value. Hence

$$\lambda_t'^*(s) = -\left(\frac{\partial \mathcal{H}(\cdot)}{\partial t}\right)^* = 0. \tag{B.29}$$

Furthermore, the travel time is a strictly monotonically increasing function that may activate constraint (B.24k) only at the final instance. Consequently, if λ_t^* is known, it will be possible to remove the nonlinear constraint on travel time (B.25) and adjoin the product of $\lambda_t^*(s)$ and the nonlinear function $\sqrt{\frac{\mathrm{m}}{2E(s)}}$ to the objective function. This implies that the dynamic OCP can yet again be formulated as a bi-level program

$$\min_{\lambda_\mathrm{t}} \int_0^{s_\mathrm{H}} \left(\frac{\mathrm{c_{eg}} P_\gamma(E^*(\lambda_\mathrm{t},s), F^*(\lambda_\mathrm{t},s)) + \lambda_\mathrm{t}}{\sqrt{\frac{2E^*(\lambda_\mathrm{t},s)}{\mathrm{m}}}} + \mathrm{w}_1 a^{*2}(\lambda_\mathrm{t},s) + \mathrm{w}_2 j^{*2}(\lambda_\mathrm{t},s) \right) \mathrm{d}s \tag{B.30a}$$

subject to:

$$t'^*(\lambda_\mathrm{t},s) = \sqrt{\frac{\mathrm{m}}{2E^*(\lambda_\mathrm{t},s)}} \tag{B.30b}$$

$$E'^*(\lambda_\mathrm{t},s) = \mathrm{m} a^*(\lambda_\mathrm{t},s) \tag{B.30c}$$

$$a'^*(\lambda_\mathrm{t},s) = j^*(\lambda_\mathrm{t},s) \tag{B.30d}$$

$$t^*(\lambda_\mathrm{t},0) = t_0, \quad t^*(\lambda_\mathrm{t},s_\mathrm{H}) \leq t_\mathrm{H} \tag{B.30e}$$

$$[j^*(\lambda_\mathrm{t},s), F_\mathrm{brk}^*(\lambda_\mathrm{t},s), F^*(\lambda_\mathrm{t},s)] = \arg\min_{j,F_\mathrm{brk}} \int_0^{s_\mathrm{H}} \left(\frac{\mathrm{c_{eg}} P_\gamma(E,F) + \lambda_\mathrm{t}}{\sqrt{\frac{2E(s)}{\mathrm{m}}}} + \mathrm{w}_1 a^2(s) + \mathrm{w}_2 j^2(s) \right) \mathrm{d}s \tag{B.30f}$$

subject to: (B.24c)-(B.24i), $E(0) = E_0$, $a(0) = a_0$

where all constraints involving travel time have been moved to the top level, while the bottom level, (B.30f), generates optimal control trajectories parameterised in λ_t. Similarly as before, the goal is to separate the two optimisation levels. One way to do this is by trying different values for λ_t and then using search methods, e.g. Newton or bisection, to find λ_t^* that minimises the top level's cost.

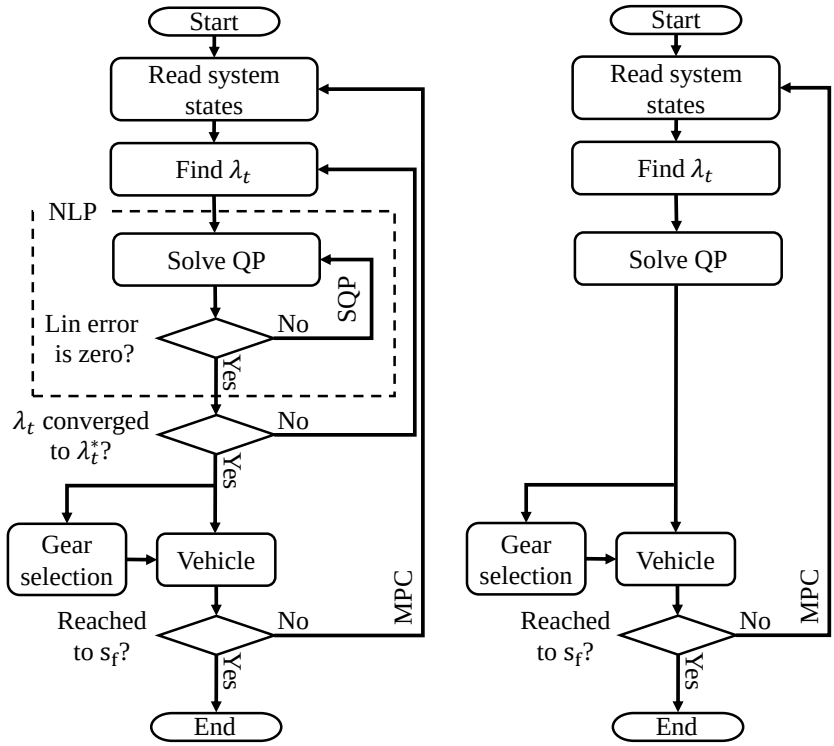

(a) With three nested loops.

(b) Without two innermost loops to solve NLP using SQP, and to find λ^*.

Figure 3: Flowchart of the proposed algorithm to solve NLP in MPC framework.

By assuming that problem (B.30f) is an NLP that can be solved with SQP, the procedure for solving the mixed-integer problem (B.24) will consist of three nested loops as illustrated in Fig. 3a. The outermost loop updates the MPC horizon, the middle loop finds the optimal value for λ_t and the innermost loop sequentially solves a QP in order to find the solution of problem (B.30f) for a given value of λ_t. The procedure is still computationally inefficient, as it requires solving multiple QPs for given multiple λ_t values in each MPC update. Our goal is to eliminate the inner most loops and for a given λ_t, solve only a single QP in each MPC update, as illustrated in Fig 3b.

4.3 Updating the time costate over the MPC loop

To eliminate the loop on finding λ_t^*, it is considered that the optimal energy consumption corresponds in general to driving slow, so it can be assumed that the vehicle will use the entire travel time, i.e. $t^*(\lambda_\mathrm{t}, s_\mathrm{H}) \approx t_\mathrm{H}$. Hence, the objective of the top level program in (B.30) is transformed to minimising maximum travel time difference, as

$$\min_{\lambda_\mathrm{t}} ||t^*(\lambda_\mathrm{t}, s_\mathrm{H}|\zeta) - t_\mathrm{H}(\zeta)|| \tag{B.31}$$

where $||\cdot||$ may indicate any norm.

For the case that the problem (B.30) is solved in SHMPC framework, the final time instance and the final point of the horizon are fixed regardless of the update instance ζ, i.e. $t_\mathrm{H}(\zeta) = \mathrm{t_f}$ and $\zeta + s_\mathrm{H}(\zeta) = \mathrm{s_f}$, $\forall\zeta$.

Lemma 1: *If predicted disturbances do not change and there is no miss-match between the control and plant model, then for an SHMPC implementation of problem* (B.30) *and for a given* λ_t*, it holds,*

$$t^*(\lambda_\mathrm{t}, s_\mathrm{H}|\zeta) = t^*(\lambda_\mathrm{t}, s_\mathrm{H}|\zeta + \delta\zeta), \quad \forall\delta\zeta \in [0, \mathrm{s_f} - \zeta], \tag{B.32}$$

i.e. the optimal travel time at the end of the horizon does not change for different SHMPC updates.

Proof. The proof follows directly from Bellman's principle of optimality, i.e. *any tail of an optimal trajectory is an optimal solution as well* [8]. □

For an MHMPC, Lemma 1 does not hold even if disturbances are predicted exactly and there is no model miss-match. This is because new information is added as the prediction horizon moves forward at each MPC update. However, if the prediction horizon is much longer than the interval between two consecutive updates, then for different ζ, it can be assumed

$$t^*(\lambda_\mathrm{t}, s_\mathrm{H}|\zeta) - t_\mathrm{H}(\zeta) \approx t^*(\lambda_\mathrm{t}, s_\mathrm{H}|\zeta^+) - t_\mathrm{H}(\zeta^+) \tag{B.33}$$

where ζ^+ is the instance of the MHMPC update following that at ζ. Fig. 4 demonstrates the overlapped curves of the final time difference versus the time costate for a CV and an EV, where $\zeta = 0\,\mathrm{m}$ and $\zeta^+ = 300\,\mathrm{m}$. Thus, it is also possible for an MHMPC to update the time costate over the MPC loop.

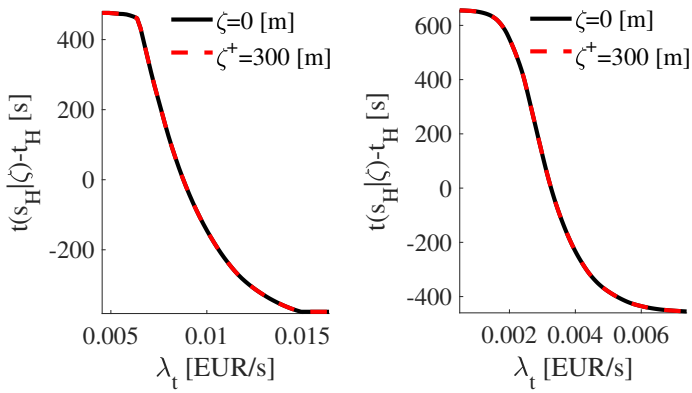

(a) For CV case study. (b) For EV case study.

Figure 4: Difference between calculated time at the end of horizon and the desired maximum time for varying time costate using MHMPC scheme, where $\zeta = 0\,\text{m}$ and $\zeta^+ = 300\,\text{m}$. Overlap of the curves for different ζ values shows that λ_t can be evaluated only once per each MPC update, rather than waiting for a full convergence.

Problem (B.31) is then solved by a derivative free Newton method, where the Newton iterates are spread across the MPC updates without waiting for a full convergence, i.e. by performing one Netwon step per update. A flowchart of the proposed algorithm is depicted in Fig. 3b, while more details on the Newton method is provided in Appendix 1.

4.4 Real-time iterations SQP over the MPC loop

For a given λ_t it remains to solve problem (B.30f). It will be shown later, in Section 5, that for the case of conventional and electric vehicle powertrians, problem (B.30f) is indeed a smooth NLP that can be solved by SQP. However, instead of sequentially solving a QP until linearization error is equal to zero, it is computationally efficient to spread the SQP over MPC updates, which is provided by RTI. The idea is to solve only a single QP per MPC update, without waiting for a full convergence. The obtained solution is possibly sub-optimal, but due to the contractivity of the RTI scheme as shown in [46], the real-time iterates quickly approach the optimal solution during the runtime of the process. Alternative algorithm for real-time solving of the NLPs has been

presented in [47].

As the SQP is stopped prematurely, it is important to show that the obtained solution by solving a single QP is feasible in the original NLP. Feasibility can be guaranteed if the domain of the QP, obtained by linearizing the nonlinear constraints in problem (B.30f), is an inner approximation of the feasible set of the NLP (B.30f). This is indeed the case for conventional and electric vehicle powertrians, which will be shown in Section 5.

5 Application to CV and EV

This section proposes several steps that show how the computationally efficient algorithm proposed in Section 4 is applied to a CV and an EV.

5.1 Conventional vehicle

A conventional powertrain includes an ICE to transform chemical fuel energy to mechanical propulsion energy through a multiple-gear transmission.

A static fuel mass rate map for a given pair of rotational speed and engine torque is obtained by gathering steady-state data from a dynamic simulation model of a diesel engine, presented in [48]. Subsequently, efficiency map and torque limits are derived, see Fig. 5. According to the efficiency isolines, it is desirable to avoid operating the ICE at low speed and torque, where efficiency is low.

Fig. 5 also illustrates a negative torque limit for an additional braking system, including a retarder, a compression release engine brake and/or an exhaust pressure governor. The additional braking is preferred over the service braking in order to reduce wear and avoid lock up of the braking pads. Using (B.10), the negative torque is translated to negative force on the wheel side as

$$F_{\mathrm{brk}} = F_{\mathrm{A}} + F_{\mathrm{S}}, \tag{B.34}$$

where F_{S} and F_{A} are forces by the service brakes and the additional braking system. The minimum negative additional force limit for a given kinetic energy is

$$F_{\mathrm{Amin}}(E) = \min_{\gamma} F_{\gamma \mathrm{A}}(E, \gamma) \tag{B.35}$$

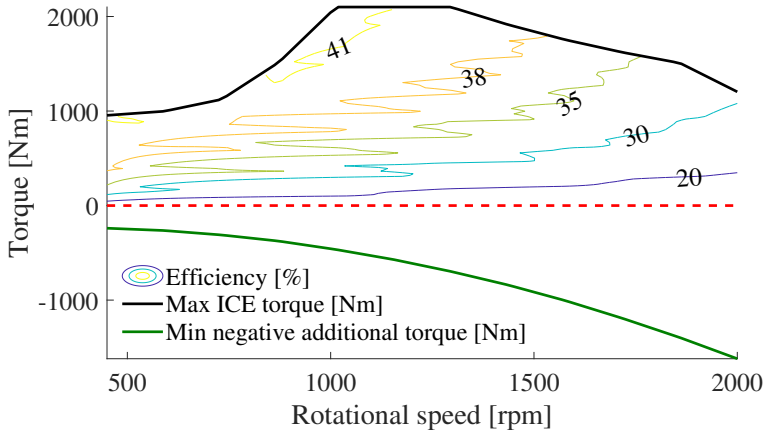

Figure 5: Steady-state efficiency map and maximum torque limit of the ICE. The negative torque limit illustrates the braking capability of the additional braking system that includes a retarder, an exhaust pressure governor and/or a compression release engine brake.

where $F_{\gamma \mathrm{A}}$ denotes the minimum negative additional force for each gear. The lower bound on the traction force is zero, i.e. $F_{\gamma \min}(E) = 0$.

The two-dimensional fuel mass rate map of the ICE translates to a three-dimensional map on the wheels side. This three-dimensional map, denoted as $\mu_{\mathrm{w}}(E, F, \gamma)$, can be expressed in terms of kinetic energy, traction force and gear using (B.5) and (B.10). Subsequently, a map, which represents the parametric internal power function, $P_{\mathrm{w}}(E, F, \gamma)$, can be derived as

$$P_{\mathrm{w}}(E, F, \gamma) = \mu_{\mathrm{w}}(E, F, \gamma) Q_{\mathrm{lhv}} \tag{B.36}$$

where Q_{lhv} is diesel heating value.

The bi-level program (B.25), can be extended for a CV case study, including the negative force region, which originates from the summation of negative additional force and service braking force, as

$$\min_{j, F_{\mathrm{brk}}} \int_0^{s_{\mathrm{H}}} \left(\frac{\mathrm{c_{eg}} P_{\mathrm{w}}(E, F, \gamma^*)}{\sqrt{\frac{2E(s)}{\mathrm{m}}}} + \mathrm{w}_1 a^2(s) + \mathrm{w}_2 j^2(s) \right) \mathrm{d}s \tag{B.37a}$$

subject to: (B.24b)-(B.24k)

$$\gamma^*(s) = \begin{cases} \arg\min_\gamma P_{\mathrm{w}}(E, F, \gamma), & \text{if } F + F_{\mathrm{brk}} \geq 0. \\ \arg\max_\gamma F_{\gamma \mathrm{A}}(E, \gamma), & \text{if } F_{\mathrm{Amin}}(E) \leq F + F_{\mathrm{brk}} < 0 \\ \arg\min_\gamma F_{\gamma \mathrm{A}}(E, \gamma), & \text{if } \underline{\mathrm{F}_{\mathrm{brk}}} \leq F + F_{\mathrm{brk}} < F_{\mathrm{Amin}}(E) \end{cases} \tag{B.37b}$$

$$\text{subject to: } \gamma(s) \in \{1, 2, ..., \gamma_{\max}\} \tag{B.37c}$$

$$F(s) + F_{\mathrm{brk}}(s) \in [\underline{\mathrm{F}_{\mathrm{brk}}}, F_{\gamma \max}(E)] \tag{B.37d}$$

Note that the traction force, F, and the total braking force, F_{brk}, cannot have non-zero values simultaneously, i.e. it is not the case that $F > 0$ and $F_{\mathrm{brk}} < 0$ at the same time.

To approach the offline-optimal gear selection problem (B.37), it is possible to grid the feasible sets of kinetic energy and total force, i.e. $F + F_{\mathrm{brk}}$. To this end, in the positive force region, for any feasible combination of longitudinal velocity (kinetic energy) and traction force, the optimal gear is the one that minimises energy consumption. In the negative force region, if the total demanded force is higher than the minimum negative additional force, the highest possible gear is selected, which avoids unnecessary down-shifting. However, if total demanded force is lower than the minimum negative additional force, the lowest possible gear is selected, since it provides the most possible negative additional force, see Fig. 6. The remaining demanded negative force is covered by the service brakes.

The optimal brake specific fuel consumption (BSFC) map and maximum traction force curve are depicted in Fig. 7. The optimal BSFC refers to the minimum burnt fuel, which is obtained by optimising the internal power in (B.27).

The internal power drawn from fuel using (B.27), is approximated by the following expression

$$P_\gamma(v, F) \approx \mathrm{p}_{\mathrm{e}0} + \mathrm{p}_{\mathrm{e}1} v^3(s) + \mathrm{p}_{\mathrm{e}2} v(s) F(s) \tag{B.38}$$

with $\mathrm{p}_{\mathrm{e}0}, \mathrm{p}_{\mathrm{e}1}, \mathrm{p}_{\mathrm{e}2} \geq 0$. During a single driving mission, the parameters $\mathrm{p}_{\mathrm{e}0}, \mathrm{p}_{\mathrm{e}1}$ and $\mathrm{p}_{\mathrm{e}2}$ are assumed constant, otherwise we will need to apply robust control methods to tackle possible uncertainties.

As illustrated in Fig. 8, for the studied engine model it is sufficient to use a first order term in F, although it is possible to include higher order

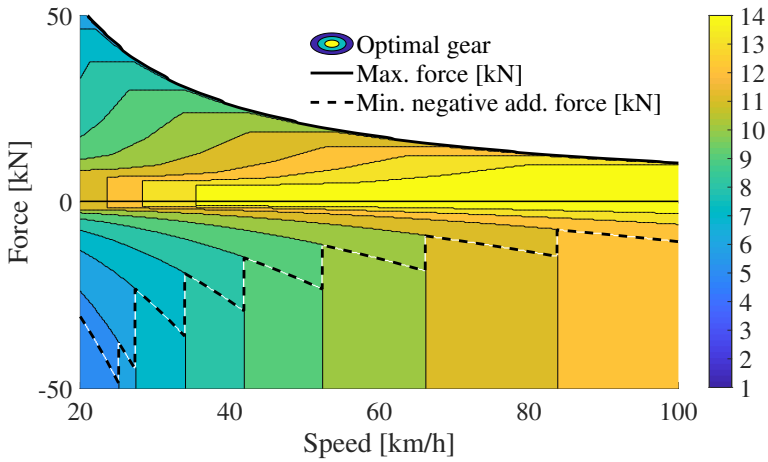

Figure 6: Offline-optimised gear map together with maximum traction force and minimum negative additional force. In the positive force region, the optimal selected gear is the one that minimises fuel consumption, which for the studied powertrain coincides with the highest feasible gear. In the negative force region, if the total force is lower than the minimum negative additional force, the lowest possible gear is selected, since it provides the most possible negative additional force. The remaining demanded negative force is covered by the service brakes. However, if the total force is higher than the minimum negative additional force, to avoid unnecessary down-shifting, the highest possible gear is selected.

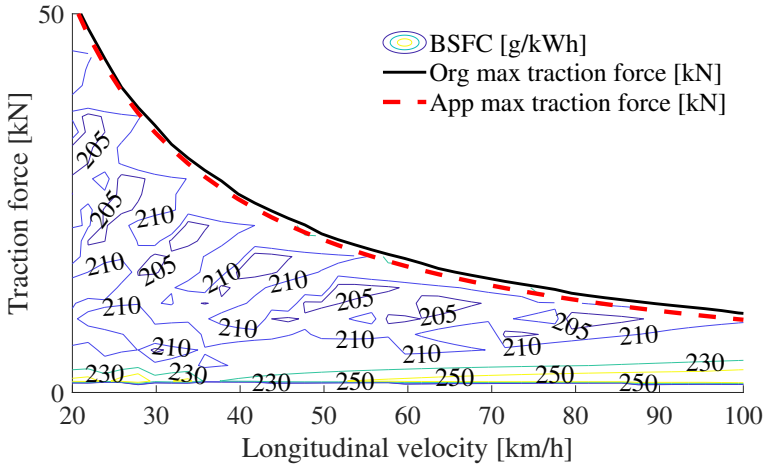

Figure 7: Offline-optimised BSFC map together with original and approximate maximum traction force as well as minimum negative additional force. The approximate limit is an inner approximation for the longitudinal velocities above 8 km/h.

terms as well, without significant increase in computational effort. Similar expressions for model abstraction of fuel mass rate are exploited in [26] and several references therein. Using (B.5) and (B.38), the stage cost (B.30f) transforms into

$$V_{\mathrm{CV}}(\cdot,\lambda_{\mathrm{t}}) \approx \frac{\mathrm{c_{eg}}(\mathrm{p_{e0}}+\lambda_{\mathrm{t}}^{*})\sqrt{\mathrm{m}}}{\sqrt{2E(s)}} + \frac{2\mathrm{p_{e1}}}{\mathrm{m}}E(s) + \\ + \mathrm{p_{e2}}F(s) + \mathrm{w_1}a^2(s) + \mathrm{w_2}j^2(s) \tag{B.39}$$

which is a convex second order cone function in terms of E, a, j, F and F_{brk}.

The maximum traction force limit, see Fig. 7, is approximated by

$$F_{\gamma\max}(E) \approx \min\left\{\overline{F}, \mathrm{y_0} + \frac{\mathrm{y_1}\sqrt{\mathrm{m}}}{\sqrt{2E(s)}}\right\} \tag{B.40}$$

where $\overline{F}$ is the maximum constant traction force, and $\mathrm{y_1}$ resembles the maximum engine power, as it can be alternatively written as a division of power with vehicle speed. The coefficients $\mathrm{y_0}$ and $\mathrm{y_1}$ are obtained by solving a linear

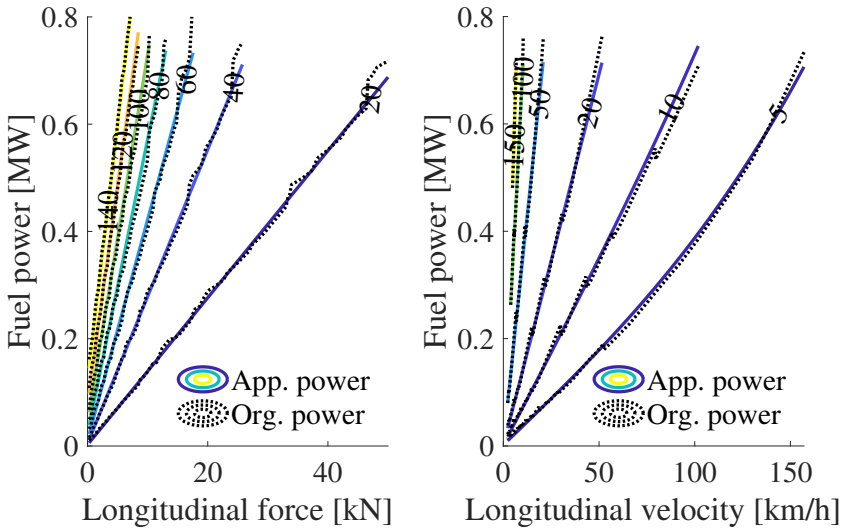

(a) Internal power versus longitudinal force for a given longitudinal velocity.

(b) Internal power versus longitudinal velocity for a given longitudinal force.

Figure 8: Original and approximated internal power drawn from fuel for a given longitudinal velocity and traction force.

program, see Appendix 2 for details. The approximated force limit (B.40) is an inner approximation of the original force for speeds above 8 km/h, see Fig. 7, which is acceptable for the highway scenarios investigated in this paper.

The problem (B.30) with the stage cost (B.39) is non-convex nonlinear program, because of the nonlinear term $\mathrm{y}_1/\sqrt{E(s)}$ in (B.40). Due to the sign of $\mathrm{y}_1 \geq 0$, this term is a convex function (a convex problem, though, requires a concave function here). It is possible to transform (B.30) to a convex second order cone program (SOCP) by linearizing the maximum force limit in (B.40). Note that linearizing any convex function about any trajectory, is always an inner approximation. Since the inner approximation is conservative, it is guaranteed that despite possibly being sub-optimal, all obtained solutions (if such solutions exist) are also feasible in the original non-convex problem. For more details, see Appendix 3.

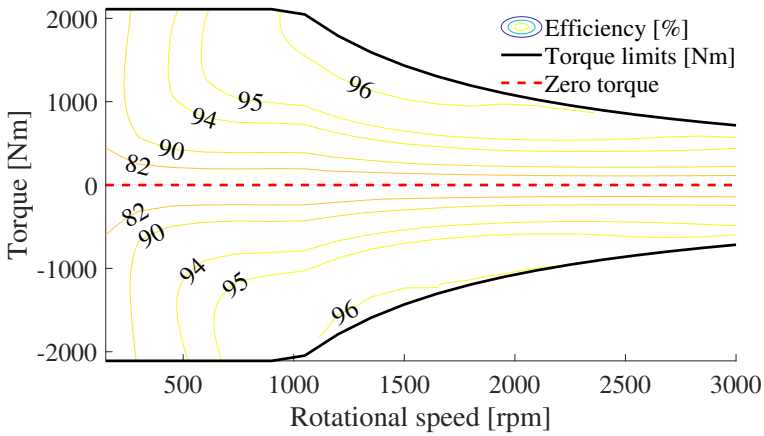

Figure 9: Steady-state efficiency map of EM together with shaft torque limits.

5.2 Fully electric vehicle

In the fully electric powertrain, the EM converts electricity to mechanical power in motoring mode, whereas it converts mechanical power to electricity in generating mode of operation. In the generating mode, the energy is recuperated and stored in the electric battery, when decreasing kinetic energy by braking or decreasing potential energy while rolling downhill. Note that the electric powertrain is assumed to have a single-gear transmission system.

For a given pair of rotational speed and torque, EM efficiency map is shown in Fig. 9, using static internal electric battery power. In Fig. 9, positive and negative torque regions correspond to the motoring and the generating modes of operation, respectively.

It is assumed that a single-gear transmission system conveys the power from the battery to the wheels. Therefore, there is no need for offline gear optimisation, i.e. $P_\gamma(v, F) = P_{\mathrm{w}}(v, F, \gamma)$.

The internal power drawn from the electric battery is approximated by the following expression

$$\begin{aligned} P_\gamma(v, F) \approx {} & \mathrm{p}_{\mathrm{m}0} + \mathrm{p}_{\mathrm{m}1} v^3(s) + \mathrm{p}_{\mathrm{m}2} v(s) F(s) + \\ & + \mathrm{p}_{\mathrm{m}3} v(s) F^2(s) \end{aligned} \tag{B.41}$$

with $\mathrm{p}_{\mathrm{m}0}, \mathrm{p}_{\mathrm{m}1}, \mathrm{p}_{\mathrm{m}2}, \mathrm{p}_{\mathrm{m}3} \geq 0$. Fig. 10 demonstrates that the approximated

model describes well the original internal battery power.

Using (B.5), (B.9) and (B.41), the stage cost (B.30f) transforms into

$$V_{\mathrm{EV}}(\cdot,\lambda_{\mathrm{t}}) \approx \frac{\mathrm{c_{eg}}(\mathrm{p_{m0}}+\lambda_{\mathrm{t}}^{*})\sqrt{\mathrm{m}}}{\sqrt{2E(s)}} + \frac{2\mathrm{p_{m1}}}{\mathrm{m}}E(s) + \mathrm{p_{m2}}F(s) + \\ + \mathrm{p_{m2}}F^{2}(s) + \mathrm{w_1}a^{2}(s) + \mathrm{w_2}j^{2}(s). \tag{B.42}$$

The traction force limits, see Fig. 11, are approximated by

$$F_{\gamma\min}(E) \approx \max\left\{\underline{F}, \mathrm{x_0} + \frac{\mathrm{x_1}\sqrt{\mathrm{m}}}{\sqrt{2E(s)}}\right\} \tag{B.43}$$

$$F_{\gamma\max}(E) \approx \min\left\{\overline{F}, \mathrm{y_0} + \frac{\mathrm{y_1}\sqrt{\mathrm{m}}}{\sqrt{2E(s)}}\right\} \tag{B.44}$$

where $\underline{F}$ and $\overline{F}$ are constant traction force limits. The coefficients $\mathrm{x_0}$ and $\mathrm{x_1}$, similar to the $\mathrm{y_0}$ and $\mathrm{y_1}$, are the solution of the linear program given in Appendix 2.

According to the signs of $\mathrm{x_1} \leq 0$ and $\mathrm{y_1} \geq 0$, the term $\mathrm{x_1}/\sqrt{E(s)}$ is a concave function and $\mathrm{y_1}/\sqrt{E(s)}$ is a convex function. Thus, the area between the two force limits (B.43) and (B.44) include a concave force set, which leads the problem (B.30) with the stage cost (B.42) to be a non-convex nonlinear program. By linearizing the force limits, the problem (B.30) with the stage cost (B.42) can be formulated as a convex SOCP, see Appendix 3. Note that linearizing any convex function about any trajectory, is always an inner approximation, and linearizing any concave function about any trajectory, results in an outer approximation. Furthermore, the approximations are conservative, therefore, all obtained solutions are inside the feasible force area, see Fig. 11, and also feasible in the original non-convex problem.

6 Results

In this paper, simulations are carried out for the CV and the EV over the 118 km long road from Södertälje to Norrköping in Sweden, which is the same route as considered in [49]. The problems (B.66) and (B.70) are discretized using the forward Euler method. The problems are solved in an SHMPC

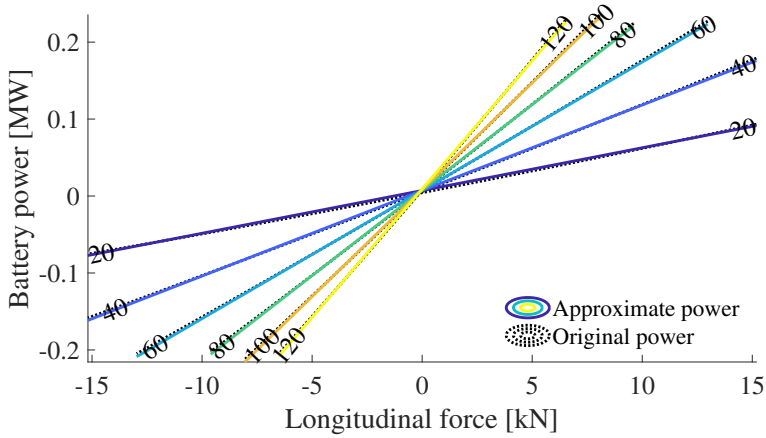

Figure 10: Original and approximated internal power drawn from the electric battery for a given longitudinal velocity and traction force.

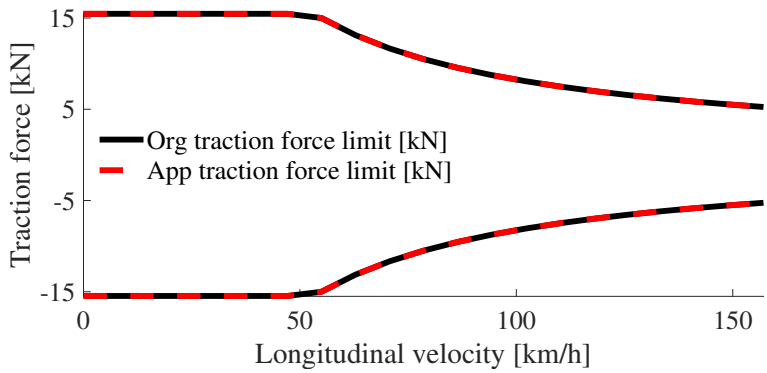

Figure 11: Original and approximated traction force limits of the EM.

Table 1: Simulation parameters

Gravitational acceleration	$g = 9.81\,\mathrm{m/s^2}$
Air density	$\rho = 1.29\,\mathrm{kg/m^3}$
Vehicle frontal area	$A_f = 10\,\mathrm{m^2}$
Rolling resistance coefficient	$c_r = 0.006$
Vehicle mass	$m = 40\,000\,\mathrm{kg}$
Aerodynamic drag coefficient	$c_d = 0.5$
Wheel radius	$r_w = 0.50\,\mathrm{m}$
Final gear ratio	$r_{fg} = 3$
Cruising set speed	$v_{cru} = 80\,\mathrm{km/h}$
Route length	$118\,\mathrm{km}$
Number of samples	$N = 500$
Fuel cost	$c^f_{eg} = 1.51\,\mathrm{EUR/litre}$
Electricity cost	$c^e_{eg} = 0.18\,\mathrm{EUR/kWh}$

framework, i.e. $s_{Hmax} \geq s_f$, where travel time at the final position (end of the route) is upper bounded by t_f, using (B.21). The simulation parameters are given in Table 1.

Within the simulations we investigate: (1) sensitivity analysis to evaluate the impact of sampling interval on the solution of the proposed algorithm; (2) how optimisation cost and optimal speed profile change for different discomfort penalties; (3) convergence properties of the algorithm; (4) computation time as a function of the number of samples in the horizon.

6.1 Sampling interval impact on total cost

To investigate the sampling interval's impact on the total cost (B.25a), we calculate normalised relative cost error for varying number of samples, as

$$\mathrm{rel}_{\mathrm{error}} = \frac{\mathrm{cost}^N_{\mathrm{tot}} - \mathrm{cost}^{1200}_{\mathrm{tot}}}{\mathrm{cost}^{1200}_{\mathrm{tot}}}, \tag{B.45}$$

for $N \in [200, 1200]$ samples, where $\mathrm{cost}^N_{\mathrm{tot}}$ and $\mathrm{cost}^{1200}_{\mathrm{tot}}$ are the total cost calculated for a sampling number of N and 1200, respectively. Note that the obtained total cost value for the finest mesh, i.e. with $N = 1200$, is the most accurate among the investigated meshes. It is observed in Fig. 12 that the

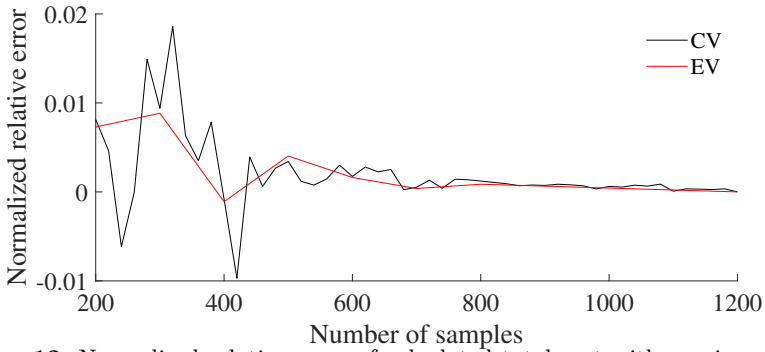

Figure 12: Normalised relative error of calculated total cost with varying number of samples. For number of samples equal to or greater than 500, the normalised relative cost error is less than 0.5 %.

normalised relative cost error is less than 0.5 % for number of samples equal to or greater than 500. Thus, in the rest of the investigations we choose the number of samples equal to 500, i.e. the sampling interval is kept at 238 m as the finer mesh for most of the simulations, unless stated otherwise.

6.2 Energy consumption vs. drivability

To study the cost components, i.e. energy cost and the cost due to penalising discomfort, we compare three case studies: Case$^{\text{fl}}$ corresponds to a case with the filtered speed, v_{fl}, which corresponds to the average driver's driving cycle. For this case, the stage costs, (B.66) and (B.70) are calculated using (B.5), (B.7) and (B.8). In Case 1, i.e. performance drive, the jerk penalty term in (B.66) and (B.70) is kept to zero; and in Case 2, i.e. comfortable drive, non-zero jerk penalty factor is used in (B.66) and (B.70). As an index to measure drivability, the root mean square (RMS) value of jerk

$$j_{\text{RMS}} = \sqrt{\frac{1}{\text{s}_\text{f}} \int_0^{\text{s}_\text{f}} j^2(s)\text{d}s} \tag{B.46}$$

is used. Note that we have observed the smooth speed profile could be achieved by only penalising jerk, thus the penalty coefficient on the acceleration, w_1, is always kept to be zero for all three cases.

There is a trade-off between the energy cost and comfort, i.e. lower values of

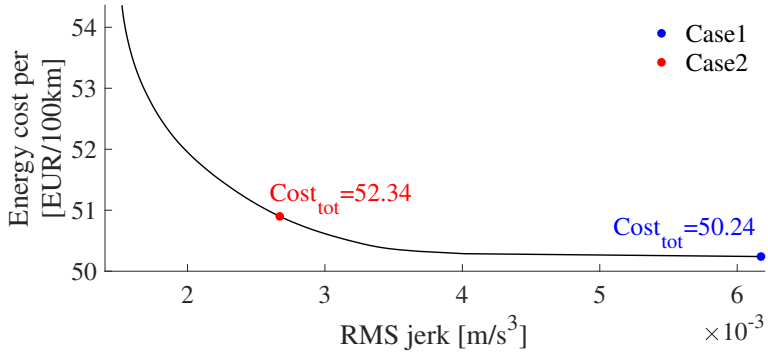

(a) Fuel cost vs. RMS jerk.

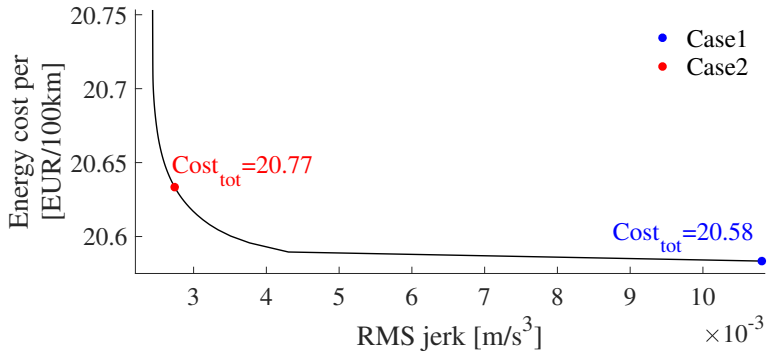

(b) Electricity cost vs. RMS jerk.

Figure 13: Energy cost investigation for different jerk penalty factors. For the large penalty factors, RMS jerk is saturated.

RMS jerk yield higher energy cost, see Fig. 1.13(a) and Fig. 1.13(b) for such trade-off for the CV and the EV respectively. Thus, vehicle manufacturers have wide range of choice to customise the vehicle's performance for a desired energy use and comfort. Note that RMS jerk saturates for large jerk penalty factors. Hereafter, the jerk penalty term in Case 2 is selected in a way that the RMS jerk is equal to $0.0027\,\mathrm{m/s^3}$ for the CV and the EV.

Optimal longitudinal velocity, acceleration and jerk profiles of Case 1 and Case 2 for the CV and the EV are demonstrated in Fig. 14. The velocity profiles without discomfort penalty, i.e. Case 1, are saw-tooth shaped and

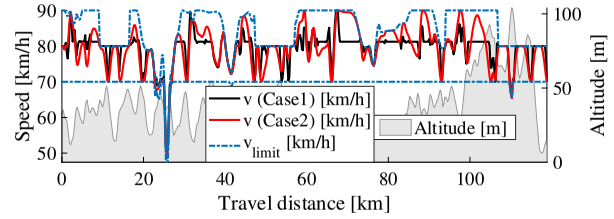

(a) Longitudinal velocity trajectories of CV.

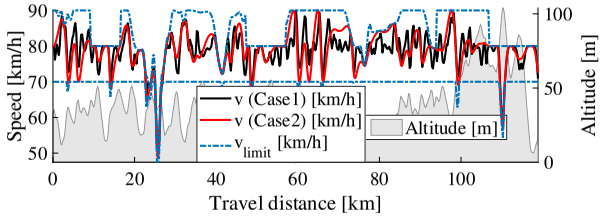

(b) Longitudinal velocity trajectories of EV.

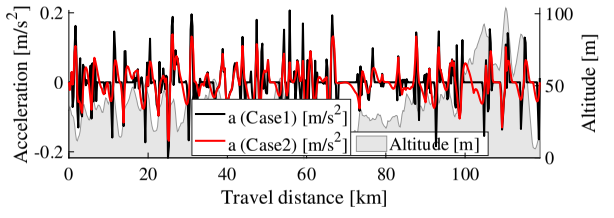

(c) Acceleration trajectories of CV.

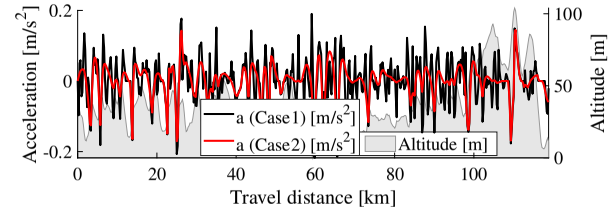

(d) Acceleration trajectories of EV.

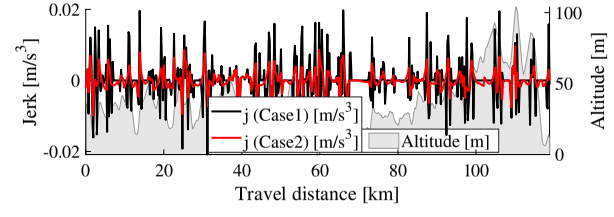

(e) Jerk trajectories of CV.

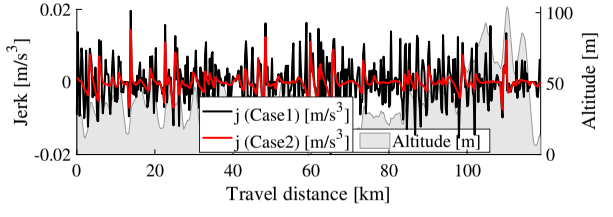

(f) Jerk trajectories of EV.

Figure 14: Optimal longitudinal velocity, acceleration and jerk trajectories for CV and EV. Case 2, i.e. which corresponds to comfortable drive, provides smoother profile and more comfortable driving. Thus, the amplitude of fluctuating acceleration and jerk is decreased.

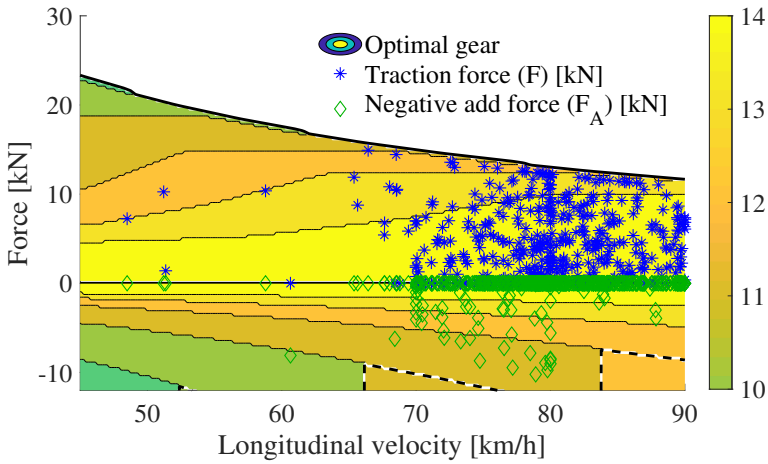

(a) Operating force-speed points of the CV and optimal gear as a contour map.

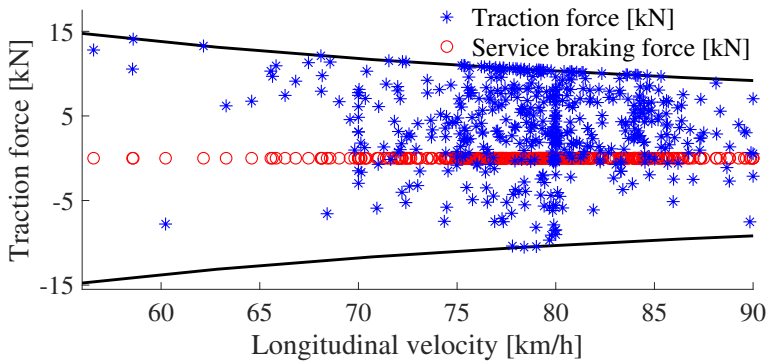

(b) Optimal force-speed points of the EV.

Figure 15: Optimal longitudinal forces vs. vehicle speed for Case 2, i.e. when jerk is penalised.

leads to more aggressive way of driving, however, the latter case provides smoother and more comfortable driving, see Fig. 1.14(a) and Fig. 1.14(b). Note that in addition to the RMS jerk, the RMS acceleration is also reduced in Case 2 compared to Case 1 for the CV and the EV, whereas the acceleration is not penalised in either cases, see Fig. 1.14(c), Fig. 1.14(d), 1.14(e) and Fig. 1.14(f).

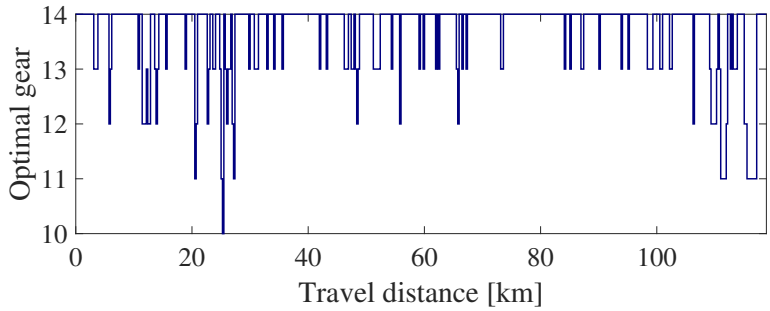

(a) Optimal gear trajectory.

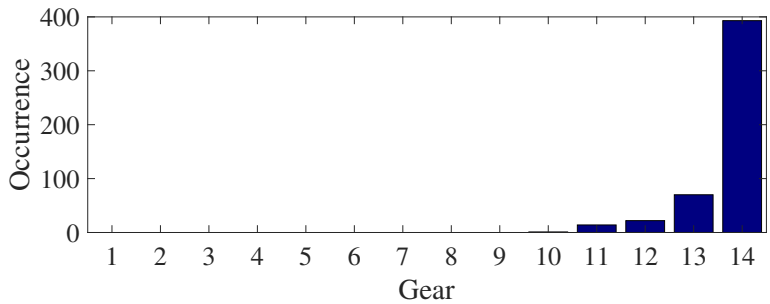

(b) Optimal gear occurrence.

Figure 16: Optimal gear profiles of CV for Case 2, i.e. which corresponds to comfortable drive. The most frequent selected gear is $\gamma = 14$.

Optimal traction and braking force points for the Case 2, i.e. comfortable drive, of CV and EV are shown in Fig. 15. Also, according to the optimal gear map in Fig. 6, for a pair of total force and longitudinal velocity, the optimal gear is chosen. The optimised gear trajectory and distribution are shown in Fig. 16, where the most frequently selected gear is $\gamma = 14$. We have observed similar results for Case 1 as well.

The cost results of the whole driving mission and their corresponding RMS jerk values for all three case studies of the CV and the EV are given in Table 2.

For the CV, the most fuel-efficient case is Case 1. There is a benefit of 11.60 % to optimize the velocity profile compared to the Case$^{\text{fl}}$, whereas the discomfort of the performance drive is accepted. Furthermore, the results

Table 2: Simulation results, energy consumption vs. drivability

CV			
Variable	Case$^{\text{fl}}$	Case 1	Case 2
Fuel cost [EUR]	65.33	59.72	60.50
Drivability cost [EUR]	2.23	0	1.71
Total cost [EUR]	67.56	59.72	62.21
Improvement [%]	-	11.60	7.92
j_{RMS} [m/s^3]	0.0026	0.0062	0.0027
$\|\|F_{\text{brk}}\|\|$ [kN]	49.46	35.27	34.07
EV			
Variable	Case$^{\text{fl}}$	Case 1	Case 2
Electricity cost [EUR]	24.55	24.47	24.52
Drivability cost [EUR]	1.68	0	0.56
Total cost [EUR]	26.23	24.47	24.69
Improvement [%]	-	6.71	5.87
j_{RMS} [m/s^3]	0.0038	0.0108	0.0027
$\|\|F_{\text{brk}} + \min(F, 0)\|\|$ [kN]	49.15	34.25	40.94

show 7.92 % reduction in total cost of Case 2 compared to the Case$^{\text{fl}}$, despite having 1.30% increase in fuel consumption compared to Case 1. As it has been expected, the proposed algorithm minimises the braking at the pads, i.e. the braking in Case 1 and Case 2 is significantly reduced compared to Case$^{\text{fl}}$.

For the EV, Case 1 provides 6.71% reduction of the total energy cost compared to Case$^{\text{fl}}$ and the total cost benefit of Case 2 is 5.87% compared to Case$^{\text{fl}}$. The comfortable drive, i.e. Case 2, leads to 0.20% increase in electricity usage compared to the performance drive, i.e. Case 1. The RMS jerk in Case 2 is reduced by 29% compared to Case$^{\text{fl}}$, i.e. the RMS jerk is reduced from 0.0038 m/s^3 to 0.0027 m/s^3.

6.3 Algorithm convergence

The convergence curve of the time costate versus shrinking prediction horizon length is shown in Fig. 17. According to the algorithm given in Appendix 1, the time costate is updated once per each MPC stage rather than waiting for the full costate convergence. It can be observed that after few initial MPC stages, the time costate converges to its optimum value. The disturbance rejection

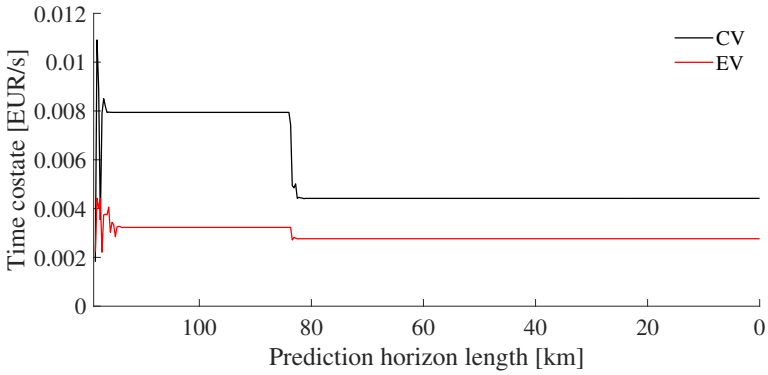

Figure 17: Travel time costate vs. prediction horizon length. The costate converges after few MPC updates, even after disturbance is introduced (at horizon length of 85 km) by suddenly increasing maximum travel time, e.g. due to traffic congestion.

properties of the algorithm are verified in Fig. 17. At the prediction horizon of 85 km, maximum travel time changes due to e.g. traffic congestion. It can be seen in Fig. 17 that the travel time costate converges to its new value, which leads the vehicle to arrive to the final position within the updated maximum travel time.

The convergence profile of the SQP algorithm is depicted in Fig. 18, where the algorithm converges to an optimum obtained by solving (B.30) in 5 iterations for both CV and EV case studies. Note that the cost value drops to within 0.4% from the optimum value in the first iteration. We exploit this behaviour through RTI in SHMPC framework, where only one QP is solved in each MPC update rather than waiting for the full SQP convergence, since the cost value in the first iteration is very close to the local optimum. Note that the cost value in iteration 0 is calculated when the vehicle is driving with the initial estimated trajectory, v_{fl}.

6.4 Computation time

The computation time profile for various sampling intervals is depicted in Fig. 19, where each QP in the SQP scheme is solved using HPIPM, known as a high-performance tool for solving QPs [50]. Here, the entire route, 118 km, is considered as the prediction horizon. The optimisation was run on a laptop

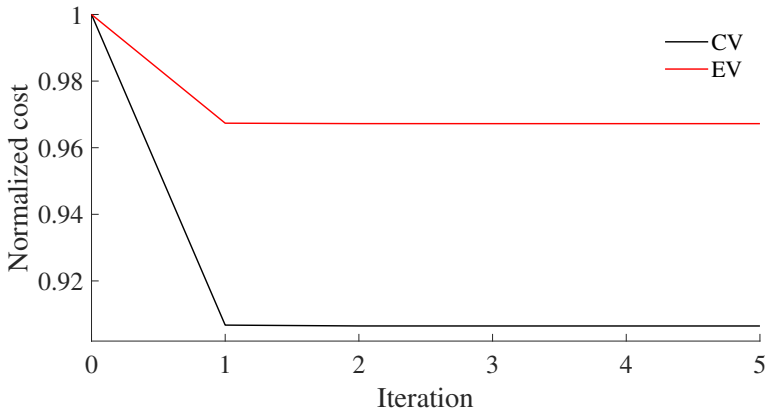

Figure 18: SQP convergence profile. The cost value drops to within 0.4% from optimum value in the first iteration. In iteration 0 the cost value is calculated when the vehicle is driving with the initial estimated trajectory, v_{fl}.

PC with 6600K CPU at 2.81GHz and 16GB RAM. The trend is that as the number of samples increases, the computation time also increases. For real-time applications, it is preferable to have small sampling interval, however the information on the topography should not be lost. In subsections 6.2 and 6.3, the number of samples is kept to 500 and the corresponding computation time for solving the problems (B.66) and (B.70) is less than 20ms, which is considerably low value for a horizon of 118 km with the sampling interval of 238 m.

7 Conclusion

In this paper a computationally efficient algorithm is proposed for eco-driving over long look-ahead horizons. To this end, a bi-level program is formulated, where integer variable, i.e. gear, is decoupled from the real-valued variables. In the bottom level, the optimal gear map is derived in a way that the total energy consumption is minimised. In the top level, the remaining online implementable NLP is formulated. To provide more comfortable way of driving, acceleration and jerk of the vehicle are penalised in the top level's objective. In the NLP, the dynamics on travel time is adjoined to the objective function,

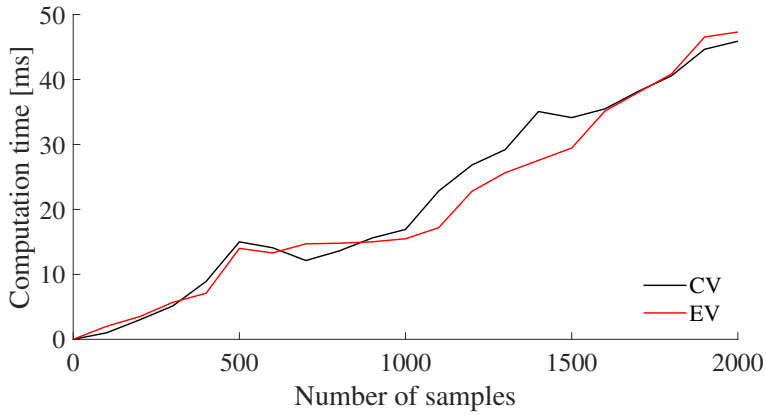

Figure 19: Computation time vs. prediction horizon length using HPIPM for various resolutions of the prediction horizon. The computation time increases linearly with the number of samples.

using the necessary PMP conditions for optimality, since: 1) the Hamiltonian is not an explicit function of the travel time; 2) the travel time is strictly monotonically increasing function; and 3) the constraint on final time may activate at the final instance. The NLP is solved by applying RIT SQP scheme in MPC framework, i.e. the time costate and the linearization trajectory are updated once per each MPC update. The proposed algorithm is applied to a CV and an EV using SHMPC framework.

According to the simulation results, there is a trade-off between cost and comfort, i.e. driving comfortably is more expensive compared to the performance drive. The energy increase because of penalising the driver's discomfort is 1.30% and 0.20% for the CV and EV, respectively, where the RMS jerk is kept to $0.0027\,\mathrm{m/s^3}$. Also, by using the proposed algorithm, the total cost is reduced up to 11.60% and 7.92% for the CV and EV, respectively, compared to the average driver's driving cycle. The computation time for the horizon of 118 km is 20 ms, the sampling interval is equal to 238 m. For on-line applications, the small computation time can enhance the optimality, since the suggested optimal state of vehicle can be updated more frequently. Also, in off-line analysis the small computation time can be applied to multi-path problems, where the optimal path of the driving vehicle in terms of energy consumption can be obtained within a small amount of time. The presented

algorithm in this paper can also be applied to HEVs as well, where the battery discharge trajectory is generated by the eco-driving supervisor and delivered to lower control layers to charge depleting or charge sustaining operation.

1 Newton method for finding optimal time costate

In this paper, a modified Newton method is applied to find the λ_{t}^{*}. Let

$$f(\lambda_{\mathrm{t}}|\zeta) = t^{*}(\lambda_{\mathrm{t}}, s_{\mathrm{H}}|\zeta) - t_{\mathrm{H}}(\zeta). \tag{B.47}$$

The rule for updating λ_{t} is

$$\lambda_{\mathrm{t}}(\zeta^{+}) = \lambda_{\mathrm{t}}(\zeta) - \frac{f(\lambda_{\mathrm{t}}|\zeta)}{\tilde{f}^{'}(\lambda_{\mathrm{t}}|\zeta)} \tag{B.48}$$

with

$$\tilde{f}^{'}(\lambda_{\mathrm{t}}|\zeta) = \min_{\lambda_{\mathrm{t}}} \left\{ f^{'}(\lambda_{\mathrm{t}}|\zeta), f^{'}_{\max} \right\}, \tag{B.49}$$

$$f^{'}(\lambda_{\mathrm{t}}|\zeta) = \frac{f(\lambda_{\mathrm{t}}|\zeta) - f(\lambda_{\mathrm{t}}|\zeta^{+})}{\lambda_{\mathrm{t}}(\zeta) - \lambda_{\mathrm{t}}(\zeta^{+})}, \tag{B.50}$$

$$f^{'}_{\max} = \frac{f_{\max} - f_{\min}}{\lambda_{\mathrm{t}}^{\min} - \lambda_{\mathrm{t}}^{\max}} \tag{B.51}$$

where $\lambda_{\mathrm{t}}^{\min} = 0\mathrm{EUR}/s$ is the minimum and $\lambda_{\mathrm{t}}^{\max}$ is the maximum time costate. Also, $f_{\min}$ and $f_{\max}$ are

$$f_{\min} = t^{*}(\lambda_{\mathrm{t}}^{\max}, s_{\mathrm{H}}|\zeta) - t_{\mathrm{H}}(\zeta), \tag{B.52}$$

$$f_{\max} = t^{*}(\lambda_{\mathrm{t}}^{\min}, s_{\mathrm{H}}|\zeta) - t_{\mathrm{H}}(\zeta). \tag{B.53}$$

To speed up the convergence to λ_{t}^{*} in (B.48), it is possible to warm start the algorithm by initialising λ_{t} at two consecutive instances $\zeta = 0$ and $\zeta = 0^{+}$, as

$$\lambda_{\mathrm{t}}(0) = \lambda_{\mathrm{t}}^{\min} - \frac{f_{\max}}{f^{'}_{\max}} \tag{B.54}$$

$$\lambda_{\mathrm{t}}(0^{+}) = \lambda_{\mathrm{t}}(0) - \frac{f(\lambda_{\mathrm{t}}|0)}{f^{'}_{\max}}. \tag{B.55}$$

where $\lambda_\mathrm{t}(0)$ is simply the intersection point of $f(\lambda_\mathrm{t}|0) = 0$ with a line connecting the two points $(\lambda_\mathrm{t}^{\min}, f_{\max})$ and $(\lambda_\mathrm{t}^{\max}, f_{\min})$.

2 Inner approximation of traction force limits

To approximate the force limits as inner approximations of the original nonlinear and non-smooth limits, a linear program is solved as:

$$\begin{aligned} &J = \min_x \left(f^T x\right) \\ &\text{subject to} \\ &Ax \leq b \end{aligned} \tag{B.56}$$

such that the area between actual force limits and their approximations is minimised. Therefore, the area between the approximated force limit and the line $F = 0$ is maximised. To this end, for the minimum force limit

$$J = \min_x \int_{\mathrm{v}_0}^{\mathrm{v}_{\max}} (\mathrm{x}_0 + \frac{\mathrm{x}_1}{v})\mathrm{d}v \tag{B.57}$$

and for the maximum force limit

$$J = \min_x \int_{\mathrm{v}_0}^{\mathrm{v}_{\max}} -(\mathrm{y}_0 + \frac{\mathrm{y}_1}{v})\mathrm{d}v. \tag{B.58}$$

Thus,

$$A = \begin{bmatrix} 1 & \frac{1}{v} \end{bmatrix}, \tag{B.59}$$

for the minimum force limit, f, b, x are defined as

$$f = -\begin{bmatrix} \mathrm{v}_{\max} - \mathrm{v}_0 \\ \ln(\mathrm{v}_{\max}) - \ln(\mathrm{v}_0) \end{bmatrix},\ b = F_{\gamma\min}(v),\ x = \begin{bmatrix} \mathrm{x}_0 \\ \mathrm{x}_1 \end{bmatrix} \tag{B.60}$$

and for the maximum force limit as

$$f = \begin{bmatrix} \mathrm{v}_{\max} - \mathrm{v}_0 \\ \ln(\mathrm{v}_{\max}) - \ln(\mathrm{v}_0) \end{bmatrix},\ b = F_{\gamma\max}(v), \quad x = \begin{bmatrix} \mathrm{y}_0 \\ \mathrm{y}_1 \end{bmatrix}. \tag{B.61}$$

The vehicle speed, v, is allowed to vary between two limits

$$v \in [\mathrm{v}_0, \mathrm{v}_{\max}]$$

where for CV v_0=8 km/h and for EV v_0=55 km/h, and $\mathrm{v}_{\max}$ is the maximum reachable speed by the vehicle. In this formulation, the idea is to minimize the area between the original force limit and the inner approximation.

3 Full statement of convex optimal energy consumption program

Here, the full statement of convex optimal energy consumption problem is given for CV and EV case studies. To this end, the nonlinear term $f(E) = 1/\sqrt{E(s)}$ in (B.40) is linearized about a trajectory $\hat{E}(s)$,

$$f^{\mathrm{lin}}(E, \hat{E}) \approx f(\hat{E}) + \left.\frac{\mathrm{d}f(E)}{\mathrm{d}E}\right|_{\hat{E}} (E(s) - \hat{E}(s)). \tag{B.62}$$

Thus, (B.40) is transformed into

$$F^{\mathrm{lin}}_{\gamma\max}(E) = \min\left\{\overline{F}, \mathrm{y}_0 + \mathrm{y}_1\sqrt{\frac{m}{2}} f^{\mathrm{lin}}(E, \hat{E})\right\} \tag{B.63}$$

and by using (B.16),

$$a^{\mathrm{lin}}_{\max}(E) = \min\left\{\overline{\mathrm{a}}, \frac{F^{\mathrm{lin}}_{\gamma\max}(E) - \mathrm{c_a}E - F_\alpha}{\mathrm{m}}\right\}. \tag{B.64}$$

Also by having $F^{\mathrm{lin}}_{\gamma\min}(E) = 0$ for the CV case study,

$$a^{\mathrm{lin}}_{\min}(E) = \max\left\{\underline{\mathrm{a}}, \frac{-\mathrm{c_a}E + \underline{\mathrm{F_{brk}}} - F_\alpha}{\mathrm{m}}\right\}. \tag{B.65}$$

The convex dynamic optimisation problem for the CV case study is now formulated as

$$\min_{j, F_{\mathrm{brk}}} \int_0^{s_{\mathrm{H}}} V_{\mathrm{CV}}(\cdot, \lambda_{\mathrm{t}}, \hat{E})\mathrm{d}s \tag{B.66a}$$

subject to:

$$E'(s) = \mathrm{m}a(s) \tag{B.66b}$$

$$a'(s) = j(s) \tag{B.66c}$$

$$F(s) = \mathrm{m}a(s) + \mathrm{c_a}E(s) - F_{\mathrm{brk}}(s) + F_{\alpha}(s) \tag{B.66d}$$

$$E(s) \in \frac{\mathrm{m}}{2}[v^2_{\min}(s), v^2_{\max}(s)] \tag{B.66e}$$

$$a(s) \in [a^{\mathrm{lin}}_{\min}(E), a^{\mathrm{lin}}_{\max}(E)] \tag{B.66f}$$

$$j(s) \in [\underline{\mathrm{j}}, \bar{\mathrm{j}}] \tag{B.66g}$$

$$F_{\mathrm{brk}}(s) \in [\underline{\mathrm{F_{brk}}}, 0] \tag{B.66h}$$

$$E(0) = E_0, \quad a(0) = a_0 \tag{B.66i}$$

After each SQP iteration, which occurs at each distance step forward, the trajectory about which that the problem is linearized is updated by moving towards the direction of the current optimal solution, i.e.

$$\hat{E}^{(i+1)}(k) = \hat{E}^{(i)}(k) + \beta(E^{*(i)}(k) - \hat{E}^{(i)}(k)). \tag{B.67}$$

where β is the step size that regulates the convergence rate.

For the EV case study, (B.43) is transformed into

$$F^{\mathrm{lin}}_{\gamma\min}(E) = \max\left\{\underline{F}, f^{\mathrm{lin}}(E, \hat{E})\right\} \tag{B.68}$$

using the linearized function, $f^{\mathrm{lin}}(E, \hat{E})$. Therefore, by using (B.16)

$$a^{\mathrm{lin}}_{\min}(E) = \max\left\{\bar{\mathrm{a}}, \frac{F^{\mathrm{lin}}_{\gamma\min}(E) - \mathrm{c_a}E - F_{\alpha}}{\mathrm{m}}\right\}. \tag{B.69}$$

Note that the maximum traction force limit for EV is approximated by (B.40). Accordingly, the maximum linearized acceleration is calculated by (B.64).

The convex dynamic optimisation problem for the EV case study is formulated as

$$\min_{j, F_{\mathrm{brk}}} \int_0^{s_{\mathrm{H}}} V_{\mathrm{EV}}(\cdot, \lambda_{\mathrm{t}}, \hat{E})\mathrm{d}s \tag{B.70a}$$

$$\text{subject to: (B.66b)-(B.66i).} \tag{B.70b}$$

Acknowledgment

This work has been financed by the Swedish Energy Agency (project number: 32226312). The authors would also like to acknowledge Martin Sivertsson from Volvo Cars, Mikael Askerdal from Volvo Truck, and Henrik Svärd and Karl Redbrandt from Scania for the support and helpful discussions during the project.

References

[1] I. T. Forum, *ITF Transport Outlook 2019*. OECD Publishing/ITF, 2019, p. 200, ISBN: 9789282103937.

[2] M. A. S. Kamal, M. Mukai, J. Murata, and T. Kawabe, "Ecological vehicle control on roads with up-down slopes", *IEEE Transactions on Intelligent Transportation Systems*, vol. 12, no. 3, pp. 783–794, 2011.

[3] ——, "Model predictive control of vehicles on urban roads for improved fuel economy", *IEEE Transactions on control systems technology*, vol. 21, no. 3, pp. 831–841, 2012.

[4] M. Vajedi and N. L. Azad, "Ecological adaptive cruise controller for plug-in hybrid electric vehicles using nonlinear model predictive control", *IEEE Transactions on Intelligent Transportation Systems*, vol. 17, no. 1, pp. 113–122, 2015.

[5] Y. Luo, T. Chen, S. Zhang, and K. Li, "Intelligent hybrid electric vehicle acc with coordinated control of tracking ability, fuel economy, and ride comfort", *IEEE Transactions on Intelligent Transportation Systems*, vol. 16, no. 4, pp. 2303–2308, 2015.

[6] G. Padilla, S. Weiland, and M. Donkers, "A global optimal solution to the eco-driving problem", *IEEE control systems letters*, vol. 2, no. 4, pp. 599–604, 2018.

[7] J. N. Barkenbus, "Eco-driving: An overlooked climate change initiative", *Energy Policy*, vol. 38, no. 2, pp. 762–769, 2010.

[8] R. Bellman, *Dynamic Programming*. New Jersey: Princeton Univ Pr, 1957.

[9] E. Hellström, M. Ivarsson, J. Åslund, and L. Nielsen, "Look-ahead control for heavy trucks to minimize trip time and fuel consumption", *Control Engineering Practice*, vol. 17, no. 2, pp. 245–254, 2009.

[10] E. Hellström, J. Åslund, and L. Nielsen, "Design of an efficient algorithm for fuel-optimal look-ahead control", *Control Engineering Practice*, vol. 18, no. 11, pp. 1318–1327, 2010.

[11] W. Dib, L. Serrao, and A. Sciarretta, "Optimal control to minimize trip time and energy consumption in electric vehicles", in *2011 IEEE Vehicle Power and Propulsion Conference*, IEEE, 2011, pp. 1–8.

[12] G. Heppeler, M. Sonntag, U. Wohlhaupter, and O. Sawodny, "Predictive planning of optimal velocity and state of charge trajectories for hybrid electric vehicles", *Control Engineering Practice*, vol. 61, pp. 229–243, 2016.

[13] H.-G. Wahl, K.-L. Bauer, F. Gauterin, and M. Holzäpfel, "A real-time capable enhanced dynamic programming approach for predictive optimal cruise control in hybrid electric vehicles", in *16th International IEEE Conference on Intelligent Transportation Systems (ITSC 2013)*, IEEE, 2013, pp. 1662–1667.

[14] L. Bühler, "Fuel-efficient platooning of heavy duty vehicles through road topography preview information", Master's thesis, KTH, Stockholm, Sweden, 2013.

[15] P. Themann, A. Zlocki, and L. Eckstein, "Energieeffiziente fahrzeuglängsführung durch v2x-kommunikation", in *Fahrerassistenzsysteme und Effiziente Antriebe*, W. Siebenpfeiffer, Ed. Wiesbaden: Springer Fachmedien Wiesbaden, 2015, pp. 27–33, ISBN: 978-3-658-08161-4.

[16] S. Boyd and L. Vandenberghe, *Convex Optimization*. Cambridge University Press, 2004.

[17] E. Hellström, J. Åslund, and L. Nielsen, "Management of kinetic and electric energy in heavy trucks", *SAE International Journal of Engines*, vol. 3, no. 1, pp. 1152–1163, 2010.

[18] T. van Keulen, B. de Jager, D. Foster, and M. Steinbuch, "Velocity trajectory optimization in hybrid electric trucks", in *American Control Conference*, Marriott Waterfront, Baltimore, MD, USA, 2010, pp. 5074–5079.

[19] T. van Keulen, B. de Jager, and M. Steinbuch, "Optimal trajectories for vehicles with energy recovery options", in *IFAC World Congress*, Milan, Italy, 2011, pp. 3831–3836.

[20] L. S. Pontryagin, V. G. Boltyanskii, R. V. Gamkrelidze, and E. F. Mishchenko, *The Mathematical Theory of Optimal Processes*. Interscience Publishers, 1962.

[21] R. F. Hartl, S. P. Sethi, and R. G. Vickson, "A survey of the maximum principles for optimal control problems with state constraints", *SIAM review*, vol. 37, no. 2, pp. 181–218, 1995.

[22] C. R. He, H. Maurer, and G. Orosz, "Fuel consumption optimization of heavy-duty vehicles with grade, wind, and traffic information", *Journal of Computational and Nonlinear Dynamics*, vol. 11, no. 6, 2016.

[23] M. Held, O. Flärdh, and J. Mårtensson, "Optimal speed control of a heavy-duty vehicle in urban driving", *IEEE Transactions on Intelligent Transportation Systems*, vol. 20, no. 4, pp. 1562–1573, 2018.

[24] M. Held, "Fuel-efficient look-ahead control for heavy-duty vehicles with varying velocity demands", PhD thesis, KTH Royal Institute of Technology, 2020.

[25] T. van Keulen, J. Gillot, B. de Jager, and M. Steinbuch, "Solution for state constrained optimal control problems applied to power split control for hybrid vehicles", *Automatica*, vol. 50, no. 1, pp. 187–192, 2014.

[26] N. Murgovski, B. Egardt, and M. Nilsson, "Cooperative energy management of automated vehicles", *Control Engineering Practice*, vol. 57, pp. 84–98, 2016.

[27] L. Johannesson, N. Murgovski, E. Jonasson, J. Hellgren, and B. Egardt, "Predictive energy management of hybrid long-haul trucks", *Control Engineering Practice*, vol. 41, pp. 83–97, 2015.

[28] L. Johannesson, M. Nilsson, and N. Murgovski, "Look-ahead vehicle energy management with traffic predictions", in *IFAC Workshop on Engine and Powertrain Control, Simulation and Modeling (E-COSM)*, vol. 48, Columbus, Ohio, USA, 2015, pp. 244–251.

[29] M. Hovgard, O. Jonsson, N. Murgovski, M. Sanfridson, and J. Fredriksson, "Cooperative energy management of electrified vehicles on hilly roads", *Control Engineering Practice*, vol. 73, pp. 66–78, 2018.

[30] S. Uebel, N. Murgovski, C. Tempelhahn, and B. Bäker, "Optimal energy management and velocity control of hybrid electric vehicles", *IEEE Transactions on Vehicular Technology*, vol. 67, no. 1, pp. 327–337, 2017.

[31] L. Guo, H. Chen, Q. Liu, and B. Gao, "A computationally efficient and hierarchical control strategy for velocity optimization of on-road vehicles", *IEEE Transactions on Systems, Man, and Cybernetics: Systems*, vol. 49, no. 1, pp. 31–41, 2018.

[32] V. Turri, B. Besselink, and K. H. Johansson, "Cooperative look-ahead control for fuel-efficient and safe heavy-duty vehicle platooning", *IEEE Transactions on Control Systems Technology*, vol. 25, no. 1, pp. 12–28, 2016.

[33] L. Guo, B. Gao, Y. Gao, and H. Chen, "Optimal energy management for hevs in eco-driving applications using bi-level mpc", *IEEE Transactions on Intelligent Transportation Systems*, vol. 18, no. 8, pp. 2153–2162, 2016.

[34] N. Stroe, S. Olaru, G. Colin, K. Ben-Cherif, and Y. Chamaillard, "A two-layer predictive control for hybrid electric vehicles energy management", *IFAC-PapersOnLine*, vol. 50, no. 1, pp. 10 058–10 064, 2017.

[35] S. Uebel, N. Murgovski, B. Baker, and J. Sjoberg, "A 2-level mpc for energy management including velocity control of hybrid electric vehicle", *IEEE Transactions on Vehicular Technology*, 2019.

[36] B. B. Hanson and T. E. Hanson, *Systems and methods for multi-mode unmanned vehicle mission planning and control*, US Patent 9,669,904, Jun. 2017.

[37] A. Hamednia, N. Murgovski, and J. Fredriksson, "Predictive velocity control in a hilly terrain over a long look-ahead horizon", *IFAC PapersOnLine*, vol. 51, no. 31, pp. 485–492, 2018.

[38] M. Diehl, "Real-time optimization for large scale nonlinear processes", PhD thesis, University of Heidelberg, 2001.

[39] M. M. Thomas, J. Kardos, and B. Joseph, "Shrinking horizon model predictive control applied to autoclave curing of composite laminate materials", in *Proceedings of 1994 American Control Conference-ACC'94*, IEEE, vol. 1, 1994, pp. 505–509.

[40] N. Murgovski, X. Hu, L. Johannesson, and B. Egardt, "Filtering driving cycles for assessment of electrified vehicles", in *Workshop for new energy vehicle dynamic system and control technology*, Beijing, China, 2013.

[41] T. Lipp and S. Boyd, "Minimum-time speed optimization along a fixed path", *International Journal of Control*, vol. 87, no. 6, pp. 1297–1311, 2014.

[42] N. Murgovski, L. Johannesson, X. Hu, B. Egardt, and J. Sjöberg, "Convex relaxations in the optimal control of electrified vehicles", in *American Control Conference*, Chicago, USA, 2015.

[43] R. de Castro, M. Tanelli, R. E. Araújo, and S. M. Savaresi, "Minimum-time path-following for highly redundant electric vehicles", *IEEE Transactions on Control Systems Technology*, vol. 24, no. 2, pp. 487–501, 2016.

[44] O. Lindgärde, M. Söderman, A. Tenstam, and L. Feng, "Optimal complete vehicle control for fuel efficiency", *Transportation Research Procedia*, vol. 14, pp. 1087–1096, 2016.

[45] A. Hamednia, N. Murgovski, and J. Fredriksson, "Time optimal and eco-driving mission planning under traffic constraints", in *Intelligent Transportation Systems (ITSC)*, Rhodos, Greece, 2020.

[46] M. Diehl, H. G. Bock, and J. P. Schlöder, "A real-time iteration scheme for nonlinear optimization in optimal feedback control", *SIAM Journal on control and optimization*, vol. 43, no. 5, pp. 1714–1736, 2005.

[47] T. Ohtsuka, "A continuation/gmres method for fast computation of nonlinear receding horizon control", *Automatica*, vol. 40, no. 4, pp. 563–574, 2004.

[48] J. Wahlström and L. Eriksson, "Modelling diesel engines with a variable-geometry turbocharger and exhaust gas recirculation by optimization of model parameters for capturing non-linear system dynamics", *Sage journals*, vol. 225, no. 7, pp. 960–986, 2012.

[49] L. Eriksson, A. Larsson, A. Thomasson, and S. C. Ab, "Heavy duty truck on open road–the aac2016 benchmark", in *IFAC Symposium on Advances in Automotive Control*, 2016.

[50] G. Frison and M. Diehl, "Hpipm: A high-performance quadratic programming framework for model predictive control", *arXiv preprint*, 2020.